



KTH Engineering Sciences

Master Thesis

Yet Another Thesis About Diagrammatic Monte Carlo

Emil Blomquist

Statistical Physics, Department of Physics,
School of Engineering Sciences
Royal Institute of Technology, SE-106 91 Stockholm, Sweden

Stockholm, Sweden 2017

Typeset in L^AT_EX

TRITA-???
ISSN ???
ISRN ???

© Emil Blomquist, September 2017
Printed in Sweden by Universitetsservice US AB, Stockholm September 2017

Abstract

...

Sammanfattning

...

Preface

...

Contents

Abstract	iii
Sammanfattning	iii
Preface	v
Contents	vii
1 Introduction	5
2 Background material	7
2.1 Quantum field theories	7
2.1.1 Single- and many-particle quantum mechanics	7
2.1.2 Second-quantization	8
2.1.3 Field operators	9
2.2 A few words about finite temperature formalism	9
2.2.1 Green's function	10
2.2.2 Bare single-particle Green's function	13
2.3 Derivation of the Fröhlich Hamiltonian	13
2.3.1 Classical picture	13
2.3.2 Quantization	19
2.4 Perturbation theory	22
2.4.1 Diagrammatic analysis	23
2.4.2 Dyson equation	27
2.5 Monte Carlo Methods	30
2.5.1 Markov processes, detailed balance and ergodicity	30
2.5.2 Metropolis-Hastings algorithm	31
3 Diagrammatic Monte Carlo	33
3.1 General idea	33
3.1.1 Example 1	34
3.1.2 Example 2	34
3.1.3 Example 3	36
3.2 Implementation	38

3.3	Bare scheme update procedures for \mathcal{G}	40
3.3.1	Results	48
3.4	Bare scheme update procedures for Σ^*	52
3.4.1	Divergent diagram	54
3.4.2	Results	56
3.4.3	Implementing Dyson equation numerically	58
3.5	Bold-line scheme ?	60
3.5.1	Skeleton diagrams	61
3.5.2	Implementation	64
3.5.3	Results	65
3.6	Numerical and analytical (!?) Results	77
4	Summary, conclusions and outlook	81
	Bibliography	83

Comments guide

- Something about an image
- Motivation for myself
- Question about something
- There is something wrong, a flaw
- Todo, things which need to be done at some point

Notations

Units

Throughout this text $k_{\text{B}} = \hbar = 1$ has been used. With this notation there no difference between wave vectors and momentum.

Fourier transform ~~remove this since it is not the case~~

A function $f(x)$ which is defined and integrable on the interval $x \in [-L/2, L/2]$ may be represented as a Fourier series. In this thesis the following convention will be used

$$c_k \equiv \int_{-L/2}^{L/2} f(x) e^{-ik \cdot x} dx \quad \Rightarrow \quad f(x) = \frac{1}{L} \sum_k c_k e^{ik \cdot x}. \quad (1)$$

where the wave vectors are given by $k = 2\pi n/L$ and $n \in \mathbb{Z}$. In the limit $L \rightarrow \infty$ the Fourier transform is defined accordingly

$$\hat{f}(k) \equiv \int_{\mathbb{R}} f(x) e^{-ik \cdot x} dx \quad \Rightarrow \quad f(x) = \frac{1}{2\pi} \int_{\mathbb{R}} \hat{f}(k) e^{ik \cdot x} dk. \quad (2)$$

How does this definition affect the conjugate variables in the derivation of the Fröhlich Hamiltonian?

Perhaps mention something about DOS and motivate

$$\frac{1}{V} \sum_{\mathbf{k}} \cdots \rightarrow \int \frac{d^3 k}{(2\pi)^3} \cdots. \quad (3)$$

TODO's

- Up in the corner: Contents \rightarrow Notations
- Rewrite the text so the word *we* is nowhere to be found
- Use either \mathbf{x} or \mathbf{r}
- In the finite temperature formalism: expectation value \rightarrow ensemble average
- Sometime: momentum \rightarrow wave vector
- Perhaps use "in spite"
- "as well as" \leftrightarrow "along with"
- set proper size of the figures in the DMC examples

- $\mathcal{G}_0, \mathcal{D}_0 \rightarrow \mathcal{G}^{(0)}, \mathcal{D}^{(0)}$. Make sure that this does not affect the zeroth order bold-line \mathcal{G}_0 !
- Remove Feynman diagram helping backgrounds
- In the beginning use wave vector instead of momentum, then since $\mathbf{p} = \hbar \mathbf{k}$ let the reader know that the terms will be used
- E vs ξ vs ε vs ϵ .
- Fix references. Make sure there is nothing unusual.

Chapter 1

Introduction

- Quantum mechanics
- Many-particle physics
- References to recent articles about polarons and DMC
- Mention something out of [1] as well as from [2].

Chapter 2

Background material

Here we shall summarize what this chapter is about

2.1 Quantum field theories

2.1.1 Single- and many-particle quantum mechanics

In quantum mechanics, utilizing the bra-ket notation, the state of a particle $|\psi\rangle$ can be projected onto the position basis $|\mathbf{x}\rangle$ to form a wave function $\langle\mathbf{x}|\psi\rangle = \psi(\mathbf{x})$. By using the Schrödinger picture, the dynamics is contained within the states $|\psi\rangle = |\psi(t)\rangle$ so that $\psi(\mathbf{x}) = \psi(\mathbf{x}, t)$ and the time evolution of which is governed by the Schrödinger equation (in the non-relativistic limit). The quantity $\psi^*(\mathbf{x}, t)\psi(\mathbf{x}, t)$ is real, and according to the Copenhagen interpretation [3] of quantum mechanics it is to be interpreted as the probability density function. From this, the expectation value of some quantity, e.g. the position of the particle, is acquired through

$$\begin{aligned}\langle\mathbf{x}(t)\rangle &= \int \mathbf{x} \psi^*(\mathbf{x}, t) \psi(\mathbf{x}, t) d^3x \\ &= \int \mathbf{x} \langle\psi(t)|\mathbf{x}\rangle \langle\mathbf{x}|\psi(t)\rangle d^3x \\ &= \langle\psi(t)| \left[\int \mathbf{x} |\mathbf{x}\rangle \langle\mathbf{x}| d^3x \right] |\psi(t)\rangle \\ &= \langle\psi(t)| \hat{\mathbf{x}} \left[\int |\mathbf{x}\rangle \langle\mathbf{x}| d^3x \right] |\psi(t)\rangle \\ &= \langle\psi(t)| \hat{\mathbf{x}} |\psi(t)\rangle.\end{aligned}\tag{2.1}$$

To reach the final equality it has been used that the position basis is an eigenbasis of the position operator $\hat{\mathbf{x}}|\mathbf{x}\rangle = \mathbf{x}|\mathbf{x}\rangle$ and the fact that this basis is orthonormal and complete so that the unity operator may be expressed as $\hat{1} = \sum_{\mathbf{x}} |\mathbf{x}\rangle \langle\mathbf{x}|$.

- Mention Hilbert space. one particle vs. many-particle Hilbert spaces?

What has been described so far is a quantum mechanical system of merely a single particle. In order to describe a system of more than one particle, this formalism need to be generalized to a many-particle description. When doing this, care need to be taken to the statistics of indistinguishable particles. That is, the state of the entire system must be symmetric to the interchange of two indistinguishable bosons and antisymmetric to the interchange of two indistinguishable fermions. In the many-particle quantum mechanics formalism, this can be rather cumbersome even when dealing with a noninteracting system. Another shortcoming with this description of quantum mechanics is that the number of particles of each species must be fixed. Hence it is not possible to have particle creation nor particle annihilation, which is necessary for certain processes.

2.1.2 Second-quantization

The second quantization [4, 5] is a Hamiltonian based method for constructing a quantum field theory. Such a theory does not have the shortcomings of having a fixed set of particles as in the case of the many-particle description of quantum mechanics.

Again the state of the total system will be described by individual single-particle states. However, instead of having explicit all the permutations of the indistinguishable single-particle states in order to incorporate the statistics, we will now express the total system state using occupation numbers. That is, in this representation the only information given is for each species of particle, the number of particles occupying what states. For example, given the following set of single-particle states $\{|\nu_i\rangle\}$ where $i = 0, 1, 2, \dots$, the expression describing a state in which $|\nu_0\rangle$ and $|\nu_2\rangle$ is occupied by three and two particles respectively would then be $|3, 0, 0, 2, 0, 0, \dots\rangle$.

In order to allow for the number of particles to be variable the Fock space is used. This space is a combination of Hilbert state spaces for any number of particles; from the empty vacuum state to a state with infinite particles. In order to create and annihilate a particle of a certain quantum number, creation \hat{c}_ν^\dagger and annihilation \hat{c}_ν operators are used. It can be shown that they are the Hermitian conjugate of one another which motivates the notation. These operators incorporate the underlying statistics of the particle at hand by a set of commutation relations. For bosons they are

$$[\hat{a}_i, \hat{a}_j^\dagger] = \delta_{ij}, \quad [\hat{a}_i, \hat{a}_j] = [\hat{a}_i^\dagger, \hat{a}_j^\dagger] = 0. \quad (2.2)$$

These commutation relations are, for each single-particle state, identical to those of the ladder operators of a harmonic oscillator. For fermions the commutation relations are identical, but the commutator is exchanged in favor of the anticommutator in order to make the state antisymmetric, i.e.

$$\{\hat{b}_i, \hat{b}_j^\dagger\} = \delta_{ij}, \quad \{\hat{b}_i, \hat{b}_j\} = \{\hat{b}_i^\dagger, \hat{b}_j^\dagger\} = 0. \quad (2.3)$$

The second-quantized Hamiltonian may be constructed by translating single- and many-particle quantum mechanical operator into the second-quantized description. In the case of a one-body operator this translation is rather intuitive. Here the second-quantization operator \hat{O} is given by [4]

$$\hat{O} = \sum_{\mu, \nu} \langle \mu | O | \nu \rangle \hat{c}_{\mu}^{\dagger} \hat{c}_{\nu}, \quad (2.4)$$

where O is the first-quantized operator, μ and ν are quantum numbers labeling the set of orthonormal single-particle states $\{|\mu\rangle\}$ and \hat{c}_{μ}^{\dagger} , \hat{c}_{μ} being the corresponding second-quantized creation and annihilation operators.

2.1.3 Field operators

When having utilized the second-quantization formalism, the quantum mechanical system is described by a quantum field. That is, rather than being an operator as in single- and many-particle quantum mechanics, the position is now a parameter, just like the time.

Field operators are creation and annihilation operators just like any other. They have gained their special name simply because they change the occupation number of single-particle eigenstates of the position operator. That is, they create or annihilate a particle at a particular position in space. Using the set of complete orthonormal single-particle wave functions $\{\psi_{\nu}(\mathbf{x})\}$ along with the corresponding creation and annihilation operators \hat{c}_{ν}^{\dagger} , \hat{c}_{ν} , these field operators may be constructed by the following superpositions [4],

$$\hat{\psi}(\mathbf{x}) \equiv \sum_{\nu} \hat{c}_{\nu} \psi_{\nu}(\mathbf{x}), \quad \hat{\psi}^{\dagger}(\mathbf{x}) \equiv \sum_{\nu} \hat{c}_{\nu}^{\dagger} \psi_{\nu}(\mathbf{x}). \quad (2.5)$$

The $\hat{\psi}(\mathbf{x})$ will annihilate a particle at position \mathbf{x} whilst the Hermitian conjugate $\hat{\psi}^{\dagger}(\mathbf{x})$ will do the opposite and create a particle at position \mathbf{x} .

2.2 A few words about finite temperature formalism

In a zero temperature quantum field theory, the Heisenberg picture is normally used when calculating observables, i.e. $O = \langle \Psi_0 | \hat{O}_H | \Psi_0 \rangle$. In this picture the operators are responsible for the time evolution of the observables whilst the state vectors are made time independent. This is achieved by letting the time evolution of the Schrödinger state vector $|\Psi_0(t)\rangle = e^{-i\hat{H}t} |\Psi_0\rangle$ be absorbed into the Heisenberg operator $\hat{O}_H(t) \equiv e^{i\hat{H}t} \hat{O}_S e^{-i\hat{H}t}$. Since $T = 0$ in such a theory, one does not need to be concerned about thermodynamics when calculating an observable, even if the initial state (is this the right word, look at electrons-holes example in Fetter) is not the vacuum one.

For a finite temperature quantum field theory and a general system, this can of course no longer hold true. In order to incorporate the thermodynamics, the observables are no longer calculated by the expectation value of merely one initial state but as an ensemble average. In the case of a system with a variable number of particles, the grand canonical ensemble should be used. The partition function is then given by $Z_G = \text{Tr} e^{-\beta(\hat{H} - \mu\hat{N})} = \text{Tr} e^{-\beta\hat{K}}$ where β is the inverse temperature, \hat{H} is the Hamiltonian, \hat{N} is the number operator, μ is the chemical potential and the trace is taken over a complete set of states. Introduced was also the grand canonical Hamiltonian $\hat{K} \equiv \hat{H} - \mu\hat{N}$. In accordance to the partition function, the statistical operator is then defined as $\hat{\rho}_G = e^{-\beta\hat{K}}/Z_G$ so that

$$O = \sum_{\nu} \langle \Psi_{\nu} | \hat{\rho}_G \hat{O}_H | \Psi_{\nu} \rangle \equiv \text{Tr} \{ \hat{\rho}_G \hat{O}_H(t) \}. \quad (2.6)$$

The operator product sandwiched between the state vectors in the equation above contain both real and imaginary exponents originating from the thermodynamics and quantum mechanics respectively. Following the Matsubara formalism [4–6], one proceeds by one introduces a new picture in order to treat the two types of exponents on an equal footing. This is a modified Heisenberg picture where a Wick rotation in time $\tau = it$ is preformed, and the Hamiltonian is exchanged in favor of the grand canonical Hamiltonian. An operator in this picture is then related to the corresponding one in the Schrödinger picture as

$$\hat{O}_K(\tau) \equiv e^{\hat{K}\tau} \hat{O}_S e^{-\hat{K}\tau}. \quad (2.7)$$

2.2.1 Green's function

The single-particle Green's function, also known as the propagator, plays a crucial role in quantum field theory. At zero temperature, in position and time representation, the single-particle Green's function is defined as

$$iG_{\alpha\beta}(x, x') \equiv \frac{\langle \Psi_0 | T[\hat{\psi}_{H\alpha}(x) \hat{\psi}_{H\beta}^{\dagger}(x')] | \Psi_0 \rangle}{\langle \Psi_0 | \Psi_0 \rangle} \quad (2.8)$$

and gives the probability amplitude of an particle to travel from one point in space and time to another one. Here $|\Psi_0\rangle$ is the ground state vector in the Heisenberg picture, $\hat{\psi}_{H\alpha}(x)$ is the α -th component of a field operator also in the Heisenberg picture, $T[\dots]$ orders the operators according to their time and x, x' being position-time four vectors. This Green's function contains observable properties such as both the ground state energy and the excitation spectrum of the system. By using the Lehman representation, the expectation value of any single-particle operator in the ground state of the system might also be extracted [4].

Above zero temperature, now working with an imaginary-time τ , the Green's function of interest is the temperature Green's function. In the imaginary-time

and position representation, the corresponding single-particle temperature Green's function is defined through

$$\mathcal{G}_{\alpha\beta}(x, x') \equiv \text{Tr}\{\hat{\rho}_G T_\tau[\hat{\psi}_{K\alpha}(x)\hat{\psi}_{K\alpha}^\dagger(x')]\}. \quad (2.9)$$

Here $\psi_{K\alpha}(x)$ is the α -th component of a field operator in the modified Heisenberg picture, $T_\tau[\dots]$ orders the operators according to their value of τ , $\text{Tr}\{\rho_G \dots\}$ is the same weighted sum of inner products as mention before and x, x' being position-imaginary-time four vectors. Since the temperature single-particle Green's function is not a function of time, it is only possible to directly extract from it observables which do not dependent on time, that is, thermodynamical observables. In order to obtain time dependent properties, one must first relate the temperature Green's function to a real-time Green's function. This is something which wont be of importance to this thesis and thus not discussed any further. From here on only the finite temperature formalism will be considered and whenever a Green's function is mention it will be understood that the single-particle temperature Green's function intended.

Assuming the Hamiltonian to time independent and translationally invariant, the Green's function will depend only on the difference $\mathbf{x} - \mathbf{x}'$ and $\tau - \tau'$ as soon shall be shown. By further imposing spin independency onto the Hamiltonian, the spin dependency of the Green's function may be factored out as $\mathcal{G}_{\alpha\beta}(\mathbf{x} - \mathbf{x}', \tau - \tau') = \delta_{\alpha\beta} \mathcal{G}(\mathbf{x} - \mathbf{x}', \tau - \tau')$. Thus, from this point and forward, when referring to a Green's function the spin dependency will be omitted.

In the case of a cubic system with a finite volume $V = l^3$, accompanied by periodic boundary conditions, the single-particle wave functions and the eigenvalues of the momentum operator are given by

$$\psi_{\mathbf{k}}(\mathbf{x}) = \frac{e^{i\mathbf{k}\cdot\mathbf{x}}}{\sqrt{V}} \quad (2.10)$$

and

$$k_i = \frac{2\pi}{l} n_i; \quad n_i = 0, \pm 1, \pm 2, \dots \quad (2.11)$$

respectively. Constructing the field operators (2.5) in terms of these, the expression for the Green's function may be transformed as

$$\begin{aligned} \mathcal{G}(\mathbf{x} - \mathbf{x}', \tau - \tau') &= \sum_{\mathbf{k}, \mathbf{p}} \psi_{\mathbf{k}}(\mathbf{x}) \psi_{\mathbf{p}}^\dagger(\mathbf{x}') \text{Tr}\{\hat{\rho}_G T_\tau[\hat{c}_{\mathbf{k}}(\tau) \hat{c}_{\mathbf{p}}^\dagger(\tau')]\} \\ &= \sum_{\mathbf{k}, \mathbf{p}} \psi_{\mathbf{k}}(\mathbf{x}) \psi_{\mathbf{p}}^\dagger(\mathbf{x}') \delta_{\mathbf{k}, \mathbf{p}} \text{Tr}\{\hat{\rho}_G T_\tau[\hat{c}_{\mathbf{k}}(\tau - \tau') \hat{c}_{\mathbf{k}}^\dagger(0)]\} \\ &= \frac{1}{V} \sum_{\mathbf{k}} e^{i\mathbf{k}\cdot(\mathbf{x} - \mathbf{x}')} \text{Tr}\{\hat{\rho}_G T_\tau[\hat{c}_{\mathbf{k}}(\tau - \tau') \hat{c}_{\mathbf{k}}^\dagger(0)]\} \\ &= \int \frac{d^3k}{(2\pi)^3} e^{i\mathbf{k}\cdot(\mathbf{x} - \mathbf{x}')} \text{Tr}\{\hat{\rho}_G T_\tau[\hat{c}(\mathbf{k}, \tau - \tau') \hat{c}^\dagger(\mathbf{k}, 0)]\}, \end{aligned} \quad (2.12)$$

where in the last equality the limit $l \rightarrow \infty$ has been taken. In order to shift the time, the hermiticity of \hat{K} allows the trace to be expressed in terms of its complete set of eigenstates $\{|\nu_{\mathbf{k}}\rangle\}$ for which $\hat{K}|\nu_{\mathbf{k}}\rangle = \xi_{\mathbf{k}}|\nu_{\mathbf{k}}\rangle$. Then, since the Hamiltonian is time independent it will commute with itself at any two times, implying that $\exp\{\hat{K}\tau - \hat{K}\tau'\} = \exp\{\hat{K}\tau\}\exp\{-\hat{K}\tau'\}$. On the other hand, in the limit of an infinite system, the Green's function in momentum space is obtained through the Fourier transform

$$\mathcal{G}(\mathbf{k}, \tau) = \int \frac{d^3k}{(2\pi)^3} e^{i\mathbf{k}\cdot\mathbf{x}} \mathcal{G}(\mathbf{k}, \tau). \quad (2.13)$$

Hence it must be the case that

$$\mathcal{G}(\mathbf{k}, \tau) = \text{Tr}\{\hat{\rho}_{\text{G}} T_{\tau}[\hat{c}(\mathbf{k}, \tau)\hat{c}^{\dagger}(\mathbf{k}, 0)]\}. \quad (2.14)$$

Assuming the ground state ensemble to be the vacuum state, i.e. $\text{Tr}\{\hat{\rho}_{\text{G}} \cdots\} \rightarrow \langle \text{vac} | \cdots | \text{vac} \rangle$, this expression further simplifies into

$$\mathcal{G}(\mathbf{k}, \tau) = \langle \text{vac} | \hat{c}(\mathbf{k}, \tau) \hat{c}^{\dagger}(\mathbf{k}, 0) | \text{vac} \rangle, \quad \tau \geq 0. \quad (2.15)$$

and is for all other imaginary-times identically zero.

In order to demonstrate some important properties of $\mathcal{G}(\mathbf{k}, \tau)$ the unity operator $\hat{1} = \sum_{\nu} |\nu\rangle\langle\nu|$, constructed in terms of the complete set of eigenstates $\{|\nu(\mathbf{k})\rangle\}$ to the grand canonical Hamiltonian $\hat{K}|\nu(\mathbf{p})\rangle = \xi_{\nu}(\mathbf{p})|\nu(\mathbf{p})\rangle$, is inserted into expression (2.14). By recalling that the annihilation operator in the modified Heisenberg picture (2.7) is given by $\hat{c}_{\mathbf{k}}(\tau) = e^{\hat{K}\tau} \hat{c}_{\mathbf{k}}(0) e^{-\hat{K}\tau}$ the expression then boils down to [7]

$$\mathcal{G}(\mathbf{k}, \tau) = \sum_{\nu} |\langle \nu | \hat{c}_{\mathbf{k}}^{\dagger} | \text{vac} \rangle|^2 e^{-(\xi_{\nu} - \xi_{\text{vac}})\tau}, \quad \tau \geq 0. \quad (2.16)$$

Here it has been used that ξ_{vac} is the vacuum energy, i.e. $\hat{K}|\text{vac}\rangle = \xi_{\text{vac}}|\text{vac}\rangle$. For the Fröhlich Hamiltonian to be considered later, $\xi_{\text{vac}} = 0$ and will therefore be ignored in the remaining calculation. Rather than working with some unknown set $\{\nu\}$, it is more convenient to parametrize using the frequency. This is done by introducing the spectral density function

$$g_{\mathbf{k}}(\omega) \equiv \sum_{\nu} \delta(\omega - \xi_{\nu}) |\langle \nu | \hat{c}_{\mathbf{k}}^{\dagger} | \text{vac} \rangle|^2, \quad (2.17)$$

through which the single-particle Green's function is expressed as

$$\mathcal{G}(\mathbf{k}, \tau) = \int g_{\mathbf{k}}(\omega) e^{-\omega\tau} d\omega, \quad \tau \geq 0. \quad (2.18)$$

Assuming the Green's function to be that of an electron ($\hat{c}_{\mathbf{k}} \rightarrow \hat{a}_{\mathbf{k}}$), the factor $|\langle \nu | \hat{a}_{\mathbf{k}}^{\dagger} | \text{vac} \rangle|^2 = |\langle \nu | \mathbf{k} \rangle|^2$ is nothing more than the overlap of the eigenstate $|\nu\rangle$ with free electron state of momentum \mathbf{k} . If there exist a stable eigenstate $|\nu_{0,\mathbf{k}}\rangle$ with energy $\xi_0(\mathbf{k})$, the spectral function should contain the term $|\langle \nu_{0,\mathbf{k}} | \mathbf{k} \rangle|^2 \delta(\omega - \xi_0(\mathbf{k}))$.

Being a stable state, the energy $\xi_0(\mathbf{k})$ is lower than the corresponding energy of any other possible eigenstate. According to (2.18), at imaginary-times $\tau \rightarrow \infty$, the sole contribution to the single-particle Green's function should come from this stable state. That is,

$$\mathcal{G}(\mathbf{k}, \tau \rightarrow \infty) = Z_0^{\mathbf{k}} e^{-\xi_0(\mathbf{k})\tau}, \quad (2.19)$$

where $Z_0^{\mathbf{k}} = |\langle \nu_{0,\mathbf{k}} | \mathbf{k} \rangle|^2$ is the bare-electron factor.

- Need to somehow introduce $E_0 = \xi_0 + \mu$. $N = 1$ since vacuum GS.

2.2.2 Bare single-particle Green's function

An eigenstate to a bare Hamiltonian, e.g. $\hat{K}_0 = \sum_{\mathbf{k}} \xi_{\mathbf{k}}^0 \hat{c}_{\mathbf{k}}^\dagger \hat{c}_{\mathbf{k}}$, is referred to as a bare or a free state. The energies $\xi_{\mathbf{k}}^0$ are known from solving the corresponding problem in first-quantization. Reusing the previous assumptions and calculations, but \hat{K} every where replaced with \hat{K}_0 , the bare Green's function in momentum space is found to be,

$$\mathcal{G}^{(0)}(\mathbf{k}, \tau) = \sum_{\mathbf{p}} |\langle \mathbf{p} | \hat{c}_{\mathbf{k}}^\dagger | \text{vac} \rangle|^2 e^{-\xi_{\mathbf{p}}^0 \tau} \quad \tau \geq 0. \quad (2.20)$$

However, this time the eigenstates are known, and using their orthonormality, the expression of the bare single-particle Green's function simplifies to

$$\mathcal{G}^{(0)}(\mathbf{k}, \tau) = e^{-\xi_0(\mathbf{k})\tau} \quad \tau \geq 0 \quad (2.21)$$

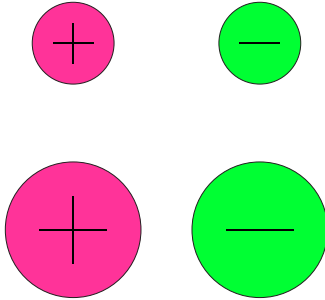
in the limit of an infinite system.

2.3 Derivation of the Fröhlich Hamiltonian

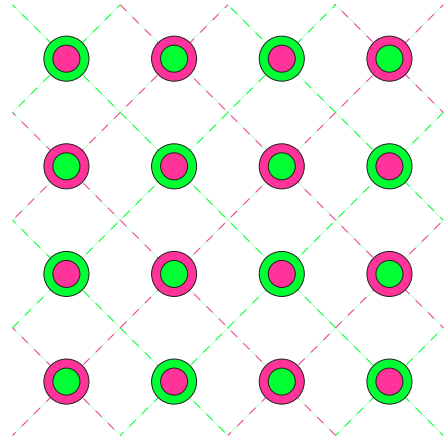
What will happen to a dielectric medium if one introduces a charged particle, and how will this particle react to changes in the dielectric medium? These are questions which Herbert Fröhlich answered in his 1954 paper *Electrons in lattice fields* [8]. In this section the original derivation will be outlined with attention directed towards details important for the thesis.

2.3.1 Classical picture

Consider a diatomic crystal, e.g. rock salt. Such a crystal is made up out of ions which pairwise have a zero net charge as illustrated in figure 2.1. By introducing a free electron into such a crystal, the crystal will become polarized due to the electric field exerted by the electron. The polarization is then described by a set of displacement vectors, one for each lattice point. In order to simplify what follows this set of displacement vectors are treated as a continuous vector field.



(a) The filled circles illustrate four types of charges. The color represent the charge sign; the ones to the left are positively charged and the ones to the right are negatively charged. The quantity of charge is represented by the size; the charges have the same charge quantity within each row, but the ones in the top row have a weaker charge than the ones in the bottom row.



(b) A layer of a diatomic crystal. This particular crystal has a face-centered cubic structure.

Figure 2.1

If this system is first looked at in a steady state situation, the polarization is determined solely by the dielectric permittivity ϵ_r . A handy quantity is the electric displacement field (CGS units)

$$\mathbf{D} = \mathbf{E} + 4\pi\mathbf{P} = \epsilon\mathbf{E} \quad (2.22)$$

where \mathbf{E} is the total electric field, \mathbf{P} is the polarization and $\epsilon = \epsilon_r\epsilon_0$ is the permittivity. Since the source of this field is given solely by the free electron, it may be thought of as an external electrical field. If the electron is at position \mathbf{x}_e , the \mathbf{D} -field at a position \mathbf{x} is given by the familiar expression

$$\mathbf{D}(\mathbf{x}, \mathbf{x}_e) = -\nabla \frac{Q}{|\mathbf{x} - \mathbf{x}_e|}, \quad (2.23)$$

so that

$$\nabla \cdot \mathbf{D}(\mathbf{x}, \mathbf{x}_e) = 4\pi q \delta(\mathbf{x} - \mathbf{x}_e). \quad (2.24)$$

Here Q is the charge of the electron and the second equality is to be thought of as valid only as a distribution. In agreement with the definition of the \mathbf{D} -field

the electric field due to the bound charges is defined as $\mathbf{E}_{\text{bound}} = -4\pi\mathbf{P}$ since $\mathbf{D} = \mathbf{E} + 4\pi\mathbf{P} = \mathbf{E} - \mathbf{E}_{\text{bound}} \equiv \mathbf{E}_{\text{free}}$.

The interaction energy, which is minimized when the \mathbf{D} -field is parallel to the polarization, is given by (why!? Dipole something? maybe postulated)

$$E_{\text{int}} = - \int_V \mathbf{D}(\mathbf{x}, \mathbf{x}_e) \cdot \mathbf{P}(\mathbf{x}) d^3x. \quad (2.25)$$

By introducing a scalar potential to the bound electric field, $\mathbf{E}_{\text{bound}} = -\nabla\Phi$, this interaction energy may be re-expressed as

$$\begin{aligned} E_{\text{int}} &= -\frac{1}{4\pi} \int_{\Omega} \mathbf{D}(\mathbf{x}, \mathbf{x}_e) \cdot \nabla\Phi(\mathbf{x}) d^3x \\ &= -\frac{1}{4\pi} \int_{\Omega \setminus V_\varepsilon} \mathbf{D}(\mathbf{x}, \mathbf{x}_e) \cdot \nabla\Phi(\mathbf{x}) d^3x - \frac{1}{4\pi} \int_{V_\varepsilon} \mathbf{D}(\mathbf{x}, \mathbf{x}_e) \cdot \nabla\Phi(\mathbf{x}) d^3x \\ &= -\frac{1}{4\pi} \int_{\Omega \setminus V_\varepsilon} \nabla \cdot [\Phi(\mathbf{x})\mathbf{D}(\mathbf{x}, \mathbf{x}_e)] d^3x + \underbrace{\frac{1}{4\pi} \int_{\Omega \setminus V_\varepsilon} \Phi(\mathbf{x}) \nabla \cdot \mathbf{D}(\mathbf{x}, \mathbf{x}_e) d^3x}_0 \\ &\quad + \underbrace{\frac{q}{4\pi} \int_{V'_\varepsilon} \frac{1}{x^2} \frac{\partial\Phi(\mathbf{x} + \mathbf{x}_e)}{\partial x} d^3x}_{\rightarrow 0 \text{ as } \varepsilon \rightarrow 0} \\ &= \frac{Q}{4\pi} \int_{-\partial V'_\varepsilon} \Phi(\mathbf{x} + \mathbf{r}_e) \nabla \frac{1}{x} \cdot d^2\mathbf{x} \\ &= Q \Phi(\mathbf{x}_e) \end{aligned} \quad (2.26)$$

Here it has both been assumed that $\Phi(\mathbf{x})$ have a continuous first derivative as well as $\Phi(\mathbf{x})\mathbf{D}(\mathbf{x}, \mathbf{x}_e) \simeq 0$ on the boundary $\mathbf{x} \in \partial\Omega$. In order to use the divergence theorem, the singularity at \mathbf{x}_e was isolated in a spherical volume V_ε with radius $\varepsilon \rightarrow 0$ centered at \mathbf{x}_e .

From this point and onwards, a system in a steady state is no longer considered and hence the time dependence is brought back. However, the solution to the time dependent version of the model clearly must agree with the time independent quantities in the limit of steady state.

Since each lattice point in the crystal is occupied by a ion, the dynamics of the system is characterized by two time scales. That is, the time it takes to displace the bound electrons relative their nuclei (deformation of ion) and the time it takes to displace the nucleus relative the lattice (deformation of lattice structure). These two types of deformation are illustrated in figure 2.2. Since the electrons are significantly lighter than their nuclei, the ion deformation time is expected to be much smaller than the time it takes to deformation the lattice. Denoting these timescales as t_{uv} and t_{ir} respectively, this translates to $t_{\text{uv}} \ll t_{\text{ir}}$ or $\omega_{\text{uv}} \gg \omega_{\text{ir}}$, where $\omega \propto 1/t$ is the corresponding characteristic frequency. The subscripts of course indicate that frequencies lie in the ultraviolet and infrared region respectively. The total

deformation, due to these two types of deformations, may then be expressed as $\mathbf{P} = \mathbf{P}_{\text{ir}} + \mathbf{P}_{\text{uv}}$.

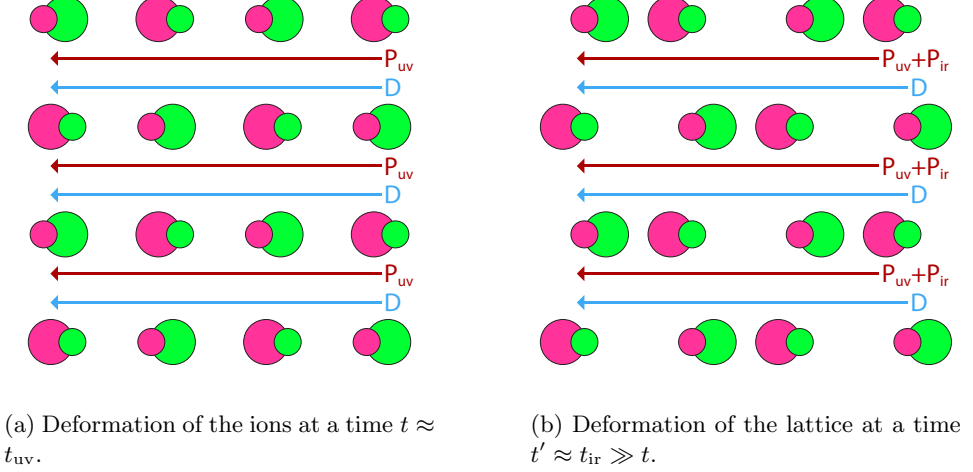


Figure 2.2

It is reasonable to further assume that each type of polarization behave as a driven harmonic oscillator, that is

$$\ddot{\mathbf{P}}_{\text{ir}}(\mathbf{x}) + \omega_{\text{ir}}^2 \mathbf{P}_{\text{ir}}(\mathbf{x}) = \frac{\mathbf{D}(\mathbf{x}, \mathbf{x}_e)}{\gamma}, \quad \ddot{\mathbf{P}}_{\text{uv}}(\mathbf{x}) + \omega_{\text{uv}}^2 \mathbf{P}_{\text{uv}}(\mathbf{x}) = \frac{\mathbf{D}(\mathbf{x}, \mathbf{x}_e)}{\delta}. \quad (2.27)$$

Here γ and δ are constants to be determined using the steady state solution

$$4\pi\mathbf{P}(\mathbf{x}) = (1 - 1/\epsilon)\mathbf{D}(\mathbf{x}, \mathbf{x}_e), \quad (2.28)$$

which follow from equation (2.22). However, since there are two unknowns to be solved for an additional relation is needed.

This second relation is the time-dependent high frequency response $\mathbf{D} = \epsilon_{\infty}\mathbf{E}$, where the rate of change ω_{∞} of the external \mathbf{D} -field satisfies $\omega_{\text{uv}} \gg \omega_{\infty} \gg \omega_{\text{ir}}$. In the case of a free electron this criterion implies that the electron must be moving extremely slowly compared to the UV timescale, but extremely quick compared to the IR timescale. Hence the UV-part of the polarization will manage to follow the changes in the \mathbf{D} -field nearly adiabatically whilst the IR-part won't have time adapt to the changes. It is therefore reasonable to assume the latter contribution to be approximately constant as well as negligible in comparison to the former contribution, i.e. $\mathbf{P} \simeq \mathbf{P}_{\text{uv}}$. Using this last approximation together with the relation of \mathbf{D} and \mathbf{E} through ϵ_{∞} , one obtains in similarity to (2.28)

$$4\pi\mathbf{P}_{\text{uv}}(\mathbf{x}) = (1 - 1/\epsilon_{\infty})\mathbf{D}(\mathbf{x}, \mathbf{x}_e). \quad (2.29)$$

By subtracting (2.29) from (2.28) a similar expression for \mathbf{P}_{ir} is found to be

$$4\pi\mathbf{P}_{\text{ir}}(\mathbf{x}) = (1/\epsilon_\infty - 1/\epsilon)\mathbf{D}(\mathbf{x}, \mathbf{x}_e). \quad (2.30)$$

Further implications of the current rate of change ω_∞ are obtained by substituting $\dot{\mathbf{P}}_{\text{uv}} \approx \omega_\infty^2 \mathbf{P}_{\text{uv}} \ll \omega_{\text{uv}}^2 \mathbf{P}_{\text{uv}}$ and $\dot{\mathbf{P}}_{\text{ir}} \approx 0$ into (2.27), which then simplifies to

$$\omega_{\text{ir}}^2 \mathbf{P}_{\text{ir}}(\mathbf{x}) = \frac{\mathbf{D}(\mathbf{x}, \mathbf{x}_e)}{\gamma}, \quad \omega_{\text{uv}}^2 \mathbf{P}_{\text{uv}}(\mathbf{x}) = \frac{\mathbf{D}(\mathbf{x}, \mathbf{x}_e)}{\delta}. \quad (2.31)$$

By finally comparing this equation to (2.29) and (2.30) the value of γ and δ , in terms of known material properties, are found to be

$$\frac{1}{\gamma} = \frac{\omega_{\text{ir}}^2}{4\pi} \left(\frac{1}{\epsilon_\infty} - \frac{1}{\epsilon} \right), \quad \frac{1}{\delta} = \frac{\omega_{\text{uv}}^2}{4\pi} \left(1 - \frac{1}{\epsilon_\infty} \right). \quad (2.32)$$

Having formulated the equation of motion for the two types of polarization, the next task is to construct one for the free electron. Since the electron was assumed to be slowly moving, one may without hesitation treat it in the non-relativistic limit. Then the only force acting on the electron is due to the bound electric field, i.e. $\mathbf{F}(\mathbf{x}_e) = q\mathbf{E}_{\text{bound}}(\mathbf{x}_e) = -q\nabla\Phi(\mathbf{x}_e)$. Thus $m\ddot{\mathbf{x}}_e = \dot{\mathbf{p}}_e = -q\nabla\Phi(\mathbf{x}_e)$ where m is an effective mass which in general is different from the electronic mass m_e . By treating \mathbf{p}_e , $\mathbf{P}_{\text{uv}}(\mathbf{r})$ and $\mathbf{P}_{\text{ir}}(\mathbf{r})$ as independent quantities, one may out of the equations of motion together with the interaction (2.26) construct the Lagrangian

$$L = \frac{\gamma}{2} \int [\dot{\mathbf{P}}_{\text{ir}}^2(\mathbf{x}) - \omega_{\text{ir}}^2 \mathbf{P}_{\text{ir}}^2(\mathbf{x})] d^3x + \frac{\delta}{2} \int [\dot{\mathbf{P}}_{\text{uv}}^2(\mathbf{x}) - \omega_{\text{uv}}^2 \mathbf{P}_{\text{uv}}^2(\mathbf{x})] d^3x \\ + \int \mathbf{D}(\mathbf{x}, \mathbf{x}_e) \cdot [\mathbf{P}_{\text{ir}}(\mathbf{x}) + \mathbf{P}_{\text{uv}}(\mathbf{x})] d^3x + \frac{\mathbf{p}_e^2}{2m}, \quad (2.33)$$

Performing a Legendre transformation, the Hamiltonian is found to be

$$H = \frac{\gamma}{2} \int [\dot{\mathbf{P}}_{\text{ir}}^2(\mathbf{x}) + \omega_{\text{ir}}^2 \mathbf{P}_{\text{ir}}^2(\mathbf{x})] d^3x + \frac{\delta}{2} \int [\dot{\mathbf{P}}_{\text{uv}}^2(\mathbf{x}) + \omega_{\text{uv}}^2 \mathbf{P}_{\text{uv}}^2(\mathbf{x})] d^3x \\ - \int \mathbf{D}(\mathbf{x}, \mathbf{x}_e) \cdot [\mathbf{P}_{\text{ir}}(\mathbf{x}) + \mathbf{P}_{\text{uv}}(\mathbf{x})] d^3x + \frac{\mathbf{p}_e^2}{2m}. \quad (2.34)$$

Since the UV-part of the polarization follows the external field nearly adiabatically, the dynamic solution \mathbf{P}_{uv} is approximatively the statical one with respect to instantaneous value of \mathbf{D} -field. Hence the contribution of \mathbf{P}_{uv} to the the Hamiltonian becomes constant so that it can be removed without affecting the dynamics, giving rise merely to an energy shift. Having removed \mathbf{P}_{uv} from the theory it is no longer necessary to keep the subscript of \mathbf{P}_{ir} and ω_{ir} for differentiation purposes, therefore it is from here on omitted.

Before proceeding with the derivation, it is important to point out that the integrals in L and H are divergent. The reason for this is the polarization, which

according to (2.29) and (2.30) is proportional to the \mathbf{D} -field which in turn is singular at $\mathbf{x} = \mathbf{x}_e$. This divergence is a consequence from disregarding the lattice structure when interpreting the displacements as a continuous vector field. If one were to calculate this integral, it would be necessary to express the polarization as a Fourier series and omit terms with a wave length smaller than that of the lattice constant.

At this point it is convenient to introduce here a complex vector field \mathbf{B} ,

$$\mathbf{B}(\mathbf{x}) = \sqrt{\frac{\gamma\omega}{2}} \left[\mathbf{P}(\mathbf{x}) + \frac{i}{\omega} \dot{\mathbf{P}}(\mathbf{x}) \right], \quad \mathbf{B}^*(\mathbf{x}) = \sqrt{\frac{\gamma\omega}{2}} \left[\mathbf{P}(\mathbf{x}) - \frac{i}{\omega} \dot{\mathbf{P}}(\mathbf{x}) \right], \quad (2.35)$$

so that

$$\mathbf{P}(\mathbf{x}) = \sqrt{\frac{1}{2\omega\gamma}} [\mathbf{B}^*(\mathbf{x}) + \mathbf{B}(\mathbf{x})], \quad \dot{\mathbf{P}}(\mathbf{x}) = i\sqrt{\frac{\omega}{2\gamma}} [\mathbf{B}^*(\mathbf{x}) - \mathbf{B}(\mathbf{x})]. \quad (2.36)$$

The reasons to why this field was introduced will become evident when quantizing the theory. The Hamiltonian, re-expressed in terms of the \mathbf{B} -field, transform into

$$H = \frac{\mathbf{p}_e^2}{2m} + \omega \int \mathbf{B}^*(\mathbf{x}) \cdot \mathbf{B}(\mathbf{x}) d^3x - \sqrt{\frac{1}{2\gamma\omega}} \int \mathbf{D}(\mathbf{x}, \mathbf{x}_e) \cdot [\mathbf{B}(\mathbf{x}) + \mathbf{B}^*(\mathbf{x})] d^3x. \quad (2.37)$$

By assuming the system to be cubic of size $V = l^3$, the \mathbf{B} -field and its complex conjugate may each be expressed in terms of a Fourier series

$$\mathbf{B}(\mathbf{x}) = \sum_{\mathbf{q}} \frac{\mathbf{q}}{q} b_{\mathbf{q}} \frac{e^{i\mathbf{q} \cdot \mathbf{x}}}{\sqrt{V}}, \quad \mathbf{B}^*(\mathbf{x}) = \sum_{\mathbf{q}} \frac{\mathbf{q}}{q} b_{\mathbf{q}}^* \frac{e^{-i\mathbf{q} \cdot \mathbf{x}}}{\sqrt{V}} \quad (2.38)$$

where the wave vectors are given according to (2.11). Next, by defining a scalar potential Ξ for the IR-part of the polarization as $4\pi\mathbf{P} = \nabla\Xi$ it is according to (2.26) possible to express the interaction energy between \mathbf{D} and \mathbf{P} as $Q\Xi(\mathbf{x}_e)$. Using (2.35) and (2.38) together with Ξ the expression for the Hamiltonian then becomes

$$H = \frac{\mathbf{p}_e^2}{2m} + \omega \sum_{\mathbf{q}} b_{\mathbf{q}}^* b_{\mathbf{q}} + \frac{1}{\sqrt{V}} \sum_{\mathbf{q}} V(q) [b_{\mathbf{q}}^* e^{-i\mathbf{q} \cdot \mathbf{r}_e} - b_{\mathbf{q}} e^{i\mathbf{q} \cdot \mathbf{r}_e}], \quad (2.39)$$

where both

$$V(q) = i \left(2\sqrt{2}\pi\alpha \right)^{1/2} \left(\frac{\omega^3}{m} \right)^{1/4} \frac{1}{q} \quad (2.40)$$

and the interaction parameter

$$\alpha = \frac{1}{2} \left(\frac{1}{\epsilon_{\infty}} - \frac{1}{\epsilon} \right) \sqrt{\frac{2m}{\omega}} Q^2 \quad (2.41)$$

has been introduced.

Here it seems as if the interaction part of the Hamiltonian is ill behaved since the $\mathbf{q} = \mathbf{0}$ term clearly is singular. This is a consequence from the periodic boundary condition which was imposed when expressing \mathbf{B} as a Fourier series. Originally the system contained only a single free electron. With a periodic boundary condition however, the system now consists of an infinite number of copies of the cube with volume V , each containing a free electron. These electrons interact with one another due to the long range Coulomb repulsion. To avoid this behavior when periodically continuing the system, one should introduce in each cube the uniform charge density $-Q/V$. Doing so would give rise to an attractive Coulomb force which for each electron would cancel the Coulomb repulsion. Such an interaction would exactly cancel the ill behaved $\mathbf{q} = \mathbf{0}$ term in the interaction part of the Hamiltonian, since the only difference would be the sign of the charge, i.e $Q \rightarrow -Q$.

2.3.2 Quantization

In order to quantize the theory, it is of utter importance to construct a set of canonical coordinates p_i and q_i for which the commutation relations are. Using (2.27) and (2.34), it is easy to verify that $\phi_i(\mathbf{x}, t)_i = [\mathbf{P}(\mathbf{x}, t)]_i$ and $\pi_i(\mathbf{x}, t) = \gamma[\dot{\mathbf{P}}(\mathbf{x}, t)]_i$ obey Hamilton's field equations

$$\dot{\phi}_i = \frac{\delta H}{\delta \pi_i}, \quad \dot{\pi}_i = -\frac{\delta H}{\delta \phi_i} \quad (2.42)$$

and thus constitutes a set of canonical field coordinates. By then employing a restricted canonical transformation $q_i = q_i(\phi, \pi)$, $p_i = p_i(\phi, \pi)$, one obtains the following set of canonical coordinates

$$q_{\mathbf{k}} = \sqrt{\frac{1}{2\omega\gamma}} [b_{\mathbf{k}}^* + b_{\mathbf{k}}], \quad p_{\mathbf{k}} = i\sqrt{\frac{\gamma\omega}{2}} [b_{\mathbf{k}}^* - b_{\mathbf{k}}]. \quad (2.43)$$

It is pretty straight forward to verify that this is in fact true. Using (2.36) and (2.38) together with the expressions for the sets of canonical coordinates one may express ϕ, π in terms of $q_{\mathbf{k}}, p_{\mathbf{k}}$ and vice versa,

$$\begin{aligned} q_{\mathbf{k}} &= \frac{1}{\sqrt{V}} \int \frac{\mathbf{k}}{k} \cdot \left[\frac{1}{\omega\gamma} \pi(\mathbf{x}) \sin \mathbf{k} \cdot \mathbf{x} + \phi(\mathbf{x}) \cos \mathbf{k} \cdot \mathbf{x} \right] d^3x \\ p_{\mathbf{k}} &= \frac{1}{\sqrt{V}} \int \frac{\mathbf{k}}{k} \cdot [\pi(\mathbf{x}) \cos \mathbf{k} \cdot \mathbf{x} - \omega\gamma \phi(\mathbf{x}) \sin \mathbf{k} \cdot \mathbf{x}] d^3x \\ \phi(\mathbf{x}) &= \frac{1}{\sqrt{V}} \sum_{\mathbf{k}} \frac{\mathbf{k}}{k} \left[q_{\mathbf{k}} \cos \mathbf{k} \cdot \mathbf{x} - \frac{1}{\omega\gamma} p_{\mathbf{k}} \sin \mathbf{k} \cdot \mathbf{x} \right] \\ \pi(\mathbf{x}) &= \frac{1}{\sqrt{V}} \sum_{\mathbf{k}} \frac{\mathbf{k}}{k} [\omega\gamma q_{\mathbf{k}} \sin \mathbf{k} \cdot \mathbf{x} + p_{\mathbf{k}} \cos \mathbf{k} \cdot \mathbf{x}]. \end{aligned} \quad (2.44)$$

Then, by showing that these coordinates satisfy the relations [9]

$$\begin{aligned} \left(\frac{\delta q_{\mathbf{k}}}{\delta \phi_i} \right)_{\phi, \pi} &= \left(\frac{\partial \pi_i}{\partial p_{\mathbf{k}}} \right)_{q, p} & \left(\frac{\delta q_{\mathbf{k}}}{\delta \pi_i} \right)_{\phi, \pi} &= - \left(\frac{\partial \phi_i}{\partial p_{\mathbf{k}}} \right)_{q, p} \\ \left(\frac{\delta p_{\mathbf{k}}}{\delta \pi_i} \right)_{\phi, \pi} &= \left(\frac{\partial \phi_i}{\partial q_{\mathbf{k}}} \right)_{q, p} & \left(\frac{\delta p_{\mathbf{k}}}{\delta \phi_i} \right)_{\phi, \pi} &= - \left(\frac{\partial \pi_i}{\partial q_{\mathbf{k}}} \right)_{q, p} \end{aligned} \quad (2.45)$$

proves that the transformation used, and the set of coordinates $q_{\mathbf{k}}, p_{\mathbf{k}}$ obtained, both are canonical.

Before promoting these new coordinates to operators, one must symmetrize the product $b_{\mathbf{q}}^* b_{\mathbf{q}}$. Up to this point, $b_{\mathbf{q}}^*$ and $b_{\mathbf{q}}$ have been complex valued variables so that the order in which they appeared in such a product does not matter. However, due to a nonzero commutation relation when promoted to operators, this will no longer be the case. In order to not favor any of the two possible orderings, they are chosen to contribute equally, i.e. $b_{\mathbf{q}}^* b_{\mathbf{q}} = (b_{\mathbf{q}}^* b_{\mathbf{q}} + b_{\mathbf{q}} b_{\mathbf{q}}^*)/2$.

By promoting the canonical coordinates to operators and imposing Bose statistics onto $\hat{q}_{\mathbf{q}}, \hat{p}_{\mathbf{q}}$, the commutation relations follow from the corresponding poisson bracket relations of classical mechanics, i.e.

$$\begin{aligned} \{q_{\mathbf{k}}, p_{\mathbf{p}}\}_{\text{PB}} &= \delta_{\mathbf{k}, \mathbf{p}} \rightarrow [\hat{q}_{\mathbf{k}}, \hat{p}_{\mathbf{p}}] = i\delta_{\mathbf{k}, \mathbf{p}} \\ \{[\mathbf{r}_e]_i, [\mathbf{p}_e]_j\}_{\text{PB}} &= \delta_{i,j} \rightarrow [[\hat{\mathbf{r}}_e]_i, [\hat{\mathbf{p}}_e]_j] = i\delta_{i,j}. \end{aligned} \quad (2.46)$$

Substituting with (2.43) into the first of these equations, and using that $[\hat{q}_{\mathbf{k}}, \hat{q}_{\mathbf{p}}] = [\hat{p}_{\mathbf{k}}, \hat{p}_{\mathbf{p}}] = 0$, one is left with the relations $[\hat{b}_{\mathbf{k}}, \hat{b}_{\mathbf{p}}^\dagger] = \delta_{\mathbf{k}, \mathbf{p}}$ and $[\hat{b}_{\mathbf{k}}, \hat{b}_{\mathbf{p}}] = 0$. Using these commutation relations the previously symmetrized terms of the Hamiltonian are rewritten as $(\hat{b}_{\mathbf{q}}^\dagger \hat{b}_{\mathbf{q}} + \hat{b}_{\mathbf{q}} \hat{b}_{\mathbf{q}}^\dagger)/2 = \hat{b}_{\mathbf{q}}^\dagger \hat{b}_{\mathbf{q}} + \frac{1}{2}$. The full Hamiltonian in quantized form then becomes

$$\hat{H} = \frac{\hat{\mathbf{p}}_e^2}{2m} + \omega \sum_{\mathbf{q}} \hat{b}_{\mathbf{q}}^\dagger \hat{b}_{\mathbf{q}} + \frac{1}{\sqrt{V}} \sum_{\mathbf{q}} V(q) \left(\hat{b}_{\mathbf{q}}^\dagger e^{-i\mathbf{q} \cdot \hat{\mathbf{r}}_e} - \hat{b}_{\mathbf{q}} e^{i\mathbf{q} \cdot \hat{\mathbf{r}}_e} \right). \quad (2.47)$$

where the zero point energy $\omega \sum_{\mathbf{q}} \frac{1}{2}$ of the oscillating ions have been omitted.

The commutation relations satisfied by $\hat{b}_{\mathbf{q}}^\dagger$ and $\hat{b}_{\mathbf{q}}$ are the same as (2.2), implying that these operators are nothing but the creation and annihilation operators of a bosonic field. The polarization field \mathbf{P} can then be thought of as being represented by a set of harmonic oscillators each corresponding to a quantized mode of vibration in the lattice, i.e. a phonon. Since the frequency of the phonons is momentum independent they it is said to be dispersionless. For optical phonons which couple to infrared radiation, this is at low momenta a good approximation as shown in the figure 2.3.

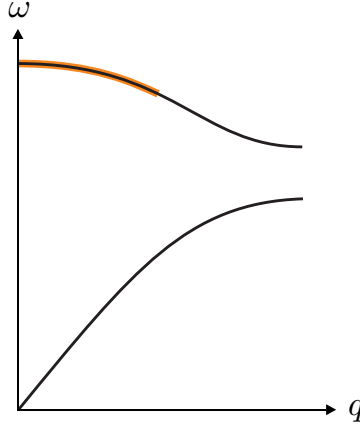


Figure 2.3: The upper and lower curves illustrate the characteristics of an optical and acoustic dispersion relation respectively. The outlined orange region suggests where the optical dispersion relation may be well approximated as momentum independent.

Having sorted out the quantization of the **B**-field, the attention is turned towards the electron which has not yet undergone second-quantization. In order to achieve this, the recipe (2.4) is used which translates a one-body operator from first to second-quantization. By using the allowed momenta (2.11) as occupation numbers for the electron state, one obtains

$$\begin{aligned}
 \frac{\hat{\mathbf{p}}_e^2}{2m} &\rightarrow \sum_{\mathbf{p}} \frac{p^2}{2m} \hat{a}_{\mathbf{p}}^\dagger \hat{a}_{\mathbf{p}}, \\
 e^{-i\mathbf{q} \cdot \hat{\mathbf{r}}_e} &\rightarrow \sum_{\mathbf{k}, \mathbf{p}} \langle \mathbf{k} | e^{-i\mathbf{q} \cdot \hat{\mathbf{r}}_e} | \mathbf{p} \rangle \hat{a}_{\mathbf{k}}^\dagger \hat{a}_{\mathbf{p}} \\
 &= \sum_{\mathbf{k}, \mathbf{p}} \langle \mathbf{k} | \left[\int |\mathbf{x}\rangle \langle \mathbf{x}| d^3x \right] e^{-i\mathbf{q} \cdot \hat{\mathbf{r}}_e} \left[\int |\mathbf{y}\rangle \langle \mathbf{y}| d^3y \right] | \mathbf{p} \rangle \hat{a}_{\mathbf{k}}^\dagger \hat{a}_{\mathbf{p}} \\
 &= \sum_{\mathbf{k}, \mathbf{p}} \hat{a}_{\mathbf{k}}^\dagger \hat{a}_{\mathbf{p}} \int d^3x \frac{e^{-i\mathbf{k} \cdot \mathbf{x}}}{\sqrt{V}} e^{-i\mathbf{q} \cdot \mathbf{x}} \frac{e^{i\mathbf{p} \cdot \mathbf{x}}}{\sqrt{V}} \\
 &= \sum_{\mathbf{k}, \mathbf{p}} \hat{a}_{\mathbf{k}}^\dagger \hat{a}_{\mathbf{p}} \delta(\mathbf{k} + \mathbf{q} - \mathbf{p}) \\
 &= \sum_{\mathbf{p}} \hat{a}_{\mathbf{p}-\mathbf{q}}^\dagger \hat{a}_{\mathbf{p}}
 \end{aligned} \tag{2.48}$$

and similarly

$$e^{i\mathbf{q}\cdot\hat{\mathbf{r}}_e} \rightarrow \sum_{\mathbf{p}} \hat{a}_{\mathbf{p}+\mathbf{q}}^\dagger \hat{a}_{\mathbf{p}}. \quad (2.49)$$

Substituting with this into the Hamiltonian and using that interaction term is symmetric with respect to \mathbf{q} , the fully second-quantized Hamiltonian becomes

$$\hat{H} = \sum_{\mathbf{p}} \frac{p^2}{2m} \hat{a}_{\mathbf{p}}^\dagger \hat{a}_{\mathbf{p}} + \omega \sum_{\mathbf{q}} \hat{b}_{\mathbf{q}}^\dagger \hat{b}_{\mathbf{q}} + \frac{1}{\sqrt{V}} \sum_{\mathbf{q}, \mathbf{p}} V(q) \left(\hat{b}_{\mathbf{q}}^\dagger - \hat{b}_{-\mathbf{q}} \right) \hat{a}_{\mathbf{p}-\mathbf{q}}^\dagger \hat{a}_{\mathbf{p}}. \quad (2.50)$$

The grand canonical Hamiltonian \hat{K} , which is used extensively in the finite temperature field theory, is obtained by adding chemical potentials to \hat{H} . But, since there is no conservation law regarding the number of phonons it must be the case that $\mu_{\text{phonon}} = 0$. Thus

$$\hat{K} = \sum_{\mathbf{p}} \left(\frac{p^2}{2} - \mu \right) \hat{a}_{\mathbf{p}}^\dagger \hat{a}_{\mathbf{p}} + \sum_{\mathbf{q}} \hat{b}_{\mathbf{q}}^\dagger \hat{b}_{\mathbf{q}} + \frac{1}{\sqrt{V}} \sum_{\mathbf{q}, \mathbf{p}} V(q) \left(\hat{b}_{\mathbf{q}}^\dagger - \hat{b}_{-\mathbf{q}} \right) \hat{a}_{\mathbf{p}-\mathbf{q}}^\dagger \hat{a}_{\mathbf{p}} \quad (2.51)$$

where for convenience $m = \omega = 1$ has been used.

2.4 Perturbation theory

Assume the Hamiltonian to be time-independent in the Schrödinger picture and expressible as the sum $\hat{K} = \hat{K}_0 + \hat{K}_1$, where \hat{K}_1 contains the interactions of the theory without which the problem would be exactly solvable. However, if this interaction is weak enough, it is reasonable to treat it perturbatively by expanding with respect to some small interaction parameter α . In order to do so it is necessary to introduce yet a new picture, the interaction picture. In the finite temperature formalism, operators in the interaction picture are related to the ones in the Schrödinger picture through $\hat{O}_I(\tau) = e^{\hat{K}_0\tau} \hat{O}_S e^{-\hat{K}_0\tau}$. Within this picture, it is possible to express the ensemble average of a τ -ordered product of operators by the perturbation series

$$\begin{aligned} & \text{Tr}\{\hat{\rho}_G T_\tau[\hat{A}_K(\tau_a) \hat{B}_K(\tau_b) \cdots \hat{F}_K(\tau_f)]\} \\ &= \\ & \frac{\sum_{n=0}^{\infty} \frac{(-1)^n}{n!} \int_0^\beta d\tau_1 \cdots \int_0^\beta d\tau_n \text{Tr}\left\{e^{-\beta\hat{K}_0} T_\tau[\hat{K}_1(\tau_1) \cdots \hat{K}_1(\tau_n) \hat{A}(\tau_a) \hat{B}(\tau_b) \cdots \hat{F}(\tau_f)]\right\}}{\sum_{n=0}^{\infty} \frac{(-1)^n}{n!} \int_0^\beta d\tau_1 \cdots \int_0^\beta d\tau_n \text{Tr}\left\{e^{-\beta\hat{K}_0} T_\tau[\hat{K}_1(\tau_1) \cdots \hat{K}_1(\tau_n)]\right\}}. \end{aligned} \quad (2.52)$$

In both the nominator and denominator of the expression above, there is the frequently appearing factor

$$\text{Tr}\{e^{-\beta\hat{K}_0} T_\tau[\hat{A} \hat{B} \cdots \hat{F}]\}. \quad (2.53)$$

It was first proved by Matsubara [6] that this factor could be rewritten as the sum of all possible permutations of contractions $\hat{A} \hat{B} \cdots \equiv \text{Tr}\{\hat{\rho}_{G0} T_\tau[\hat{A} \hat{B}]\}$ amongst the

product of operators $\hat{A}\hat{B}\cdots\hat{F}$. Here $\hat{\rho}_{G0}$ is the bare statistical operator, defined in accordance with $\hat{\rho}_G$ but having the full Hamiltonian replaced by the noninteracting part only. In the case of a creation and an annihilation operator, the contraction,

$$\hat{c}_{\mathbf{k}}(\tau) \cdot \hat{c}_{\mathbf{k}}^\dagger(\tau') = \text{Tr}\{\hat{\rho}_{G0} T_\tau[\hat{c}_{\mathbf{k}}(\tau) \hat{c}_{\mathbf{k}}^\dagger(\tau')]\} = \mathcal{G}^{(0)}(\mathbf{k}, \tau), \quad (2.54)$$

is nothing but the definition of the bare propagator in momentum space (2.14). All other types of contractions amongst such operators turn out to be zero, i.e.

$$\hat{c}_{\mathbf{k}}(\tau) \cdot \hat{c}_{\mathbf{k}}(\tau') = \hat{c}_{\mathbf{k}}^\dagger(\tau) \cdot \hat{c}_{\mathbf{k}}^\dagger(\tau') = \hat{c}_{\mathbf{k}}(\tau) \cdot \hat{c}_{\mathbf{p}}^\dagger(\tau') = 0 \quad \forall \quad \mathbf{k} \neq \mathbf{p}. \quad (2.55)$$

Hence only a small part of all terms in (2.53) survive, and these are the ones which may be represented pictorially in terms of Feynman diagrams. Further the denominator of (2.52) will serve to precisely cancel out any unconnected diagram part from the nominator. What is left of the perturbations series is then an infinite number of connected Feynman diagrams which are easily constructed from a set of Feynman rules.

2.4.1 Diagrammatic analysis

The constituents of the resulting Feynman diagrams are easily obtained just by analyzing the Hamiltonian (2.51). Using the vacuum ground state ensemble, the bare electronic and phononic propagators, referred to as $\mathcal{G}^{(0)}$ and $\mathcal{D}^{(0)}$ respectively, are given according to (2.21) and represented as

$$0 \xrightarrow[\mathbf{p}]{} \tau = \mathcal{G}^{(0)}(\mathbf{p}, \tau) = \exp \left\{ - \left(\frac{p^2}{2} - \mu \right) \tau \right\} \quad \tau \geq 0, \quad (2.56)$$

$$0 \text{ --- } \mathbf{q} \text{ --- } \tau = \mathcal{D}^{(0)}(\mathbf{q}, \tau) = \exp \{-\tau\} \quad \tau \geq 0. \quad (2.57)$$

Since any propagator going backwards in time is identically zero, it is possible to use the convention that the momentum is carried in the direction of increased time, which throughout this paper will be towards the right. Then, by examining the interaction part of the Hamiltonian, the possible vertices and their contribution are

found out to be

$$= \frac{V(\mathbf{q})}{\sqrt{V}}$$

(2.58)

with $V(\mathbf{q})$ as defined in (2.40).

In this thesis only the electronic single-particle Green's function will be studied in terms of Feynman diagrams. Hence the operators $\hat{A} \hat{B} \cdots \hat{F}$ in the perturbation series (2.52) are replaced by $\hat{a}_{\mathbf{p}} \hat{a}_{\mathbf{p}}^{\dagger}$ as to coincide with the definition (2.14) of $\mathcal{G}(\mathbf{p}, \tau)$. In order to construct the relevant diagrams, the Feynman rules [4] dictate:

1. Draw all topologically distinct diagrams with $2n + 1$ electron lines and n phonon lines.
2. With each particle line associate a factor $\mathcal{G}^{(0)}$ in case of an electron, and $\mathcal{D}^{(0)}$ in case of a phonon.
3. Each vertex contributes with the factor $V(\mathbf{q})/\sqrt{V}$, where \mathbf{q} is the momentum of the phonon connected to this vertex.
4. Conserve the total momentum at every vertex.
5. The external legs should both be assigned the external momentum \mathbf{p} of the interacting Green's function $\mathcal{G}(\mathbf{p}, \tau)$. The ingoing external leg should start at the imaginary-time 0 and the outgoing external leg should terminate at τ .
6. For each of the n internal momenta, sum over all allowed momentum values.
7. For each of the n internal imaginary-times, integrate from 0 to β .
8. Multiply each diagram with the factor $(-1)^n$.

In this thesis the single-particle Green's function will be studied in the limit $V \rightarrow \infty$. Hence the sums over internal momenta should be replaced according to

$$\frac{1}{V} \sum_{\mathbf{k}} \cdots \rightarrow \int \frac{d^3 k}{(2\pi)^3} \cdots \quad (2.59)$$

Further more this will be studied at $T = 0$ implying that the upper limit of the imaginary-time integrals becomes infinite.

Since the ground state ensemble is equal to that of vacuum, the propagators become identically zero for negative imaginary-times. Because of this, the contribution from diagrams containing tadpoles, electron loops or similar structures vanish. This is illustrated in figure 2.4.

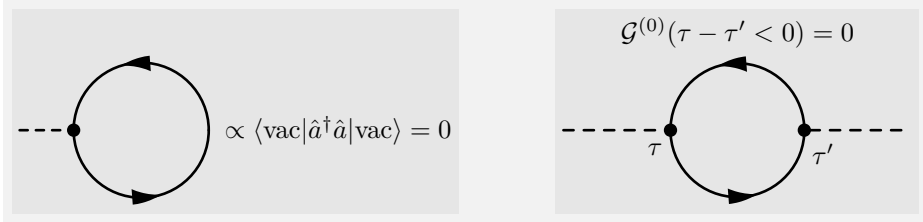


Figure 2.4: A tadpole and an electron loop both of which are equal to zero due to the ground state ensemble of vacuum.

Then the only contributing diagrams are those where all electron propagators follow after one another in a line, and phonon propagators spawn and die on the

vertices on that line. That is,

$$\begin{aligned}
 \mathcal{G}(\mathbf{p}, \tau) = & \text{Diagram 1} + \text{Diagram 2} \\
 & + \text{Diagram 3} \\
 & + \text{Diagram 4} \\
 & + \dots
 \end{aligned}$$

The diagrams are Feynman diagrams representing terms in the expansion of $\mathcal{G}(\mathbf{p}, \tau)$. Each diagram consists of a horizontal line with arrows pointing to the right, representing a fermion line. Vertices are marked with dots on the line. Dashed lines represent boson loops.

- Diagram 1:** A single horizontal line from 0 to τ with momentum \mathbf{p} and a right-pointing arrow.
- Diagram 2:** A horizontal line from 0 to τ with momentum \mathbf{p} . A dashed loop with momentum \mathbf{q} connects vertex τ_1 to vertex τ_2 . The segment between τ_1 and τ_2 has momentum $\mathbf{p} - \mathbf{q}$. The segment after τ_2 has momentum \mathbf{p} .
- Diagram 3:** A horizontal line from 0 to τ with momentum \mathbf{p} . Two dashed loops are present. The first loop with momentum \mathbf{q} connects τ_1 to τ_2 . The second loop with momentum \mathbf{k} connects τ_3 to τ_4 . The segments between vertices have momenta $\mathbf{p} - \mathbf{q}$, \mathbf{p} , $\mathbf{p} - \mathbf{k}$, and \mathbf{p} respectively.
- Diagram 4:** A horizontal line from 0 to τ with momentum \mathbf{p} . Two overlapping dashed loops are present. The first loop with momentum \mathbf{q} connects τ_1 to τ_2 . The second loop with momentum \mathbf{k} connects τ_2 to τ_3 . The segments between vertices have momenta $\mathbf{p} - \mathbf{q}$, $\mathbf{p} - \mathbf{q} - \mathbf{k}$, and $\mathbf{p} - \mathbf{k}$ respectively.

It is obvious that the contribution from each diagram is nonzero only when the times are ordered chronologically, i.e. $0 = \tau_0 \leq \tau_1 \leq \tau_2 \leq \dots \leq \tau_{2n-1} = \tau$. Because if this was not the case at least one propagator would propagate backwards in time and contribute with a factor of zero. Thus it is only meaningful to carry out the integrals such that this chronologization constraint is fulfilled.

Another important property of these diagrams is that they all carry a positive definite contribution to \mathcal{G} . This since the value of a propagator always is larger than or equal to zero, and the sign from the factor $(-1)^n$ cancel the i^{2n} contained within $V(\mathbf{q})^{2n}$.


- Since there is no preferred direction of the external momentum \mathbf{p} , the Green's function will depend only upon the magnitude $p = |\mathbf{p}|$, i.e. $\mathcal{G} = \mathcal{G}(\alpha, \mu, p, \tau)$.

2.4.2 Dyson equation

Working at zero temperature allows for a full Fourier representation of the single-particle Green's function, i.e.

$$G(\mathbf{x}, \tau) = \frac{1}{(2\pi)^4} \int d^3k \int d\omega e^{i(\mathbf{k} \cdot \mathbf{x} - \omega\tau)} G(\mathbf{k}, \omega) ; \quad G = \mathcal{G}, \mathcal{D}, \mathcal{G}_0, \mathcal{D}_0. \quad (2.61)$$

It so happens to be more pleasant working in \mathbf{k} - ω space for a lot of reasons but what will be of importance here is the conservation of total four momentum $k = (\omega, \mathbf{k})$ at all vertices in a Feynman diagram. In that way the external legs of a diagram no longer depend upon any internal variables and may then be factored out from the nasty integral expression. Hence it is convenient to express the interacting single-particle Green's function, here depicted as a double line, in terms of the self-energy $\Sigma(k)$ as



$$= \text{single line } k + \text{single line } k \circlearrowleft \Sigma(k) \text{ single line } k, \quad (2.62)$$

where

$$\Sigma(k) = \text{diagram 1} + \text{diagram 2} + \text{diagram 3} + \dots$$

Diagram 1: A horizontal line with four vertices. The first two vertices are connected by a dashed arc labeled q above and $k-q$ below. The next two vertices are connected by a dashed arc labeled q above and $k-q$ below. The first and third vertices are connected by a dashed arc labeled q above and $k-q-s$ below. The second and fourth vertices are connected by a dashed arc labeled s above and $k-s$ below.

Diagram 2: A horizontal line with four vertices. The first two vertices are connected by a dashed arc labeled q above and $k-q$ below. The next two vertices are connected by a dashed arc labeled s above and $k-s$ below. The first and third vertices are connected by a dashed arc labeled q above and $k-q-s$ below. The second and fourth vertices are connected by a dashed arc labeled s above and $k-s$ below.

Diagram 3: A horizontal line with four vertices. The first two vertices are connected by a dashed arc labeled q above and $k-q$ below. The next two vertices are connected by a dashed arc labeled s above and $k-s$ below. The first and third vertices are connected by a dashed arc labeled q above and $k-q-s$ below. The second and fourth vertices are connected by a dashed arc labeled s above and $k-s$ below.

(2.63)

A related quantity is the proper self-energy $\Sigma^*(k)$, which is made up by a subset of the self-energy diagrams. These diagrams are said to be irreducible, meaning that they cannot be split in two by cutting only one propagator. Examples of such diagrams are the first, third and fourth diagram in (2.63). The second diagram in the same expression can be split in half by cutting the electronic propagator with four-momenta k and is then said to be a reducible diagram. With this definition of the proper self-energy, the self-energy is nothing but

$$\Sigma(k) = \Sigma^*(k) + \begin{array}{c} \Sigma^*(k) \\ \uparrow k \\ \Sigma^*(k) \end{array} + \begin{array}{c} \Sigma^*(k) \\ \uparrow k \\ \Sigma^*(k) \\ \uparrow k \\ \Sigma^*(k) \end{array} + \begin{array}{c} \Sigma^*(k) \\ \uparrow k \\ \Sigma^*(k) \\ \uparrow k \\ \Sigma^*(k) \\ \uparrow k \\ \Sigma^*(k) \end{array} + \dots \quad (2.64)$$

By inserting (2.64) into (2.62), factoring out $\mathcal{G}^{(0)}(k)\Sigma^*(k)$ from every diagram but the bare propagator and identifying what is left with $\mathcal{G}(k)$, one obtains a self-consistent expression for $\mathcal{G}(k)$ known as Dyson's equation,

$$\text{double line } k = \text{single line } k + \text{double line } k \rightarrow \Sigma^*(k) \rightarrow \text{single line } k \quad (2.65)$$

Hence the equation for $\mathcal{G}(k)$ in terms of $\mathcal{G}^{(0)}(k)$ and $\Sigma^*(k)$ becomes

$$\mathcal{G}(k) = \frac{1}{1/\mathcal{G}^{(0)}(k) - \Sigma^*(k)}. \quad (2.66)$$

2.5 Monte Carlo Methods

The Monte Carlo method [10, 11] studies models of systems by stochastic computer simulations. Such a simulation rely on repeated sampling of (pseudo-)random numbers in order to obtain results for models which in principle might be either deterministic or stochastic. In physics-related problems this method is often used in order to sample a sequence of states of a physical system whose probability is given in accordance to a model Hamiltonian. Expectation values of interest may then be approximated by appropriately constructed sample means.

Usually the state space of the system at hand is too large to fully cover during a Monte Carlo simulation which will lead to statistical noise in calculated system properties. A lot of this noise may be suppressed by sampling states which represent the system well. This is known as importance sampling.

2.5.1 Markov processes, detailed balance and ergodicity

In order to sample states of the system a Markov process is used. Given an initial state x such a process will generate a new state x' on random, i.e. if the Markov process repeatedly was given the state x the new state x' would not be the same every time. The probability $P(x|x')$ of generating a state x' given x is referred to as a transition probability. In order to be a Markov process there are two criteria which the transition probabilities must fulfill; they are not allowed to change with time and they may only depend on the properties of the current states x and x' . During the course of a Monte Carlo simulation the Markov process is repeatedly fed the system state in order to generate a sequence of states. When the simulation have run for a long enough time, the frequency for which a particular state is generated will be given by a distribution corresponding to the design of the transition probabilities. When this has happened one say that the process has reached an equilibrium and the distribution has become stationary. However, in order for the succession of generated states to match the pursued probability distribution when equilibrium has been reached, it is necessary that the conditions of ergodicity and detailed balance are satisfied.

Starting with the condition of ergodicity, this is the requirement that the Markov process should be able to reach any state of the system starting from any other state in a finite simulation time. This is equal to saying that there must be at least one path of non-zero transition probabilities between any two states. This is illustrated in figure 2.5. If the process would not be ergodic, some states would never be sampled, no matter how long the simulation was running. The equilibrium distribution of the Markov process would then be such that some states would have a zero probability mass, which in general would not agree with the true distribution of the simulated physical system.

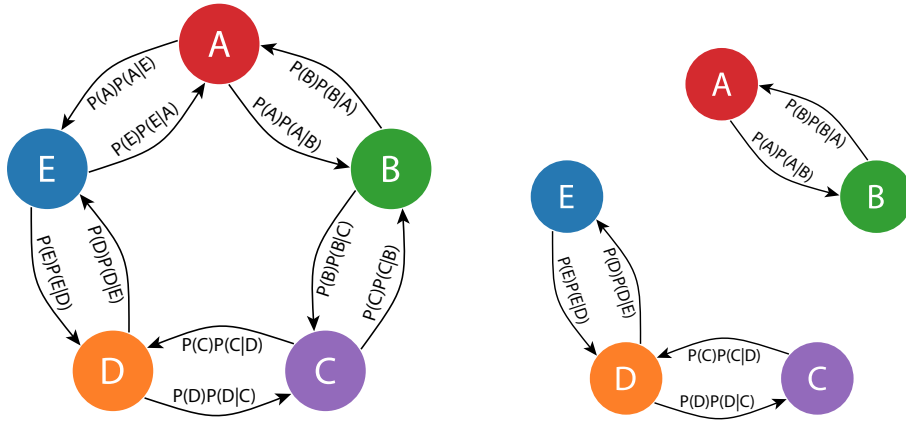


Figure 2.5: Illustrated is a state space consisting of the five possible states A, B, C, D and E, for which two Markov processes are constructed. For these processes all transitions which have a non-zero probability are depicted with an arrow. It is then clear that the Markov process to the left satisfy ergodicity whilst the one to the right does not.

Detailed balance is the requirement that the net flow of probability between any two states is exactly zero, i.e.

$$P(x) P(x|x') = P(x') P(x'|x) \quad (2.67)$$

where $P(x)$ is the probability of the system being in state x . Imposing such a condition on the transition probabilities it can be shown [11] that the Markov process must approach a simple equilibrium for which the stationary distribution is $\pi(x)$. Hence dynamics such a limit cycles are forbidden by this condition.

2.5.2 Metropolis-Hastings algorithm

The Metropolis-Hastings algorithm is a Markov chain Monte Carlo method for obtaining a sequence of random samples from a probability distribution for which direct sampling would be difficult. Briefly speaking, this algorithm is able to draw samples from any distribution $P(x)$ given that it is possible to compute the value of a function $f(x)$ which is proportional to the probability density function $\rho(x)$ of the distribution $P(x)$. The Metropolis-Hastings algorithm suggests constructing transition probabilities $P(x|x')$ in order to design a Markov process for which the stationary distribution $\pi(x)$ is chosen to be $P(x)$.

The starting point to derive the Metropolis-Hastings algorithm is to separate the transitional probabilities into two parts; the proposal $W(x|x')$ and acceptance-rejection $A(x|x')$. Here $W(x|x')$ is the conditional probability distribution of proposing state x' given state x and similarly $A(x|x')$ is the conditional probability distribution of accepting the proposed state x' given x . Expressing the transitional probability as a product of these two parts, i.e. $P(x|x') = W(x|x') A(x|x')$, the criteria of detailed balance (2.67) might be rewritten as

$$\frac{A(x|x')}{A(x'|x)} = \frac{P(x)}{P(x')} \frac{W(x'|x)}{W(x|x')} . \quad (2.68)$$

In order to fulfill the condition above, it is common to use the Metropolis choice for the acceptance,

$$A(x|x') = \min \left(1, \frac{P(x)}{P(x')} \frac{W(x'|x)}{W(x|x')} \right) = \min \left(1, \frac{f(x)}{f(x')} \frac{W(x'|x)}{W(x|x')} \right) , \quad (2.69)$$

where the proportionality between the density of P and f has been used in order to reach the last equality. The new state x' is then accepted according to $A(x|x')$. In practice this is achieved by sampling a uniform random number $a \in [0, 1]$ and accepting the proposed transition if $A(x|x') > a$, otherwise the transition is rejected. In case of the proposed state x' being rejected, the current state x is to be thought of as having been sampled yet again.

In order for the Markov process to cover as much of state space as possible, it is important to construct the proposal distributions in such a way that the acceptance ratios become as large as possible. If this is not the case the process will spend an unnecessary amount of time being rejected leaving the current state.

Chapter 3

Diagrammatic Monte Carlo

Here we shall summarize what this chapter is about

3.1 General idea

- Rename ξ_n .

Diagrammatic Monte Carlo (from here on abbreviated DMC) is a numerical method developed by Prokof'ev et al. [7] which allows to simulate quantities $Q(\{y\})$ in terms of convergent diagrammatic sums, i.e. sums of integrals with an ever increasing number of integration variables

$$Q(\{y\}) = \sum_{n=0}^{\infty} \sum_{\xi_n} \int dx_1 \dots dx_n D_n(\xi_n, \{y\}, x_1, \dots, x_n). \quad (3.1)$$

Here $\{y\}$ is a set of external variables and ξ_n indexes the different integrands of order n which are given by the function D_n . Terms corresponding to $n = 0$ are understood as being known functions of the external variables. In case of a discrete internal variable x_i , the corresponding integral is exchanged in favor of a sum.

The method is based on the Metropolis-Hastings algorithm and samples integrands from the integral sum in the $(\xi_n, \{y\}, x_1, \dots, x_n)$ parameter space. That is, a random walk is preformed between the different integrands in the integral sum, as well as between the possible values of the integration variables. In this random walk it is also permissible to include one or more of the external variables. Since the terms at $n = 0$ are known functions it is then possible to calculate the value of Q by keeping track of the frequency by which these terms are sampled, as well as the length of the sequence of sampled terms.

To clarify any ambiguities, the main idea behind the DMC method will next be demonstrated by a few simple examples.

3.1.1 Example 1

In this example the task is to compute $1 + C$, where for convenience it is assumed that $C > 1$ is a constant. The integral sum (3.1) will then contain merely two constant zeroth order terms, making the parameter space discrete with the two possibilities $\xi_0 = 0$ and $\xi_0 = 1$ corresponding to the terms 1 and C respectively.

To follow the recipe of the Metropolis-Hastings algorithm, the function D_n is regarded as proportional to the probability density function

$$\rho(x) = \frac{D_n(x)}{\sum_y D_n(y)} = \frac{D_n(x)}{1 + C} ; \quad x \in \{\xi_0 = 0, \xi_0 = 1\}, \quad (3.2)$$

allowing it to be substituted against f in (2.69) so that a sequence of ξ_0 's may be sampled from the corresponding probability distribution P . Since there are only the two states 1 and C in parameter space, there can be at most four types of transitions amongst them. By introducing the corresponding transition probabilities: $P(1|C)$, $P(C|1)$, $P(1|1)$ and $P(C|C)$, the Markov process to be simulated may then be illustrated as in figure (3.1).

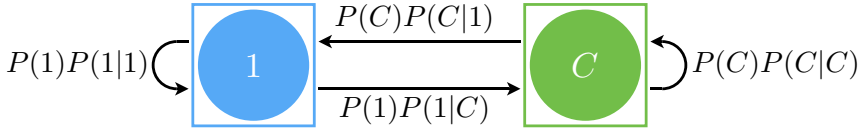


Figure 3.1: Caption this plz!

To simplify matters, the proposal distributions $W(1|C)$, $W(1|1)$, $W(C|1)$ and $W(C|C)$ are all chosen to have the same probability of $1/2$. Then, according to (2.69), the acceptance-rejection ratios will be given by $A(1|1) = A(1|C) = A(C|C) = 1$ and $A(C|1) = 1/C$. By keeping track of how many times $\xi_0 = 0$ appears in the generated sequence, lets say N_0 times, as well as the the total length N of the sequence, it is possible to calculate $1 + C$. This since

$$N_0 \propto \rho(1) \propto 1, \quad N - N_0 \propto \rho(C) \propto C \quad \Rightarrow \quad \frac{N_0}{N - N_0} = \frac{1}{C} \quad (3.3)$$

so that

$$1 + C = 1 + \frac{N - N_0}{N_0}. \quad (3.4)$$

3.1.2 Example 2

In this second example the task is to compute the sum $1 + \int_a^b x dx$. Instead of having of having two zeroth order terms as in the first example, there is now a zeroth and first order term. This implies that the parameter space is no longer

completely discrete with merely two possible states. Similarly to the first example, the zeroth order term is still represented in parameter space by the state $\xi_0 = 0$. On the other hand, the first order term corresponds to the infinite number of states ($\xi_1 = 0, x \in [a, b]$). This notation of the states in parameter space is a little cumbersome, however, by assuming $b > a > 1$ it is possible to create a one-to-one mapping which maps $\xi_0 = 0$ and ($\xi_1 = 0, x \in [a, b]$) onto $x = 1$ and $x \in [a, b]$ respectively. Again the function D_n is regarded as proportional the probability density function

$$\rho(x) = \frac{D_n(x)}{\sum_y D_n(y)} = \frac{D_n(x)}{1 + \int_a^b x \, dx} ; \quad x \in \{1\} \cup [a, b]. \quad (3.5)$$

in order for the Markov process to generate states according to the probability distribution P corresponding to this choice of ρ . To cover the whole parameter space so that ergodicity is satisfied, it is more than sufficient to consider four types of transitions with corresponding transition probabilities $P(1|1)$, $P(1|x)$, $P(x|1)$ and $P(x|x')$. Here it is understood that $x, x' \in [a, b]$ and thus corresponds to a state of the first order term. This Markov process may be illustrated as figure 3.2.

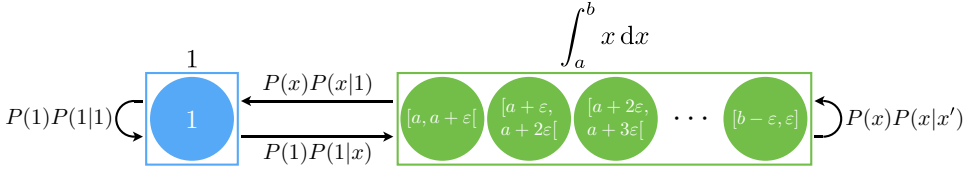


Figure 3.2: Caption this plz!

In order to construct proposal distributions to or from the first order term, it is convenient to introduce the collection of states referred to as f containing all states $x \in [a, b]$. Using this notation, the proposal distributions are chosen to be

$$\begin{aligned} W(1|1) &= \frac{1}{2} & W(1|x) &= W(1|f) U_{a,b}(x) = \frac{1}{2} \frac{1}{b-a} \\ W(x|1) &= W(f|1) = \frac{1}{2} & W(x|x') &= W(f|f) U_{a,b}(x') = \frac{1}{2} \frac{1}{b-a}. \end{aligned} \quad (3.6)$$

The quantities $W(1|1)$, $W(1|f)$, $W(f|1)$ and $W(f|f)$ are simply the probability of proposing a state corresponding to a certain term in the integral series and have been set equally probable. Also $U_{a,b}(x) = [b-a]^{-1}$ is the uniform probability distribution on the interval $[a, b]$ from which x is sampled. Then, from the proposal distributions follow the acceptance ratios

$$\begin{aligned} A(1|1) &= 1 & A(1|x) &= \min\left(1, [b-a]x\right) \\ A(x|1) &= \min\left(1, [b-a]^{-1}x^{-1}\right) & A(x|x') &= \min\left(1, x^{-1}x'\right). \end{aligned} \quad (3.7)$$

If then $x = 1$ appears N_0 number of times in the sequence of states with length N , it follows from (3.3) and (3.4) that

$$1 + \int_a^b x \, dx = 1 + \frac{N - N_0}{N_0} . \quad (3.8)$$

3.1.3 Example 3

In this third and final example, the task is to compute

$$1 + \int_a^b dx e^{-x} + \int_{a'}^{b'} dy \int_{a''}^{b''} dz e^{-y-z} , \quad (3.9)$$

which is more similar to the actual problem. This integral sum consists of a zeroth, first and second order term. By assuming that $b > a > 1$, a one-to-one mapping similar to the one used in the previous example may be preformed here as well. Again the zeroth and first order terms are chosen to be represented by $x = 1$ and $x \in [a, b]$ respectively, whilst the second order term is to be represented by $x = (y, z) \in [a', b'] \times [a'', b'']$.

Analogously to the former examples the function D_n is normalizable and may thus be thought of as a non-normalized probability density function. Hence a Markov process is used to generate a sequence of parameter space states from a probability distribution P corresponding to D_n . This time the Markov process is designed to have the seven types of transitions illustrated in figure 3.3.

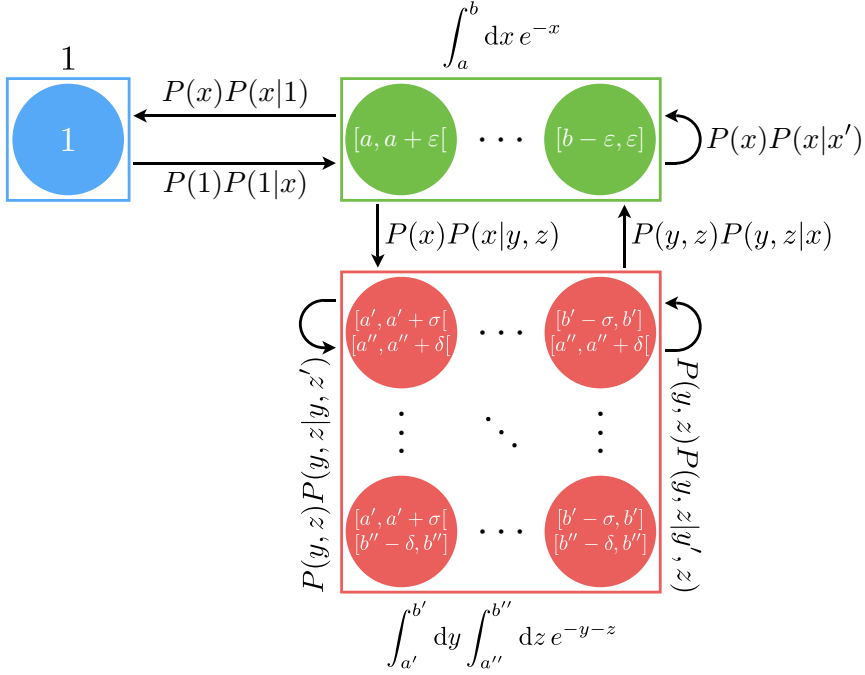


Figure 3.3: Caption this plz!

In order to construct transition probabilities it is convenient to introduce the collection of states f and ff . These contain all states in parameter space corresponding the first and second order term respectively. The transition probabilities are then chosen as

$$\begin{aligned}
 W(1|x) &= W(1|f) U_{a,b}(x) & W(x|y, z) &= W(f|ff) U_{a',b'}(y) U_{a'',b''}(z) \\
 W(x|1) &= W(f|1) & W(y, z|y', z) &= W(ff|ff) W(ff|y') U_{a',b'}(y') \\
 W(y, z|x) &= W(ff|f) U_{a,b}(x) & W(y, z|y, z') &= W(ff|ff) W(ff|z') U_{a'',b''}(z') \\
 W(x|x') &= W(f|f) U_{a,b}(x'), & &
 \end{aligned} \tag{3.10}$$

where

$$\begin{aligned}
 W(1|f) &= 1 \\
 W(f|1) &= W(f|f) = W(f|ff) = \frac{1}{3} \\
 W(ff|f) &= W(ff|ff) = W(ff|y') = W(ff|z') = \frac{1}{2}.
 \end{aligned} \tag{3.11}$$

The discrete proposal distributions $W(ff|y')$ and $W(ff|z')$ correspond to choosing to update either the y or the z part of the total parameter state. Having all of this

information it is then trivial to calculate the acceptance ratios, which become

$$\begin{aligned}
W(1|x) &= \min\left(1, \frac{1}{3}[b-a]e^{-x}\right) \\
W(x|1) &= \min\left(1, 3[b-a]^{-1}e^x\right) \\
W(x|x') &= \min\left(1, e^{x-x'}\right) \\
W(x|y, z) &= \min\left(1, \frac{2}{3}[b'-a'] [b''-a''] [b-a]^{-1} e^{x-y-z}\right) \\
W(y, z|x) &= \min\left(1, \frac{3}{2}[b'-a']^{-1} [b''-a'']^{-1} [b-a] e^{y+z-x}\right) \\
W(y, z|y', z') &= \min\left(1, e^{y-y'}\right) \\
W(y, z|y, z') &= \min\left(1, e^{z-z'}\right).
\end{aligned} \tag{3.12}$$

By defining N_0 and N in accordance to what was done in the previous example, the value of the sum is then approximated by

$$1 + \int_a^b dx e^{-x} + \int_{a'}^{b'} dy \int_{a''}^{b''} dz e^{-y-z} = 1 + \frac{N - N_0}{N_0}. \tag{3.13}$$

3.2 Implementation

——— [continue here](#) ———

The task at hand is now to implement the DMC method in order to calculate the electronic single-particle Green's function $\mathcal{G}(\alpha, \mu, \mathbf{p}, \tau)$. The integral series (3.1) will then be nothing but the diagrammatic series (2.60), with the external parameters $\{y\} = \{\alpha, \mu, \mathbf{p}, \tau\}$. The integration variables x_i 's must therefore correspond to the internal imaginary-times and momenta, where the internal momenta are chosen to be those of the phonon propagators. By then representing the internal momenta in spherical coordinates $\mathbf{q} = (q \sin \theta \cos \varphi, q \sin \theta \sin \varphi, q \cos \theta)$, the momentum integrals should be replaced according to

$$\int \frac{d^3 q}{(2\pi)^3} \rightarrow \int_{q=0}^{\infty} \int_{\theta=0}^{\pi} \int_{\varphi=0}^{2\pi} \frac{q^2 \sin \theta dq d\theta d\varphi}{(2\pi)^3}. \tag{3.14}$$

The beauty of this is realized when recalling that each phonon brings with it a factor $V(q)^2 \propto q^{-2}$, whose momentum dependence exactly cancel with that of the integral. For example, the expression corresponding the first order diagram then becomes

$$- \int_0^\tau d\tau_2 \int_0^{\tau_2} d\tau_1 \int_0^\infty dq \int_0^\pi d\theta \int_0^{2\pi} d\varphi \mathcal{G}_0(\mathbf{p}, \tau_1) \mathcal{G}_0(\mathbf{p}-\mathbf{q}, \tau_2-\tau_1) \tilde{\mathcal{D}}_0(\mathbf{q}, \tau_2-\tau_1) \mathcal{G}_0(\mathbf{p}, \tau-\tau_2), \tag{3.15}$$

where $\tilde{\mathcal{D}}_0(\mathbf{q}, \tau)$ is a phonon propagator which has absorbed the factor $q^2 \sin \theta (2\pi)^{-3}$ originating from the integral, the interaction potential $V(q)^2$ along with the factor -1 from the Feynman rules. Thus

$$\tilde{\mathcal{D}}_0(\mathbf{q}, \tau) = \frac{2\sqrt{2}\pi\alpha}{(2\pi)^3} \sin \theta \exp\{-\tau\} \quad (3.16)$$

which is a quantity always larger than or equal to zero. The integrand of each and every integral in the integral series will be entirely made up out of \mathcal{G}_0 's and $\tilde{\mathcal{D}}_0$'s which implies that every contribution to \mathcal{G} is a positive contribution. This will simplify the DMC implementation since it won't be necessary to calculate what sign each sampled parameter space state comes with.

The external parameters \mathbf{p} and τ will be the only ones allowed to change during the Markov process. Including α and/or μ would cause the parameter space to increase and the statistics to be spread out. Thus more computation time would be needed to calculate quantities to the same level of certainty as having α and μ fixed.

The value of the propagator \mathcal{G} will be computed at the discrete set of points $\mathbf{p}_i = \Delta p(0.5 + i) \hat{\mathbf{e}}_z$ and $\tau_j = \Delta \tau(0.5 + j)$ where $i = 0, 1, 2, \dots, N-1$, $j = 0, 1, 2, \dots, M-1$ and the resolution is chosen in terms of Δp and $\Delta \tau$. To calculate $\mathcal{G}(\mathbf{p}_i, \tau_j) = \mathcal{G}_{i,j}$, both a bin N_0 and a two dimensional histogram N are used, even though \mathbf{p} and τ will be continuous variables. Thus the bin $N_{i,j}$ of the histogram will be covering the range $p \in [p_i - \Delta p/2, p_i + \Delta p/2]$ and $\tau \in [\tau_j - \Delta \tau/2, \tau_j + \Delta \tau/2]$ of the external parameter values. The value of every bin in the histogram along with N_0 are initially put to zero. Then, each time a parameter space state is sampled, it will be checked whether or not this state belongs to the zeroth order term $\mathcal{G}_0(\mathbf{p}, \tau)$. If this is the case, the value of N_0 is increased by 1, if not, the bin in the histogram according to the external parameters is increased by 1. By doing this, the quantities N_0 and $N_{i,j}$ can be shown to be proportional to

$$\begin{aligned} N_0 &\propto \int_0^{N\Delta p} dp \int_0^{M\Delta \tau} d\tau \mathcal{G}_0(\mathbf{p}, \tau) \\ &= \Delta p \Delta \tau \sum_{k,l} \mathcal{G}_0(\mathbf{p}_k, \tau_l) + \mathcal{O}([\Delta p]^3 + [\Delta \tau]^3) \end{aligned} \quad (3.17)$$

and

$$\begin{aligned} N_{i,j} &\propto \int_{p_i-0.5}^{p_i+0.5} dp \int_{\tau_j-0.5}^{\tau_j+0.5} d\tau [\mathcal{G}(\mathbf{p}, \tau) - \mathcal{G}_0(\mathbf{p}, \tau)] \\ &= \Delta p \Delta \tau [\mathcal{G}(\mathbf{p}_i, \tau_j) - \mathcal{G}_0(\mathbf{p}_i, \tau_j)] + \mathcal{O}([\Delta p]^3 + [\Delta \tau]^3) \end{aligned} \quad (3.18)$$

respectively. Omitting the errors due to discretization, the interacting electronic propagator is then found to be

$$\mathcal{G}(\mathbf{p}_i, \tau_j) = \mathcal{G}_0(\mathbf{p}_i, \tau_j) + N_{i,j} \frac{\sum_{k,l} \mathcal{G}_0(\mathbf{p}_k, \tau_l)}{N_0}. \quad (3.19)$$

On the other hand, if the external momentum where to be held fixed at \mathbf{p}_0 , the value of \mathcal{G} at the set of imaginary-times $\{\tau_j\}$ would similarly become

$$\mathcal{G}(\mathbf{p}_0, \tau_j) = \mathcal{G}_0(\mathbf{p}_0, \tau_j) + N_j \frac{\sum_l \mathcal{G}_0(\mathbf{p}_0, \tau_l)}{N_0}. \quad (3.20)$$

Here the histogram N has only one dimension corresponding to the different τ_j .

- introduce τ_{\max} and p_{\max} .
- Quickly mention the code implementation. momenta belongs to lines, time to nodes. Nodes instead of vertices in order to keep things general (when sampling Σ^*)

3.3 Bare scheme update procedures for \mathcal{G}

What remains to be discussed is how the sampling of states in parameter space occurs. As the name Diagrammatic Monte Carlo suggest, the diagrammatic representation of the integral series will be used. That is, the functions D_n in the integral series (3.1) is to be though of as a Feynman diagram (without the integrals). The random walk, which is used to simulate the Markov process, will thus be in terms of such diagrams. It is then important that each and every such diagram must be possible to reach in order to cover all of parameter space and thus maintaining ergodicity. To make sure that this actually is the case, a set of update procedures [7] have been constructed.

Change of diagram length in time, type 1



Figure 3.4: The only affected parameter is the highlighted imaginary-time of the end point node.

This update procedure merely changes the external imaginary-time parameter τ , which is nothing but the diagram length in time. In the first update type this is

achieved by altering the time of the end point node in the diagram, i.e. $\tau \rightarrow \tau'$, as illustrated in figure 3.4. The only affected quantity of such an update will be the value of the very last \mathcal{G}_0 in the diagram so that

$$\frac{D_n(\tau')}{D_n(\tau)} = \frac{\mathcal{G}_0(\mathbf{p}, \tau' - \tau_{2n})}{\mathcal{G}_0(\mathbf{p}, \tau - \tau_{2n})} = \frac{\exp\left\{-\left(\frac{p^2}{2} - \mu\right)\tau'\right\}}{\exp\left\{-\left(\frac{p^2}{2} - \mu\right)\tau\right\}} \quad (3.21)$$

Now consider an exponential distribution on the interval $[\tau_{2n}, \tau_{\max}]$ with rate parameter $\lambda = p^2/2 - \mu$ of which the density is

$$\rho(\tau) = \frac{\lambda e^{-\lambda(\tau - \tau_{2n})}}{1 - e^{-\lambda(\tau_{\max} - \tau_{2n})}}. \quad (3.22)$$

By sampling τ' from such a distribution, the ratio $W(\tau'|\tau)/W(\tau|\tau')$ will be the inverse of D'_n/D_n . Hence the acceptance ratio $A(\tau|\tau')$ of this update procedure becomes 1, and any proposed τ' is always accepted.

Change of diagram length in time, type 2

- Mention something about the probability of choosing a node on random will cancel is chosen uniformly. Tell the reader that this is also the case for all other updates procedures as long as nothing else is said.



Figure 3.5: The highlighted τ 's are the parameters affected by this update.

This update procedure also changes the external imaginary-time parameter, although it does so in a slightly different by letting any \mathcal{G}_0 in the diagram be lengthen or shortened in time, not just the last one. This is achieved by randomly picking any but the leading node in the diagram to assign a new imaginary-time τ'_k from the interval $[\tau_{k-1}, \tau_{\max} - (\tau - \tau_k)]$. In order to only modify the length of the electronic propagator just in front of the chosen node, every node proceeding this node must clearly have the difference $\tau'_k - \tau_k$ added to its time. This is illustrated in figure 3.5.

This update does not merely affect the one \mathcal{G}_0 , but phonon propagators with start and end points on different sides of the chosen node would also have their

length modified by the difference $\tau'_k - \tau_k$. If there are m such phonons, the quota of the diagram values become

$$\begin{aligned} \frac{D_n(\tau')}{D_n(\tau)} &= \frac{\mathcal{G}_0(\mathbf{p}, \tau_k - \tau_{k-1}) \prod_{i=0}^{m-1} \tilde{\mathcal{D}}_0(\mathbf{q}_i, \Delta\tau_i)}{\mathcal{G}_0(\mathbf{p}, \tau'_k - \tau_{k-1}) \prod_{j=0}^{m-1} \tilde{\mathcal{D}}_0(\mathbf{q}_j, \Delta\tau_j + [\tau'_k - \tau_k])} \\ &= \frac{\exp \left\{ - \left(\frac{p^2}{2} - \mu + m \right) \tau'_k \right\}}{\exp \left\{ - \left(\frac{p^2}{2} - \mu + m \right) \tau_k \right\}}, \end{aligned} \quad (3.23)$$

where $\Delta\tau_i$ is the length in time of the i th phonon propagator. By sampling the τ'_k from an exponential distribution with rate parameter $\lambda = p^2/2 - \mu + m$, the acceptance ration for this update procedure also becomes unity.

This second version of the change of diagram length update procedure is more complex than the first one, and may therefore be chosen less often. In a worst case scenario the complexity scales as $\mathcal{O}(2n)$, due to figuring out the number of phonons m just discussed. Only one of the procedures changing the length of the diagram would be sufficient, but having an over complete set of update procedures is necessarily not something negative and could potentially enhance the statistics.

Change of external momentum



Figure 3.6: This update procedure changes the momentum of every \mathcal{G}_0 in the diagram by the external momentum difference $\mathbf{p}' - \mathbf{p}$. Surely it must be the case that $\mathbf{p}_0 = \mathbf{p}_{2n} = \mathbf{p}$ and the same is of course true in primed case as well.

Since there is no preferred direction of the Hamiltonian (2.50), the Green's function \mathcal{G} becomes dependent merely upon the magnitude of the external momentum \mathbf{p} . [\(this is supposed to have been discussed at an earlier point!\)](#) This update procedure is thus constructed to keep the direction constant while changing only the magnitude $p \rightarrow p'$. In order to satisfy momentum conservation at each vertex, the \mathcal{G}_0 's are chosen to absorb the external momentum difference $\mathbf{p}' - \mathbf{p}$ leaving the value of

the $\tilde{\mathcal{D}}_0$'s the same. This is illustrated in figure 3.6. The ratio of the diagram value after to before such an update then becomes

$$\begin{aligned} \frac{D_n(\mathbf{p}')}{D'_n(\mathbf{p})} &= \frac{\prod_{i=0}^{2n} \mathcal{G}_0(\mathbf{p}'_i, \tau_{i+1} - \tau_i)}{\prod_{j=0}^{2n} \mathcal{G}_0(\mathbf{p}_j, \tau_{j+1} - \tau_j)} \\ &= \exp \left\{ -\frac{1}{2} \sum_{i=0}^{2n} \left([\mathbf{p}_i + (\mathbf{p}' - \mathbf{p})]^2 - p_i^2 \right) (\tau_{i+1} - \tau_i) \right\} \\ &= \exp \left\{ -\frac{\tau}{2} \left([p' - p]^2 + 2\langle \mathbf{p} \rangle_{0,2n} \cdot [\mathbf{p}' - \mathbf{p}] \right) \right\} \end{aligned} \quad (3.24)$$

where the mean electronic momentum is defined as

$$\langle \mathbf{p} \rangle_{k,l} \equiv \sum_{i=k}^l \frac{\tau_{i+1} - \tau_i}{\tau} \mathbf{p}_i. \quad (3.25)$$

- [Introduce \$p_{\min}\$ earlier in the thesis](#)

By sampling $p' \in [p_{\min}, p_{\max}]$ using a truncated half-normal distribution whose corresponding normal distribution would have the standard deviation $\sigma = 1/\sqrt{\tau}$, the fraction of the proposal distributions take the value

$$\frac{W(\mathbf{p}'|\mathbf{p})}{W(\mathbf{p}|\mathbf{p}')} = \exp \left\{ -\frac{\tau}{2} (p^2 - p'^2) \right\} \quad (3.26)$$

so that the acceptance ratio is found to be

$$\begin{aligned} A(p|p') &= \min \left(1, \exp \left\{ -(\mathbf{p}' - \mathbf{p}) \cdot (\langle \mathbf{p} \rangle_{0,2n} - \mathbf{p}) \tau \right\} \right) \\ &= \min \left(1, \exp \left\{ -(p' - p) (\langle p_z \rangle_{0,2n} - p) \tau \right\} \right). \end{aligned} \quad (3.27)$$

In the final equality the vectors has ben represented in a Cartesian coordinate system with the z -axis parallel to the external momentum. On average $\langle p_z \rangle_{0,2n}$ should not differ to much from p , implying that both the exponential and the acceptance ration should be close to unity most of the time. This of course being the reason why the update procedure is constructed the way it is.

Perhaps $\langle p_z \rangle_{0,2n} = p$ on average?

Change of transferred momentum magnitude

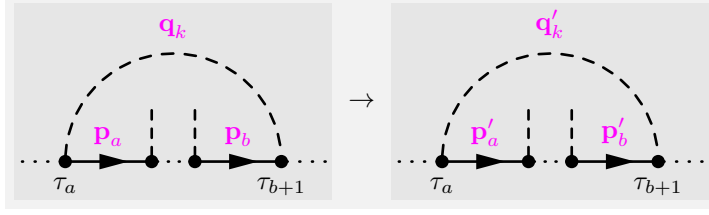


Figure 3.7: The momentum transferred via an internal phonon propagator is updated. In order obey momentum conservation at every vertex, electronic propagators beneath the phonon arc absorb the momentum difference.

This update procedure is designed to be very similar to that of the external momentum. However, the main difference of course being that the magnitude of momentum transferred via a phonon propagator is updated rather than the external momentum. In order to achieve this, a \tilde{D}_0 is randomly picked and has a new momentum magnitude assigned to it $q_k \rightarrow q'_k$ while keeping the direction fixed. In order to conserve momentum at the two vertices connected to the phonon propagator, the \mathcal{G}_0 's located beneath the phonon arc should absorb the momentum difference $\mathbf{q}_k - \mathbf{q}'_k$. This is illustrated in figure 3.7. Since the $\tilde{D}(\mathbf{q}, \tau)$'s does not depend on the magnitude $q = |\mathbf{q}|$, the ratio of diagram values become

$$\begin{aligned}
 \frac{D_n(\mathbf{q}'_k)}{D_n(\mathbf{q}_k)} &= \frac{\prod_{i=a}^b \mathcal{G}_0(\mathbf{p}'_i, \tau_{i+1} - \tau_i)}{\prod_{j=a}^b \mathcal{G}_0(\mathbf{p}_j, \tau_{j+1} - \tau_j)} \\
 &= \exp \left\{ -\frac{1}{2} \sum_{i=a}^b \left([\mathbf{p}_i + (\mathbf{q}_k - \mathbf{q}'_k)]^2 - p_i^2 \right) (\tau_{i+1} - \tau_i) \right\} \\
 &= \exp \left\{ -\frac{\tau_{b+1} - \tau_a}{2} ([q_k - q'_k]^2 + 2\langle \mathbf{p} \rangle_{a,b} \cdot [\mathbf{q}_k - \mathbf{q}'_k]) \right\},
 \end{aligned} \tag{3.28}$$

which indeed is similar to (3.24). Following in the footsteps of the previous update procedure, $q'_k \in [0, \infty[$ is sampled from a half-normal distribution whose corresponding normal distribution would have the standard deviation $\sigma = 1/\sqrt{\tau_{b+1} - \tau_a}$. The acceptance ration is then found to be,

$$A(\mathbf{q}_k | \mathbf{q}'_k) = \min \left(1, \exp \left\{ -(\mathbf{q}_k - \mathbf{q}'_k) \cdot (\langle \mathbf{p} \rangle_{a,b} + \mathbf{q}_k) [\tau_{b+1} - \tau_a] \right\} \right). \tag{3.29}$$

It is reasonable to assume that on average, $\langle \mathbf{p} \rangle_{a,b} + \mathbf{q}_k$ does not differ too much from the external momentum \mathbf{p} . Hence this update procedure should have an acceptance

ration close to unity at low external momenta whilst performing worse at higher external momenta.

Change of transferred momentum direction

This update procedure changes the direction $(\theta_k, \varphi_k) \rightarrow (\theta'_k, \varphi'_k)$ of the momentum transferred via a phonon propagator. As in the previous update procedure, the electronic propagators below the phonon arc absorb the momentum difference $\mathbf{q}_k - \mathbf{q}'_k$ which is illustrated in figure 3.7. This time, since $\tilde{\mathcal{D}} \propto \sin \theta$ the ratio of the diagram values becomes slightly different

$$\begin{aligned} \frac{D_n(\mathbf{q}'_k)}{D_n(\mathbf{q}_k)} &= \frac{\sin \theta'_k \prod_{i=a}^b \mathcal{G}_0(\mathbf{p}'_i, \tau_{i+1} - \tau_i)}{\sin \theta_k \prod_{j=a}^b \mathcal{G}_0(\mathbf{p}_j, \tau_{j+1} - \tau_j)} \\ &= \frac{\sin \theta'_k}{\sin \theta_k} \exp \left\{ -\frac{\tau_{b+1} - \tau_a}{2} ([\mathbf{q}_k - \mathbf{q}'_k]^2 + 2\langle \mathbf{p} \rangle_{a,b} \cdot [\mathbf{q}_k - \mathbf{q}'_k]) \right\}. \end{aligned} \quad (3.30)$$

By sampling the azimuthal angle uniformly on the interval $\varphi'_k \in [0, 2\pi]$, and the polar angle $\theta'_k \in [0, \pi]$ from a probability distribution whose density $\rho(\theta'_k) = \frac{1}{2} \sin \theta'_k$, one obtains the acceptance ratio

$$A(\mathbf{q}_k | \mathbf{q}'_k) = \min \left(1, \exp \left\{ -\frac{\tau_{b+1} - \tau_a}{2} ([\mathbf{q}_k - \mathbf{q}'_k]^2 + 2\langle \mathbf{p} \rangle_{a,b} \cdot [\mathbf{q}_k - \mathbf{q}'_k]) \right\} \right). \quad (3.31)$$

Vertex shift in time



Figure 3.8: The imaginary-time of internal node k is updated.

This update procedure changes the imaginary-time $\tau_k \rightarrow \tau'_k$ of a randomly chosen internal node whilst keeping the chronological ordering, i.e. $\tau_{k-1} < \tau'_k < \tau_{k+1}$. The procedure is illustrated in figure 3.8, and as can be seen, it does only affect the three propagators connected to the node so that

$$\begin{aligned} \frac{D_n(\tau'_k)}{D_n(\tau_k)} &= \frac{\mathcal{G}_0(\mathbf{p}_{k-1}, \tau'_k - \tau_{k-1}) \mathcal{G}_0(\mathbf{p}_k, \tau_{k+1} - \tau'_k) \tilde{\mathcal{D}}_0(\mathbf{q}_k, \pm(\tau_l - \tau'_k))}{\mathcal{G}_0(\mathbf{p}_{k-1}, \tau_k - \tau_{k-1}) \mathcal{G}_0(\mathbf{p}_k, \tau_{k+1} - \tau_k) \tilde{\mathcal{D}}_0(\mathbf{q}_k, \pm(\tau_l - \tau_k))} \\ &= \exp \left\{ -\left[\frac{p_{k-1}^2}{2} - \frac{p_k^2}{2} \mp 1 \right] (\tau' - \tau) \right\}. \end{aligned} \quad (3.32)$$

Here the upper sign is used if $\tau_l > \tau_k$, meaning that the phonon propagator is leaving to node l from node k . If instead $\tau_l < \tau_k$, the lower sign should be used and the situation becomes the opposite. By sampling τ'_k from the interval $[\tau_{k-1}, \tau_{k+1}]$ using an exponential distribution with rate parameter $\lambda = p_{k-1}^2/2 - p_k^2/2 \mp 1$, the acceptance ration becomes unity.

Change of diagram structure

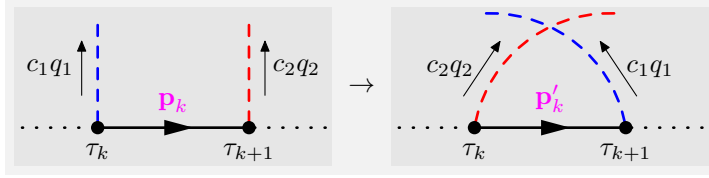


Figure 3.9: The diagram structure is modified by interchanging the phonon propagators connected to two neighboring nodes. **Blue face:** \mathbf{q}_1 and \mathbf{q}_2

This update procedure, as illustrated in figure 3.9, interchange the two phonon propagators connected to a pair of randomly selected neighboring nodes. In order to conserve momentum, the \mathcal{G}_0 connected to both of the selected nodes must absorb the difference $\mathbf{p}'_k - \mathbf{p}_k = c_1 \mathbf{q}_1 - c_2 \mathbf{q}_2$. Here the c_i tells whether the propagator is propagating towards any of the two nodes ($c_i = -1$) or if it is propagating away from any of the two nodes ($c_i = 1$). The ratio of the diagram value prior to and after the update then becomes

$$\begin{aligned} \frac{D_n(\xi'_n)}{D_n(\xi_n)} &= \frac{\mathcal{D}_0(\mathbf{q}_1, c_1[\tau_i - \tau_{k+1}]) \mathcal{D}_0(\mathbf{q}_2, c_2[\tau_j - \tau_k]) \mathcal{G}_0(\mathbf{p}'_k, \tau_{k+1} - \tau_k)}{\mathcal{D}_0(\mathbf{q}_1, c_1[\tau_i - \tau_k]) \mathcal{D}_0(\mathbf{q}_2, c_2[\tau_j - \tau_{k+1}]) \mathcal{G}_0(\mathbf{p}_k, \tau_{k+1} - \tau_k)} \\ &= \exp \left\{ - \left[\frac{(\mathbf{p}_k + c_1 \mathbf{q}_1 - c_2 \mathbf{q}_2)^2}{2} - \frac{p_k^2}{2} - c_1 + c_2 \right] (\tau_{k+1} - \tau_k) \right\}. \end{aligned} \quad (3.33)$$

Other than the pair of nodes to be picked, there are no parameters to be sampled in order to change the diagram structure in this way. Thus $W(\xi_n | \xi'_n) = W(\xi'_n | \xi_n)$ and the update procedure should be accepted according to

$$A(\xi_n | \xi'_n) = \min \left(1, \frac{D_n(\xi'_n)}{D_n(\xi_n)} \right). \quad (3.34)$$

Change of diagram order

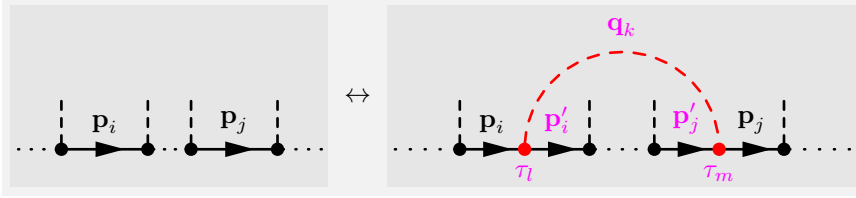


Figure 3.10: An illustration of the change of diagram order procedure.

This final update procedure which is illustrated in figure 3.10, is the only one which changes the order of the diagram at hand. To increase the diagram order, an electronic propagator $\mathcal{G}_{0,i}$ is selected on random and then split at a time τ_l , which is sampled uniformly on the interval $[\tau_i, \tau_{i+1}]$. After this, another imaginary time τ_m is sampled on the interval $\tau_m \in [\tau_l, \tau]$ using an exponential distribution with a rate parameter $\lambda = 1$. The $\mathcal{G}_{0,j}$ which happen to occupy the imaginary-time τ_m is split in twice at that point as well. For each of the two times τ_l and τ_m , a node is inserted so that the loose ends of the \mathcal{G}_0 's have something to connect to. The two newly introduced nodes are then further connected to a new phonon propagator $\tilde{\mathcal{D}}_0$, for which the momentum \mathbf{q}_k is sampled according to the *change of transferred momentum* procedures introduced earlier. In order to obey momentum conservation at each node, the \mathcal{G}_0 's under the newly added phonon arc have their momentum subtracted by \mathbf{q}_k . In this way, the probability distribution of increasing the diagram order becomes

$$\begin{aligned}
 W(n|n+1) &= P_R(n) \frac{1}{2n+1} \frac{1}{\tau_{i+1} - \tau_i} \frac{e^{-(\tau_m - \tau_l)}}{1 - e^{-(\tau - \tau_l)}} \frac{\sin \theta_k}{2} \frac{1}{2\pi} \\
 &\times \sqrt{\frac{2(\tau_m - \tau_l)}{\pi}} \exp \left\{ -\frac{q_k^2}{2} (\tau_m - \tau_l) \right\}.
 \end{aligned} \tag{3.35}$$

Here $P_R(n)$ is the probability of choosing to raise the diagram order once having selected the *change of diagram order* procedure. Of course the corresponding probability of choosing to lower the diagram order is then nothing but $1 - P_R(n)$. Further

more, the ratio of the diagram value prior to and after the update is realized to be

$$\begin{aligned} \frac{D_{n+1}}{D_n} &= \tilde{D}_0(\mathbf{q}_k, \tau_m - \tau_l) \frac{\prod_{i=l}^{m-1} \mathcal{G}_0(\mathbf{p}_i - \mathbf{q}_k, \tau_{i+1} - \tau_i)}{\prod_{i=l}^{m-1} \mathcal{G}_0(\mathbf{p}_i, \tau_{i+1} - \tau_i)} \\ &= \frac{2\sqrt{2}\pi\alpha}{(2\pi)^3} \sin \theta_k \exp \left\{ - \left[\frac{q_k^2}{2} + 1 - \langle \mathbf{p} \rangle_{l,m-1} \cdot \mathbf{q}_k \right] (\tau_m - \tau_l) \right\}. \end{aligned} \quad (3.36)$$

The procedure of lowering the diagram order is much more simplistic; it is only necessary to randomly pick a \tilde{D} which is to be removed. Hence $W(n+1|n) = (1 - P_R(n+1)) [n+1]^{-1}$, and by introducing the quantity

$$\begin{aligned} R(n|n+1) &= \frac{D_{n+1}}{D_n} \frac{W(n+1|n)}{W(n|n+1)} \\ &= \frac{1 - P_R(n+1)}{P_R(n)} \frac{\alpha}{\sqrt{\pi}} \frac{2n+1}{n+1} \frac{\tau_{i+1} - \tau_i}{\sqrt{\tau_m - \tau_l}} \\ &\quad \times \left[1 - e^{-(\tau - \tau_l)} \right] \exp \left\{ [\langle \mathbf{p} \rangle_{l,m-1} \cdot \mathbf{q}_k] (\tau_m - \tau_l) \right\} \end{aligned} \quad (3.37)$$

the acceptance ratios may be expressed as

$$A(n|n+1) = \min(1, R(n|n+1)) \quad , \quad A(n+1|n) = \min(1, 1/R(n|n+1)) \quad . \quad (3.38)$$

By requiring that

$$\frac{1 - P_R(n+1)}{P_R(n)} = \frac{\sqrt{\pi}}{2\alpha} \quad \Rightarrow \quad P_R(n) = P_R = \left[1 + \frac{\sqrt{\pi}}{2\alpha} \right]^{-1} \quad (3.39)$$

these acceptance ratios become independent of the coupling constant α and less dependent of the diagram order n

Clearly it should not be possible to lower the diagram order any further than $n = 0$. Also, one could think of implementing a maximum order n_{\max} for which the diagram order should not be able to rise above. To achieve this, it is extremely important not to set $P_R = 1$ and $P_R = 0$ at $n = 0$ and $n = n_{\max}$ respectively, since this would ruin the detailed balance. Rather one should approach this by simply refusing such an update. For example, if the procedure to increase the diagram order happen to be chosen when $n = n_{\max}$, it should be refused and a new update procedure chosen instead.

- [Check the acceptance ratio!](#)

3.3.1 Results

- [Result should be independent on weight of each update function](#)

Here follow some results obtained when simulating \mathcal{G} using the bare scheme update procedures described above. The external momentum \mathbf{p} has been fixed during these simulations in order to not spread the statistics out over external parameters for which the data is not shown.

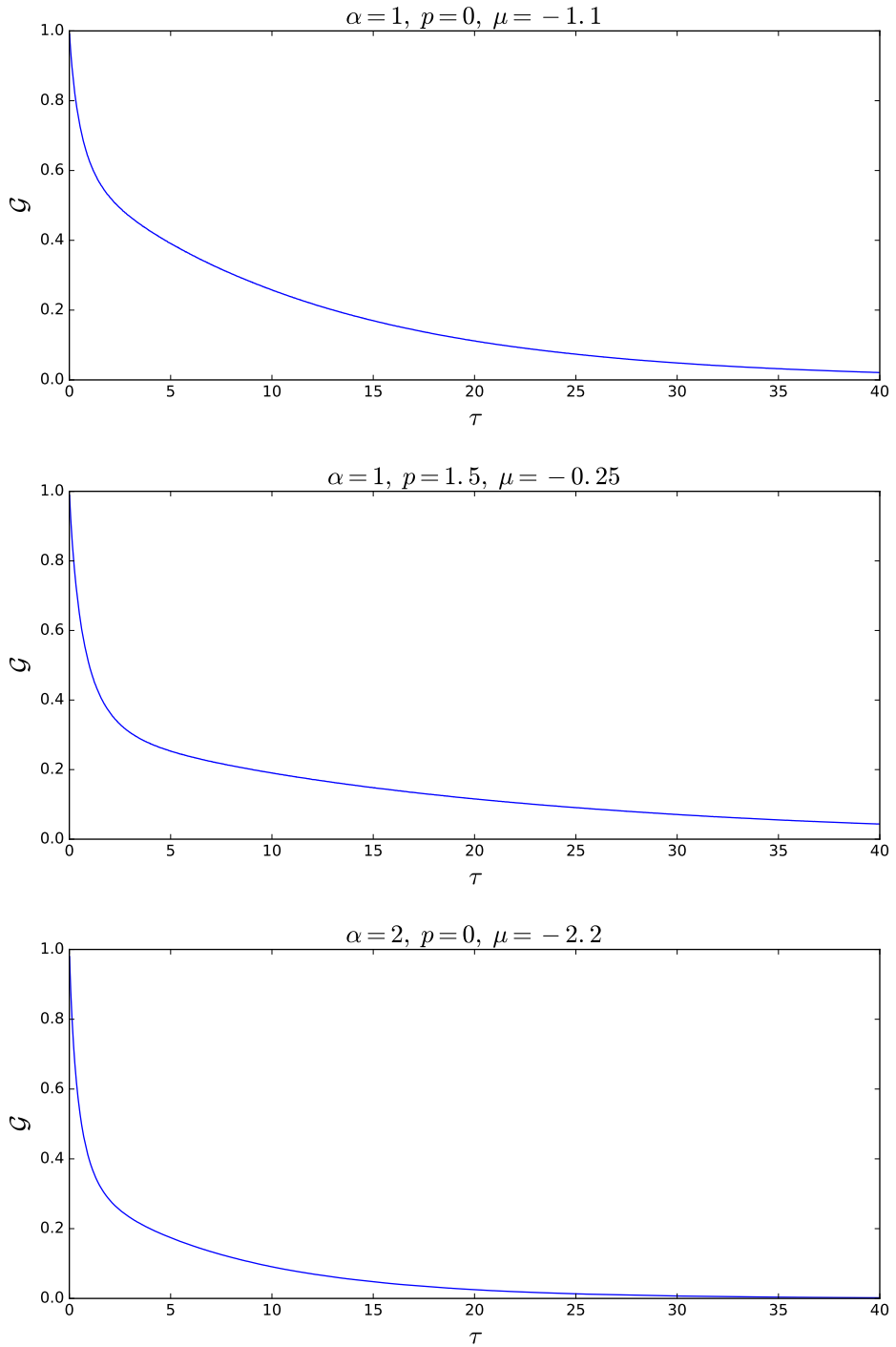


Figure 3.11: The acquired value of $\mathcal{G}(p = 0, \tau)$ after 80 minutes of core time. Here $\tau_{max} = 40$ and $\Delta\tau = 0.02$ has been used.

τ	$\mathcal{G}(0, 1, -1.1)$	$\mathcal{G}(1.5, 1, -0.25)$	$\mathcal{G}(0, 2, -2.2)$
0.01	0.9906	0.9881	0.9797
1.01	0.6242	0.4938	0.3922
2.01	0.5225	0.3631	0.2808
3.01	0.4673	0.3066	0.2314
4.01	0.4259	0.2745	0.1993
5.01	0.3907	0.2528	0.1738
6.01	0.359	0.2365	0.1524
7.01	0.3301	0.223	0.1339
8.01	0.3041	0.2113	0.1176
9.01	0.2797	0.2003	0.1031
10.01	0.2573	0.1902	0.09057
11.01	0.2374	0.1806	0.07967
12.01	0.2175	0.1715	0.07009
13.01	0.2003	0.1635	0.0617
14.01	0.1844	0.1552	0.05428
15.01	0.1695	0.1476	0.04763
16.01	0.156	0.1409	0.04189
17.01	0.1436	0.1341	0.03696
18.01	0.1319	0.1276	0.03243
19.01	0.1213	0.1216	0.02866
20.01	0.1116	0.1157	0.02498
21.01	0.1025	0.1103	0.02211
22.01	0.09434	0.1051	0.01937
23.01	0.08689	0.09985	0.01701
24.01	0.07983	0.09523	0.01492
25.01	0.07363	0.0909	0.01322
26.01	0.06764	0.08651	0.01168
27.01	0.06217	0.0825	0.01027
28.01	0.05718	0.07844	0.009083
29.01	0.05272	0.07471	0.007966
30.01	0.04861	0.07102	0.007016
31.01	0.04458	0.06742	0.006182
32.01	0.04098	0.06404	0.005393
33.01	0.03794	0.06131	0.004762
34.01	0.03482	0.05836	0.00411
35.01	0.0319	0.05525	0.003671
36.01	0.02945	0.05269	0.003204
37.01	0.02723	0.05022	0.002901
38.01	0.02509	0.04788	0.002536
39.01	0.02288	0.04576	0.002207
39.99	0.02102	0.04357	0.001962

Table 3.1: Some values of $\mathcal{G}(p, \alpha, \mu)$ from the plots in figure 3.11.

3.4 Bare scheme update procedures for Σ^*

Rather than calculating $\mathcal{G}(\mathbf{p}, \tau)$ directly using DMC, it is also possible and even so preferred (motivate this from papers. Cover more diagrams and so on...) to instead simulate the proper self energy $\Sigma^*(\mathbf{p}, \tau)$, from which the electronic propagator is calculated using the Dyson equation (2.66). In order to do this, the random walk must now cover diagrams without external legs but also be able to reach the bare propagator \mathcal{G}_0 for normalization purposes. This is easily accomplished by a slight modification of some of the update procedures introduced in the previous section, and will be discussed in more detail shortly.

Before that however, it is important to realize that no longer all types of diagrams ($n > 0$) should be binned. In order to calculate Σ^* it is critical that the histogram merely have contributions from irreducible diagrams. Then, in similarity to (3.19) and (3.20) the value of Σ^* is calculated in terms N_0 and N in the following way

$$\Sigma^*(\mathbf{p}_i, \tau_j) = N_{i,j} \frac{\sum_{k,l} \mathcal{G}_0(\mathbf{p}_k, \tau_l)}{N_0}, \quad \Sigma^*(\mathbf{p}_0, \tau_j) = N_j \frac{\sum_l \mathcal{G}_0(\mathbf{p}_0, \tau_l)}{N_0}. \quad (3.40)$$

An easy way to check whether or not a diagram is irreducible, is to store the current momentum of every \mathcal{G}_0 present in the diagram within a hash table. If one or more momenta are found to be equal to that of the external momentum, the diagram must clearly be reducible and should thus not be binned. Since the complexity of a search in a hash table is $\mathcal{O}(1)$, this implementation should not limit the performance of the algorithm. To recapitulate, all self energy diagrams (together with the bare propagator for normalization purposes) should be sampled, but only proper ones are allowed to increment the bins values $N_{i,j}$ of the histogram.

Now, returning to the update procedures, there are only two which need to be modified. The others stay the same but might have some trivial change of notation for quantities, such as $\langle \mathbf{p} \rangle_{0,2n} \rightarrow \langle \mathbf{p} \rangle_{0,2n-1}$ in the case of the *change of external momentum* procedure.

Change of diagram length in time, type 1

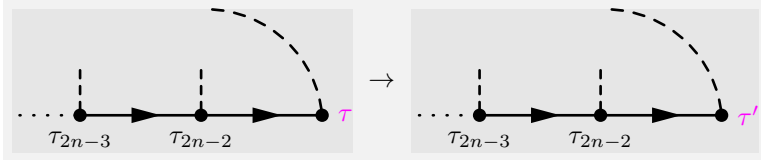


Figure 3.12: An illustration of the first kind of update procedure for changing the length of a diagram without external legs.

At $n > 0$, there is now a phonon propagator connected to the end point node of the diagram as depicted in figure 3.12. Thus, in accordance with the *change of diagram length in time, type 2* update procedure,

$$\frac{D_n(\tau')}{D_n(\tau)} = \exp \left\{ - \left[\frac{p^2}{2} - \mu + 1 \right] (\tau' - \tau) \right\}. \quad (3.41)$$

Hence, to maintain the acceptance ratio at unity, the only modification needed is to change the rate parameter of the distribution from which τ' is sampled, i.e. $\lambda \rightarrow \lambda' = \lambda + 1$.

Change of diagram order

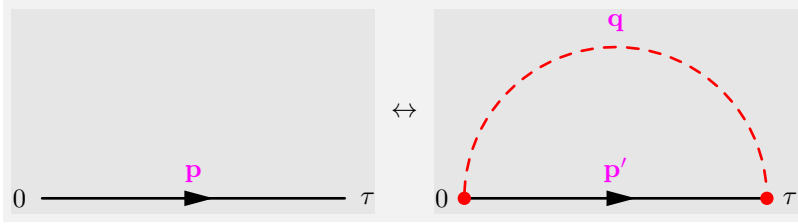


Figure 3.13: An illustration of the change of diagram order procedure between zeroth and first order diagrams.

In order to prevent generating diagrams with external legs, it is necessary only to modify the transition between a zeroth and a first order diagram. Instead of sampling two times where new nodes then will be inserted for the phonon to connect to, the already existing start and end point node of diagram will be used. This is illustrated in figure 3.13. Other than that this transition is no different from the ordinary *change of diagram order* update procedure so that

$$W(n = 0 | n = 1) = P_R \frac{\sin \theta_k}{2} \frac{1}{2\pi} \sqrt{\frac{2\tau}{\pi}} \exp \left\{ - \frac{q_k^2}{2} \tau \right\}. \quad (3.42)$$

The acceptance ratio may thus be expressed as previously (3.38) with

$$\begin{aligned} R(n = 0 | n = 1) &= \frac{D_{n=1}}{D_{n=0}} \frac{W(n = 1 | n = 0)}{W(n = 0 | n = 1)} \\ &= \frac{1 - P_R}{P_R} \frac{\alpha}{\sqrt{\pi}} \frac{1}{\sqrt{\tau}} \exp \left\{ [\langle \mathbf{p} \rangle_{l,m-1} \cdot \mathbf{q}_k - 1] \tau \right\}. \end{aligned} \quad (3.43)$$

The transitions procedure between diagrams of order $n > 0$, as introduce in section 3.3, can not add any external legs since both the start and end point node

of the diagram will be connected to phonons. However, there are now $2n - 1$ rather than $2n + 1$ number of \mathcal{G}_0 's to chose from when sampling the starting point time of the phonon propagator. Hence the " $2n + 1$ " in equation (3.35) and (3.37) should be replaced by " $2n - 1$ " to incorporate this.

3.4.1 Divergent diagram

It can be shown that the first order self energy diagram $\Sigma^{*(1)}(\mathbf{p}, |tau)$ is proportional to $1/\sqrt{\tau}$ and thus diverges when $\tau \rightarrow 0$. It is not possible to capture such a behavior using a histogram since the function to be approximated has a too large second derivative in the vicinity of the singularity. To show this, consider the mean value of a function $f(x)$ on the interval $x_i - \Delta x/2 < x < x_i + \Delta x/2$ with $f(x_i)$ expanded in terms of the small parameter Δx , i.e.

$$\begin{aligned}
 & \frac{1}{\Delta x} \int_{x_i - \Delta x/2}^{x_i + \Delta x/2} f(t) dt \\
 &= \frac{1}{\Delta x} \int_{x_i - \Delta x/2}^{x_i + \Delta x/2} f(x_i + [t - x_i]) dt \\
 &= \frac{1}{\Delta x} \int_{x_i - \Delta x/2}^{x_i + \Delta x/2} [f(x_i) + f'(x_i) [t - x_i] + \frac{1}{2} f''(x_i) [t - x_i]^2 + \dots] dt \\
 &= f(x_i) + \frac{1}{24} f''(x_i) [\Delta x]^2 + \mathcal{O}([\Delta x]^4).
 \end{aligned} \tag{3.44}$$

In order for this mean value to be well approximated by $f(x_i)$, it is required that $f''(x_i) [\Delta x]^2 \ll f(x_i)$. However, in the case of $f(x) = 1/\sqrt{x}$ and $x_i = \Delta x/2$ this is not fulfilled, no matter the size of Δx , since $f''(x_i) [\Delta x]^2 = 3\sqrt{2}/\sqrt{\Delta x}$ whilst $f(x_i) = 2/\sqrt{\Delta x}$. The ability of a histogram to approximate the function $1/\sqrt{x}$ in the vicinity of $x = 0$ is illustrated in figure 3.14.

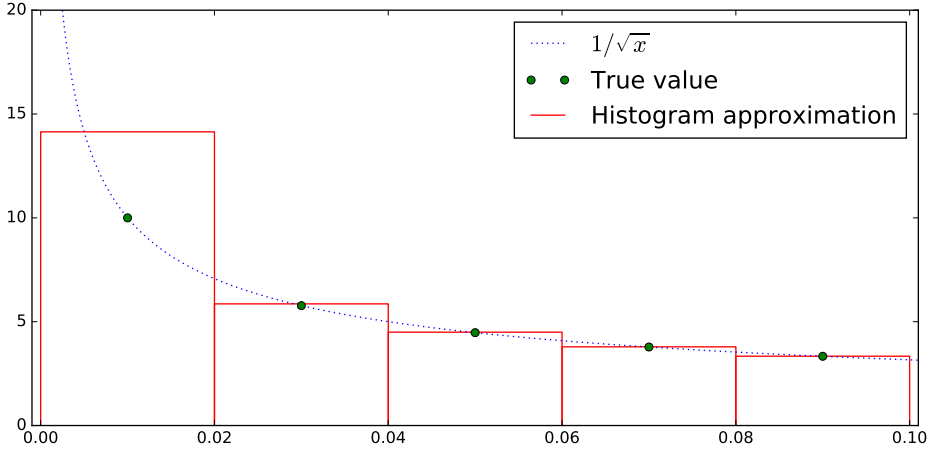


Figure 3.14: The function $1/\sqrt{x}$ approximated by a histogram with bin size $\Delta x = 0.02$ in the vicinity of $x = 0$. As can be seen, the approximative value at $x_0 = 0.01$ is quite far off from the true one.

Remove vertical lines for the legend to be true

The true value of the first order self energy diagram at zero external momentum is

$$\Sigma^{*(1)}(\mathbf{p} = \mathbf{0}, \tau) = \frac{\alpha}{\sqrt{\pi}} \frac{e^{-(1-\mu)\tau}}{\sqrt{\tau}} \quad \tau \geq 0. \quad (3.45)$$

When approximating this function with a histogram of bin size $\Delta\tau$, the value of the bin corresponding to τ_i becomes

$$\begin{aligned} \langle \Sigma^{*(1)}(\mathbf{p} = \mathbf{0}) \rangle_j &= \frac{1}{\Delta\tau} \int_{\tau_j - \Delta\tau/2}^{\tau_j + \Delta\tau/2} \Sigma^{*(1)}(\mathbf{p} = \mathbf{0}, t) dt \\ &= \frac{1}{\Delta\tau} \frac{\alpha}{\sqrt{1-\mu}} \left[\operatorname{erf} \left\{ \sqrt{(1-\mu) \left(\tau_j + \frac{\Delta\tau}{2} \right)} \right\} - \operatorname{erf} \left\{ \sqrt{(1-\mu) \left(\tau_j - \frac{\Delta\tau}{2} \right)} \right\} \right] \end{aligned} \quad (3.46)$$

However, for external momentum $\mathbf{p} \neq \mathbf{0}$ it seems next to impossible to find an analytical expression of $\Sigma^{*(1)}(\mathbf{p}, \tau)$ due to cumbersome integrals. Nevertheless, by the usage of Monte Carlo integration these integrals may be calculated to an extremely good precision in a matter of seconds.

In order to find out whether a value of $\Sigma^{*(1)}(\mathbf{p}_i, \tau_j)$ should be calculated using DMC or Monte Carlo integration, it is reasonable to look at the difference $\Delta\Sigma_j^{*(1)} = \langle \Sigma^{*(1)}(\mathbf{p} = \mathbf{0}) \rangle_j - \Sigma^{*(1)}(\mathbf{p} = \mathbf{0}, \tau_j)$. For times $\tau_j < \tau_{\text{threshold}}$ where this difference is

larger than a threshold value ε , Monte Carlo integration should be used, otherwise DMC will be sufficient. The DMC code written during this master project has the threshold set to $\varepsilon = 0.001$. In table 3.2 the value of $\Delta\Sigma_j^{*(1)}$ is given for the first six j 's.

j	0	1	2	3	4	5	6
$\Delta\Sigma_j^{*(1)}$	2.34	0.0486	0.0133	0.0058	0.00314	0.00193	0.00129

Table 3.2: Here $\Delta\Sigma_j^{*(1)}$ is calculated for different values of j . The parameters used are $\alpha = 1$, $\mu = -1.1$ and $\Delta\tau = 0.02$.

It is crucial that there will be no contribution from $\Sigma^{*(1)}$ to the histogram N for times where it is calculated using Monte Carlo integration. However, to avoid such a double contribution it is as simple as to not bin a first order self energy diagram if the length τ of which belongs to a bin $N_{i,j}$ of time $\tau_j < \tau_{\text{threshold}}$.

3.4.2 Results

Here follow some results obtained when simulating Σ^* using the bare scheme update procedures described above. For the same reasons as given before the external momentum \mathbf{p} has again been kept fixed during these simulations .

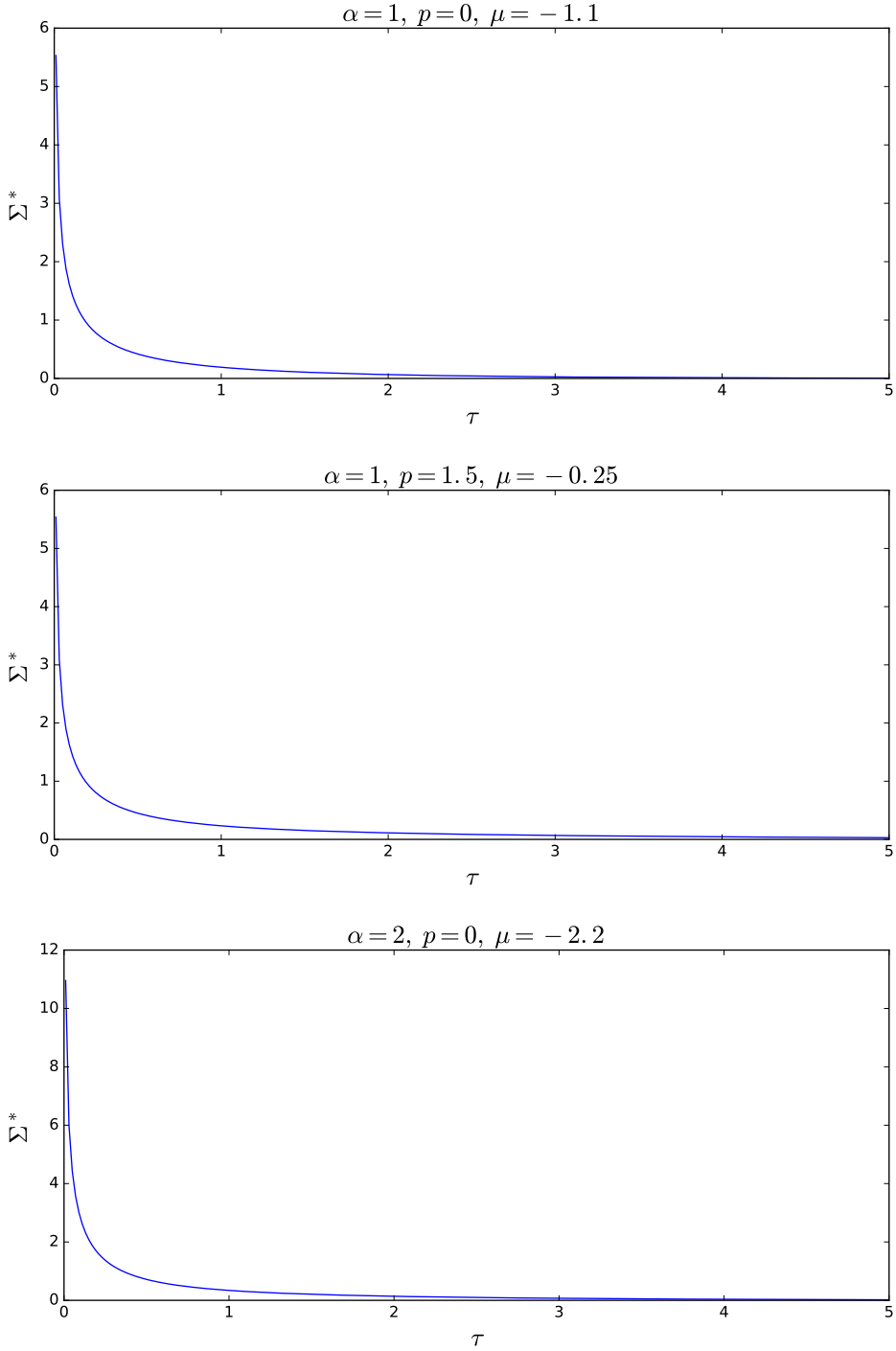


Figure 3.15: The acquired value of $\Sigma^*(p=0, 0 \leq \tau \leq 5)$ after 80 minutes of core time. Here $\tau_{max} = 40$ and $\Delta\tau = 0.02$ has been used.

τ	$\Sigma^*(0, 1, -1.1)$	$\Sigma^*(1.5, 1, -0.25)$	$\Sigma^*(0, 2, -2.2)$
0.01	5.531	5.537	10.96
0.21	0.892	0.9145	1.591
0.41	0.5063	0.5362	0.8721
0.61	0.3417	0.3757	0.5845
0.81	0.2484	0.2877	0.4318
1.01	0.1889	0.2312	0.3366
1.21	0.1481	0.1924	0.2724
1.41	0.1184	0.1638	0.2249
1.61	0.09575	0.1419	0.1887
1.81	0.07845	0.1248	0.1613
2.01	0.0643	0.1114	0.1377
2.21	0.05323	0.0994	0.1191
2.41	0.04421	0.08949	0.103
2.61	0.03667	0.08083	0.08986
2.81	0.03072	0.07354	0.07825
3.01	0.02576	0.06704	0.06804
3.21	0.02159	0.06117	0.05961
3.41	0.01814	0.05634	0.05227
3.61	0.01523	0.05141	0.046
3.81	0.01287	0.04739	0.04028
4.01	0.0109	0.04374	0.03547
4.21	0.009089	0.04027	0.03091
4.41	0.007704	0.03723	0.02729
4.61	0.006375	0.03454	0.02392
4.81	0.00551	0.03193	0.02108
4.99	0.004662	0.02981	0.01871

Table 3.3: Some values of $\Sigma^*(p, \alpha, \mu)$ from the plots in figure 3.15.

3.4.3 Implementing Dyson equation numerically

It is not entirely trivial how to implement Dyson equation when having to use a discrete Fourier transform. First of all, the proper self energy must be transformed into frequency space, but due to the singularity at $\tau = 0$ it is not preferable to transform this quantity directly. However, knowing the analytical expression of this singular contribution, it can then be subtracted from the self energy so that the discrete Fourier transform may be applied to the resulting regular expression. The singular part is then Fourier transformed analytically and once in ω -space it is added to the transformed regular expression. That is,

$$\Sigma^*(\mathbf{p}_i, \omega_j) = \mathcal{F}_{\text{DFT}} \{ \Sigma^*(\mathbf{p}_i, \tau_j) - \Sigma^*_{\text{singular}}(\mathbf{p}_i, \tau_j) \} + \Sigma^*_{\text{singular}}(\mathbf{p}_i, \omega_j), \quad (3.47)$$

which is possible due to the linearity of the Fourier transform. A possible choice of the singular part is $\Sigma_{\text{singular}}^*(\mathbf{p}_i, \tau_j) = \Sigma^{*(1)}(\mathbf{p} = \mathbf{0}, \tau_j)$ for which the expression is (3.45) and thus

$$\Sigma_{\text{singular}}^*(\mathbf{p}_i, \omega_j) = \frac{\alpha}{\sqrt{1 - \mu + i\omega_j}}. \quad (3.48)$$

Having the proper self energy in momentum and frequency space, Dyson equation is given by (2.66). However, it is not possible to directly transform back to $\mathcal{G}(\mathbf{p}_i, \tau_j)$ using the inverse discrete Fourier transform. This has to do with the fact that $\mathcal{G}(\mathbf{p}, \omega)$ falls off as $1/\omega$ when $\omega \rightarrow \infty$, which is too slow. Instead one may transform the difference

$$\Delta\mathcal{G}(\mathbf{p}, \omega) = \mathcal{G}(\mathbf{p}, \omega) - \mathcal{G}_0(\mathbf{p}, \omega) = \frac{\Sigma^*(\mathbf{p}, \omega)}{(i\omega + \xi(\mathbf{p}) - \Sigma^*(\mathbf{p}, \omega))(i\omega + \xi(\mathbf{p}))} \quad (3.49)$$

which has the proportionality $\Delta\mathcal{G}(\mathbf{p}, \omega \rightarrow \infty) \propto \omega^{-5/2}$ because $\Sigma^*(\mathbf{p}, \omega \rightarrow \infty) \propto \omega^{-1/2}$. Since also the inverse Fourier transform is linear, it follows that

$$\mathcal{F}_{DFT}^{-1} \{ \Delta\mathcal{G}(\mathbf{p}_i, \omega_j) \} = \Delta\mathcal{G}(\mathbf{p}_i, \tau_j) = \mathcal{G}(\mathbf{p}_i, \tau_j) - \mathcal{G}_0(\mathbf{p}_i, \tau_j). \quad (3.50)$$

The interacting electronic propagator in τ -space is finally obtained by

$$\mathcal{G}(\mathbf{p}_i, \tau_j) = \mathcal{G}_0(\mathbf{p}_i, \tau_j) + \Delta\mathcal{G}(\mathbf{p}_i, \tau_j). \quad (3.51)$$

In figure 3.16 the relative difference between the \mathcal{G}_{Σ^*} obtained using Dyson equation and the directly simulated \mathcal{G} is plotted against τ for both $\Delta\tau = 0.02$ and $\Delta\tau = 0.01$. As can be seen the difference is smaller than the size of $\Delta\tau$ in both cases. The agreement also seems to improve somewhat linearly with smaller $\Delta\tau$, the drawback is however more noise since there is less statistics contributing to each bin N_j .

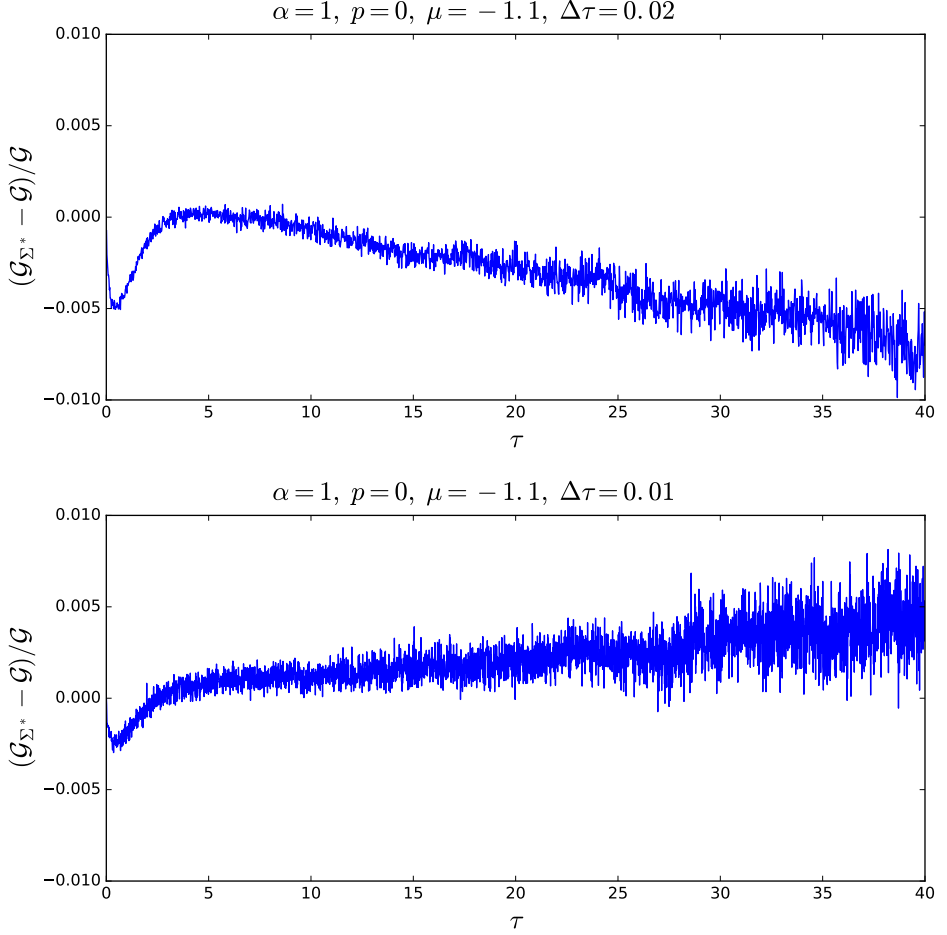


Figure 3.16: The relative difference between \mathcal{G}_{Σ^*} obtained using Dyson equation and the directly simulated \mathcal{G} . For each of these simulations a core time of 24 hours has been used.

3.5 Bold-line scheme ?

The bold-line scheme [12] is a self consistent scheme making use of bold-line tricks iteratively in order to partially or fully sum up a diagram series. Dyson equation is one such bold-line trick and is the only one to be investigated in this thesis.

Here the propagator $\mathcal{G}_{k+1} = \mathcal{G}^{(0)} + \Delta\mathcal{G}_{k+1}$ is obtained when employing Dyson equation to the self energy S_{k+1} , made up of self energy diagrams subjected to certain constraints in order to prevent double counting. However, rather than using

the bare propagator when calculating S_{k+1} , the \mathcal{G}_k computed in the previous iteration of the scheme is instead used. During the first iteration, when no propagator previously have been calculated, the bare one is used, i.e. $\mathcal{G}_0 = \mathcal{G}^{(0)}$. This scheme will converge given an appropriate choice of parameters so that $S_{m+1} \simeq S_m$ for some m . In practice, as will be shown, this convergence will happen after 4 or so iterations.

3.5.1 Skeleton diagrams

In order for certain diagrams to not contribute more than once to the \mathcal{G}_k , it is necessary to narrow down the class of allowed diagrams to a subclass of the proper self energy diagrams, referred to as skeleton diagrams [13]. This class of diagrams is characterized by the lack of insertions, i.e. diagram parts which act like self energies to some of the constituents of the diagram. It is easily realized, that the skeleton diagrams in the series of \mathcal{G} are particularly easy to identify. That is, if the phonon propagators of a self energy diagram are entirely interconnected, the diagram is a skeleton one. Here interconnected phonon propagator is referred to those who intersect with at least another one when they are all drawn on one side of the straight line of electronic propagators, as done throughout this paper. This is illustrated in figure 3.17.

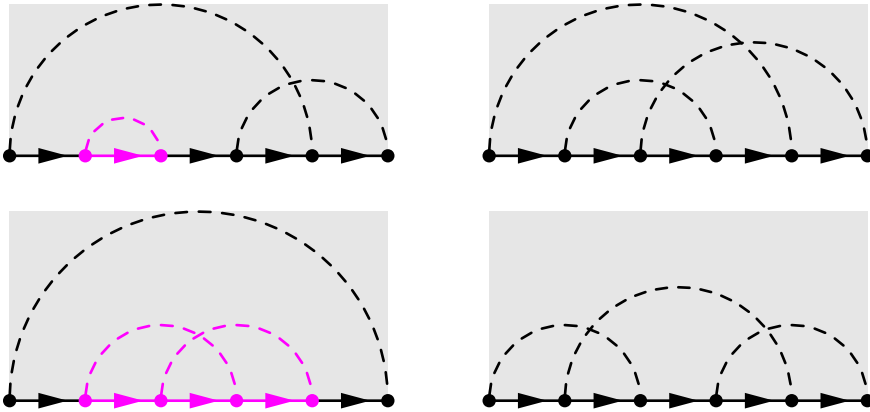


Figure 3.17: The diagrams to the left belong to the class of skeleton diagrams whilst the ones to the right merely belong to the class of proper self energy diagrams. The insertions of the proper self energy diagrams are here highlighted.

Even by restricting to merely a subset of skeleton diagrams, bounded by the diagram order $n \leq n_{\max}$, the range of diagrams contributing to \mathcal{G}_k will grow extremely fast with the bold-line iteration k . This will now be demonstrated in the case of $n_{\max} = 1$.

First iteration

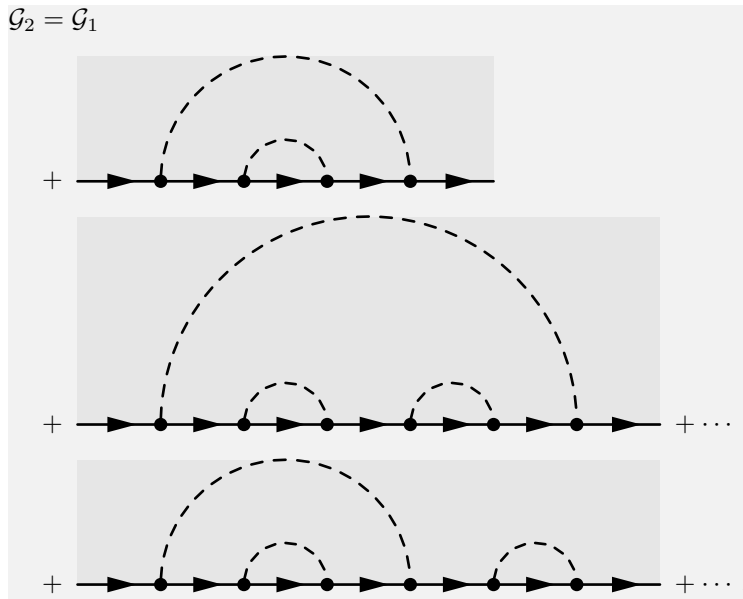
$$\begin{aligned}
 S_1 &= \text{diagram with a dashed arc over a single arrow} \\
 \mathcal{G}_1 &= \text{diagram with a red double arrow} \\
 &= \text{diagram with a single arrow} + \text{diagram with a dashed arc over a red double arrow} + \text{diagram with two dashed arcs over red double arrows} + \dots
 \end{aligned}$$

(3.52)

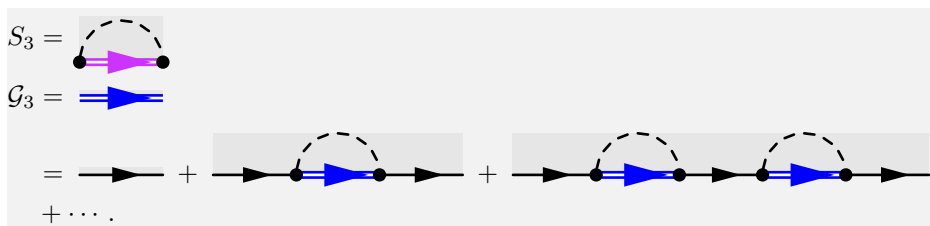
Second iteration

$$\begin{aligned}
 S_2 &= \text{diagram with a dashed arc over a red double arrow} \\
 \mathcal{G}_2 &= \text{diagram with a blue double arrow} \\
 &= \text{diagram with a single arrow} + \text{diagram with a dashed arc over a blue double arrow} + \text{diagram with two dashed arcs over blue double arrows} + \dots
 \end{aligned}$$

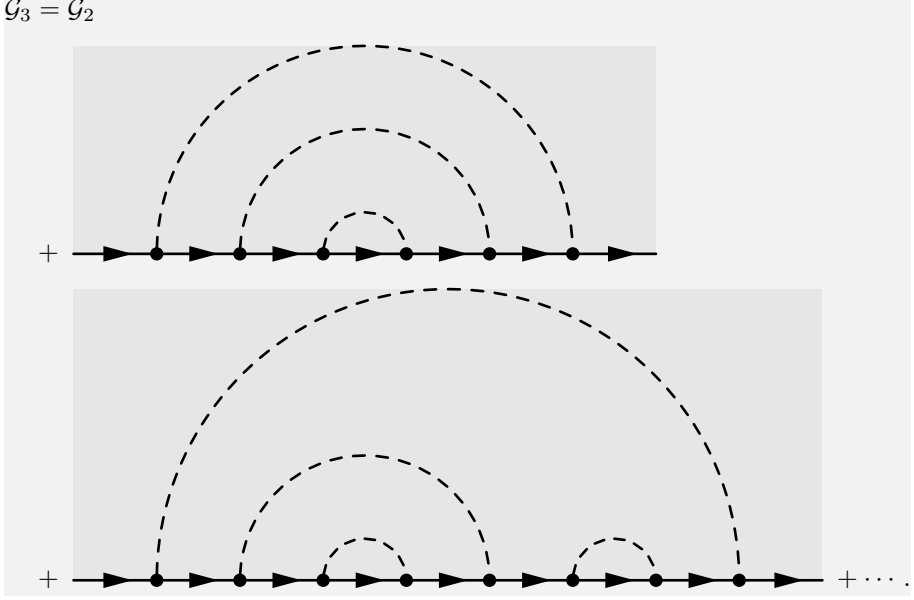
By substituting with \mathcal{G}_1 in terms of the diagram series (3.52) into the diagram series of \mathcal{G}_2 , this series, expressed in terms of the bare constituents, becomes



Third iteration



Similarly to before, by substituting with \mathcal{G}_2 into \mathcal{G}_3 , one obtains



Already at this point, a wide range of diagrams contribute to \mathcal{G}_3 . However, even if one continues this iterative process, a skeleton diagram of order $n > 1$ in which phonon propagators intersect won't be encountered in the series.

3.5.2 Implementation

The diagram update procedures, for bold-line iterations $k > 1$, need to be altered in order to account for the replacement of the bare propagators within the diagram in favor of \mathcal{G}_i . However, rather than expressing \mathcal{G}_i in terms of the difference $\Delta\mathcal{G}_k$ to the bare propagator, it is more convenient to work with an additional imaginary phase $\varphi_k(\mathbf{p}, \tau)$, so that

$$\mathcal{G}_k(\mathbf{p}, \tau) = e^{\varphi_k(\mathbf{p}, \tau)} \mathcal{G}^{(0)}(\mathbf{p}, \tau). \quad (3.53)$$

This phase is defined through

$$\varphi(\mathbf{p}, \tau) = -\tau \Delta\xi_k(p_l, \tau_m) \quad (3.54)$$

where $\Delta\xi_k$ is an additional energy

$$\Delta\xi_k(\mathbf{p}_i, \tau_j) = \frac{1}{\tau_j} \log \frac{\mathcal{G}^{(0)}(\mathbf{p}_i, \tau_j)}{\mathcal{G}_k(\mathbf{p}_i, \tau_j)}. \quad (3.55)$$

In equation (3.54), p_l and τ_m are chosen to obey $p_l - \frac{1}{2}\Delta p \leq p \leq p_l + \frac{1}{2}\Delta p$ and $\tau_m - \frac{1}{2}\Delta\tau \leq \tau \leq \tau_m + \frac{1}{2}\Delta\tau$ respectively. However, in the case of momentum

magnitudes $p > p_{N-1} + \frac{1}{2}\Delta p$, it is natural to use p_{N-1} . During the discretization it is then important to chose a large enough cutoff momentum p_{\max} in order for the true $G_k(\mathbf{p}, \tau)$ to be reasonably approximated by $e^{\varphi_k(\mathbf{p}, \tau)}\mathcal{G}^{(0)}(\mathbf{p}, \tau)$ at momentum magnitudes $p > p_{N-1} + \frac{1}{2}\Delta p$. Thus, if the p_{\max} is chosen to small, the \mathcal{G}_k wont converge to the true interacting propagator \mathcal{G} .

Now, with $\mathcal{G}_k(\mathbf{p}, \tau)$ defined in this way, the only modification needed in order for the update procedures to reflect the change $\mathcal{G}^{(0)} \rightarrow \mathcal{G}_k$, is to multiply the quota of the diagram values D'/D with the factor

$$\exp \left\{ \sum_{a \in A} \varphi(\mathbf{p}_a, \tau_a) - \sum_{b \in B} \varphi(\mathbf{p}_b, \tau_b) \right\}. \quad (3.56)$$

Here B and A is the set of affected electronic propagators before and after the update procedure respectively.

But wait, there is more. Update procedures involving the sampling of imaginary-times from an exponential distribution with momentum dependent rate parameter must further be slightly modified in order to improve the otherwise disastrous statistics. This since the quota $W(\tau'_l|\tau_l)/W(\tau_l|\tau'_l) = \exp\{-\lambda(\tau_l - \tau'_l)\}$, for certain differences $\tau_l - \tau'_l$, poorly mimics the ratio $D(\tau'_l)/D(\tau_l)$ due to the choice of rate parameter $\lambda(\mathbf{p})$. This is easily realized by comparing the $\mathcal{G}(\mathbf{p}, \tau)$'s in figure 3.11 to their corresponding bare propagators $\mathcal{G}^{(0)}(\mathbf{p}, \tau)$. In order to resolve this issue, one adds to the the original rate parameter the contribution $\Delta\lambda_k(\mathbf{p}_l)$, which is obtained by fitting an exponentially decaying function $C_k(\mathbf{p}_l)\exp\{-\Delta\lambda_k(\mathbf{p}_l)\tau\}$ to $\mathcal{G}_k(\mathbf{p}_l, \tau_j)/\mathcal{G}^{(0)}(\mathbf{p}_l, \tau_j)$ for each \mathbf{p}_l . Again $p_l - \frac{1}{2}\Delta p \leq p \leq p_l + \frac{1}{2}\Delta p$ and p_{N-1} is used for $p > p_{N-1} + \frac{1}{2}\Delta p$.

After each bold-line iteration, when calculating the value of $S_{k+1}(\mathbf{p}_i, \tau_j)$ from $N_{i,j}$, it is important to normalize using \mathcal{G}_k rather than the bare propagator $\mathcal{G}^{(0)}$. Hence, in similarity with (3.40),

$$S_{k+1}(\mathbf{p}_i, \tau_j) = N_{i,j} \frac{\sum_{l,m} \mathcal{G}_k(\mathbf{p}_l, \tau_m)}{N_0}. \quad (3.57)$$

Equally important for this to be true, is to make sure that only skeleton diagrams contribute to incrementing the bins $N_{i,j}$ of the histogram.

3.5.3 Results

Nine different simulations for an increasing value of the maximum diagram order n_{\max} has been carried out using the discretization $\Delta\tau = 0.02$, $\Delta p = 0.02$, $p_{\max} = 10$ and $\tau_{\max} = 60$. With larger n_{\max} , the statistics became significantly more contaminated by noise. Thus, in order to try and suppress this noise, the computation for each iteration in the bold-line scheme needed to be increased. The number of core hours needed quickly outgrew what was possible to calculate using a single core in a foreseeable future, hence the code was parallelized using the *Message Passing Interface* (MPI).

Depicted in figures 3.18 to 3.26 are the obtained values of S_k 's, as well as the corresponding \mathcal{G}_k 's, for an increasing value of n_{\max} . The proper self energy Σ^* and the interacting Greens function, acquired using Dyson equation, \mathcal{G} are also outlined.

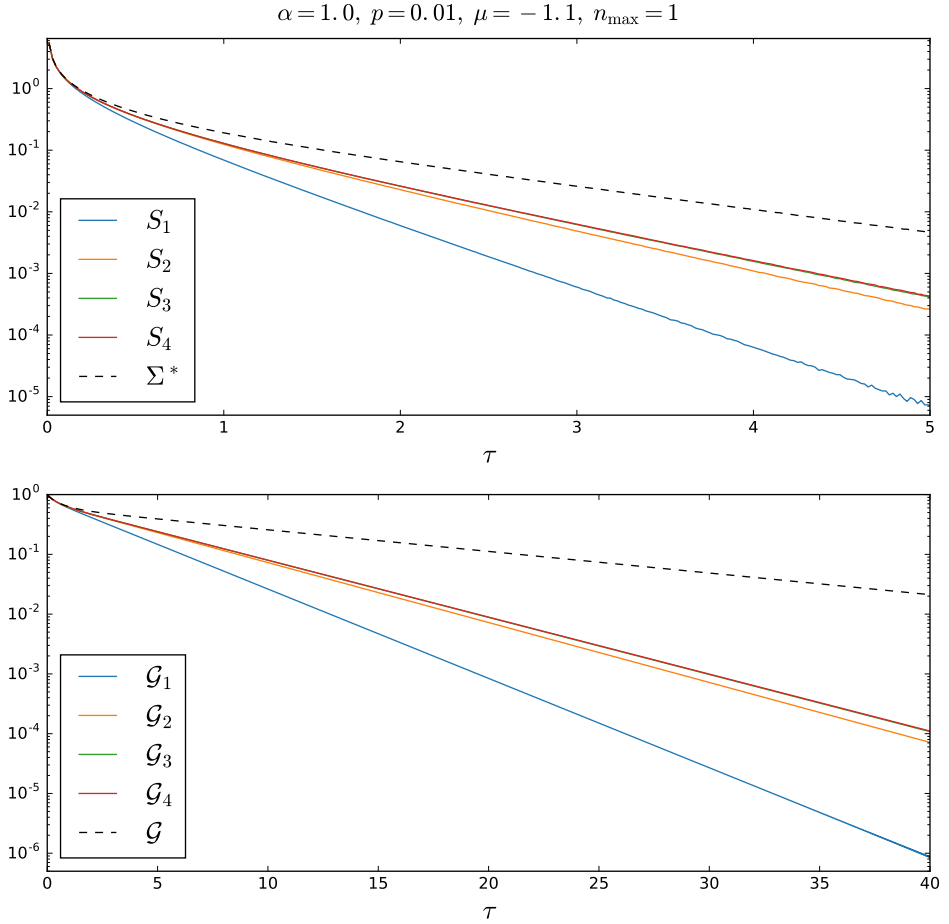


Figure 3.18: A total core time of 13 days was used for each of the four iterations in the bold-line scheme.

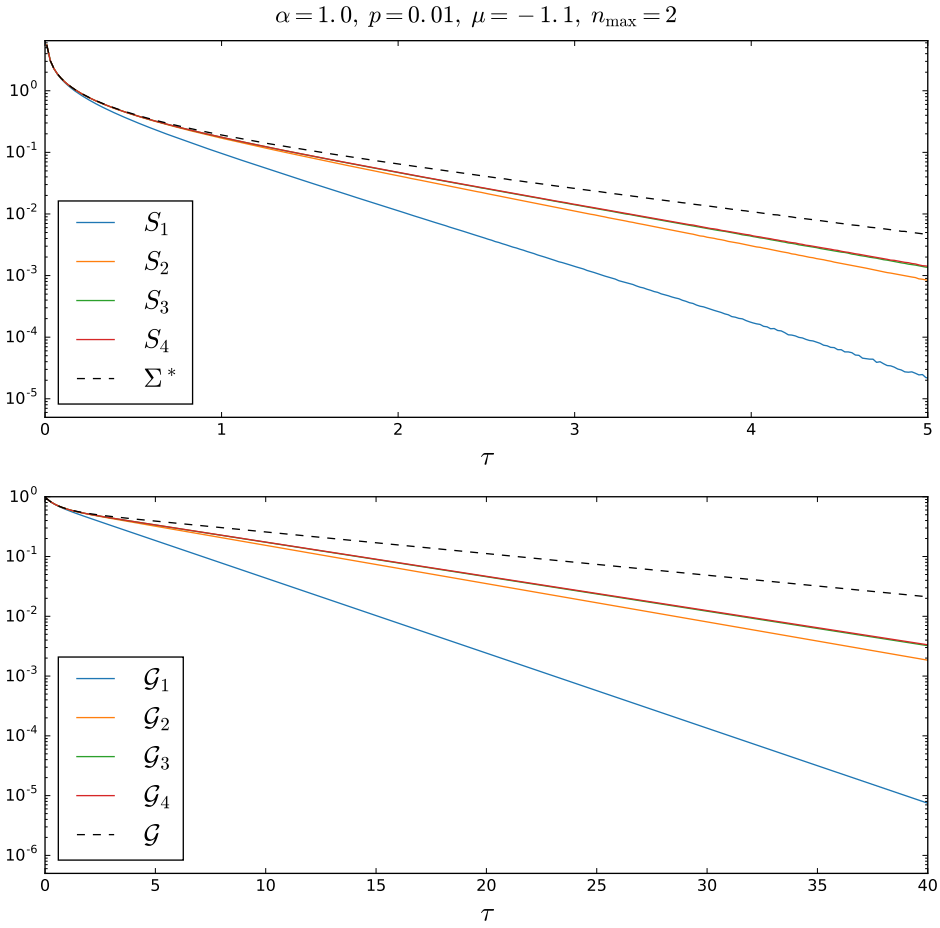


Figure 3.19: A total core time of 13 days was used for each of the four iterations in the bold-line scheme.

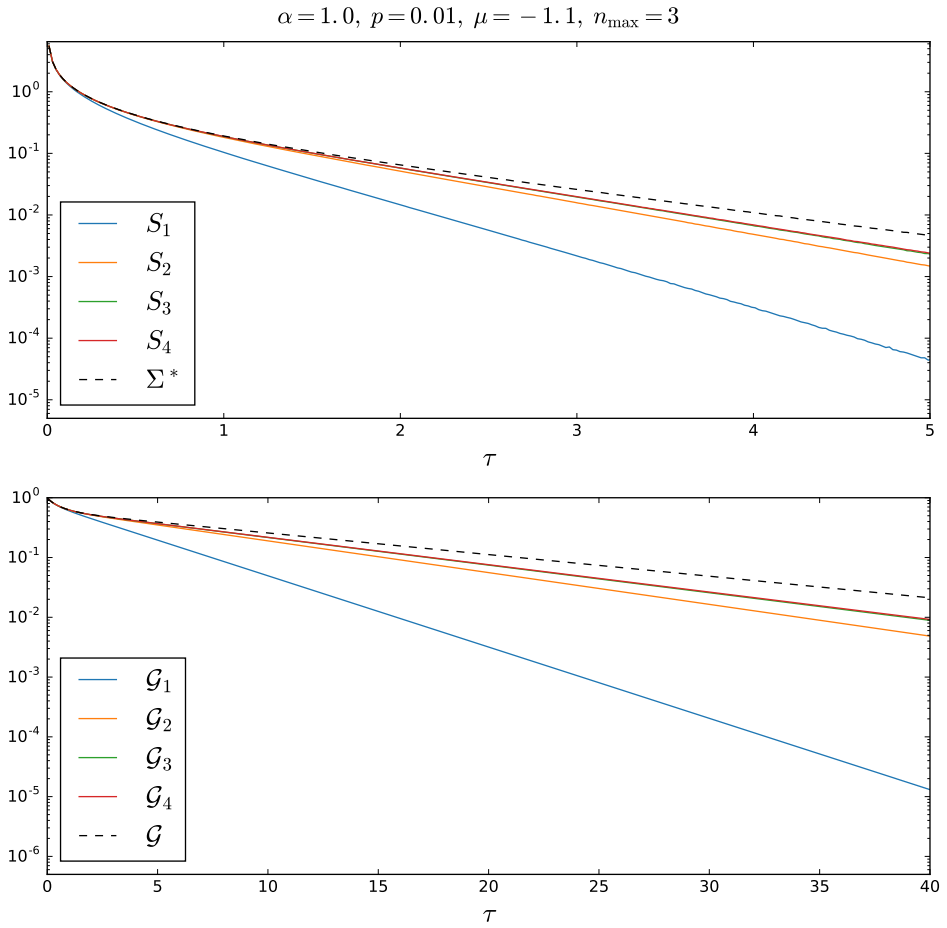


Figure 3.20: A total core time of 15 days was used for each of the four iterations in the bold-line scheme.

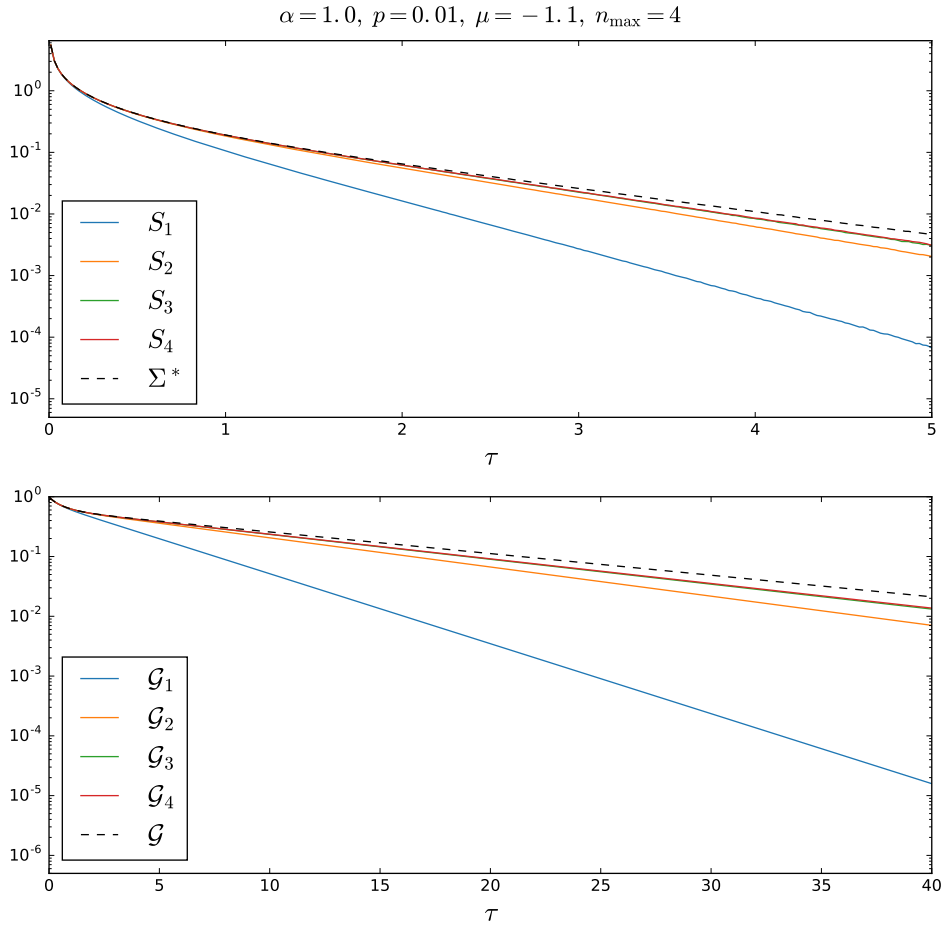


Figure 3.21: A total core time of 15 days was used for each of the four iterations in the bold-line scheme.

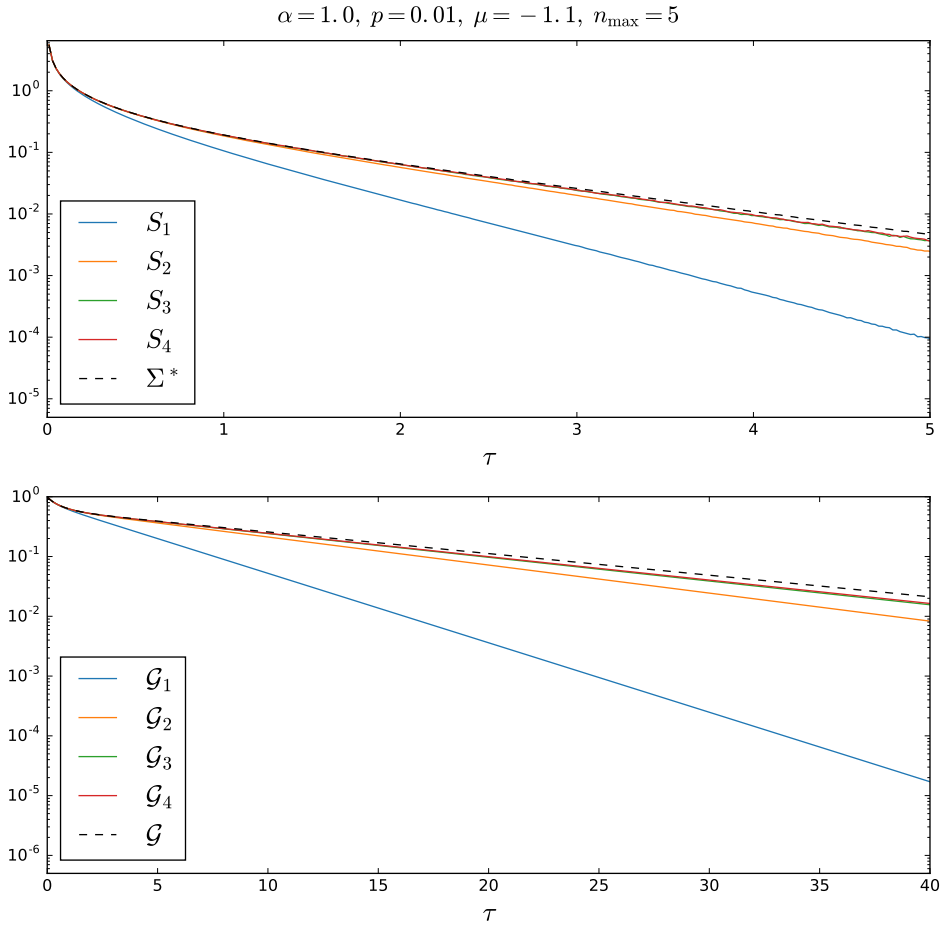


Figure 3.22: A total core time of 15 days was used for each of the four iterations in the bold-line scheme.

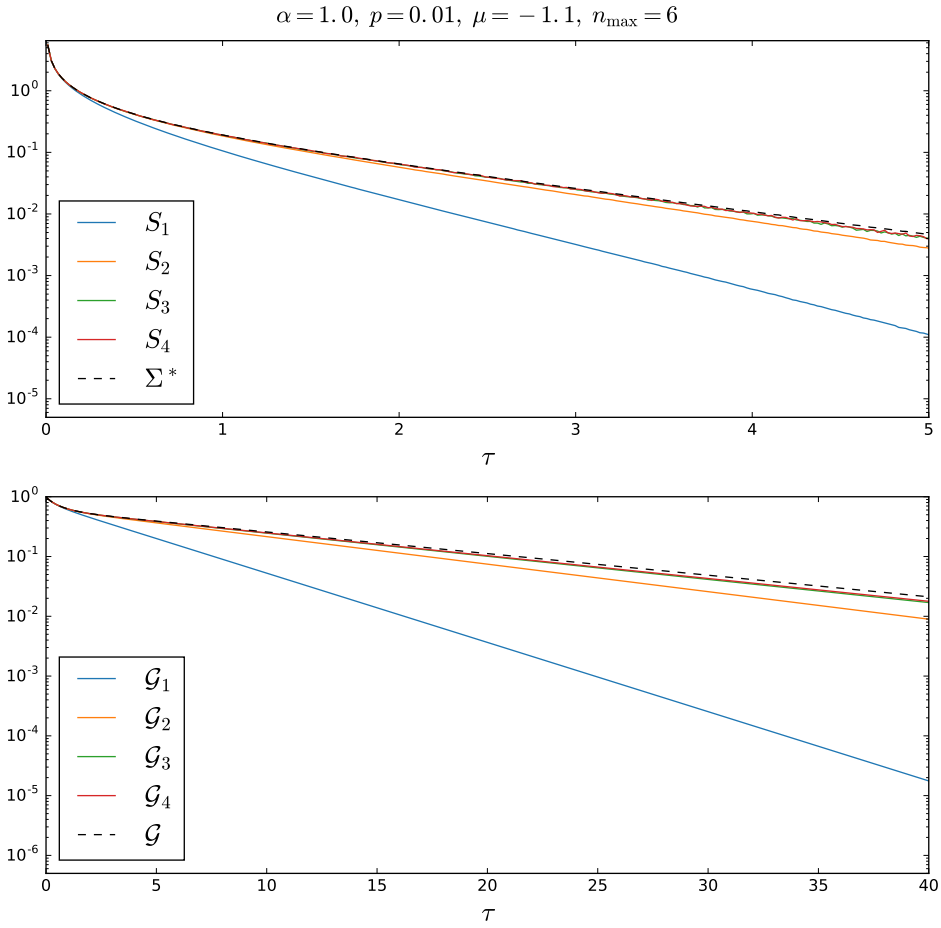


Figure 3.23: A total core time of 28 days was used for each of the four iterations in the bold-line scheme.

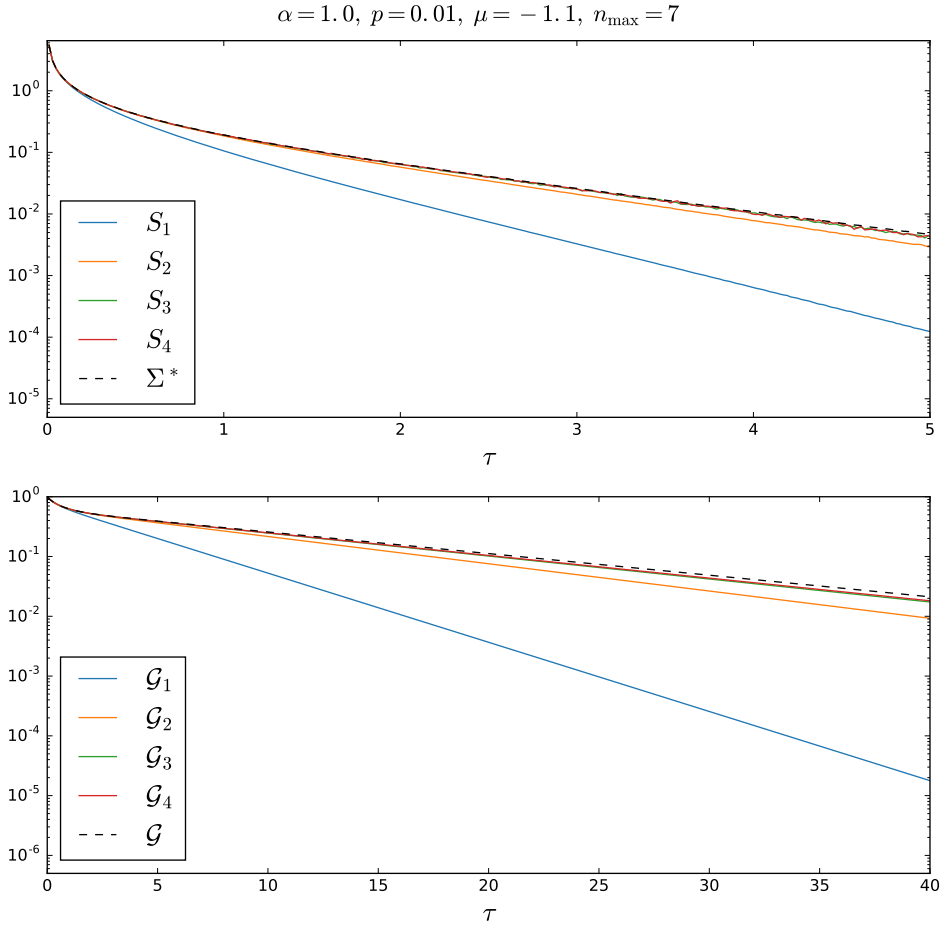


Figure 3.24: A total core time of 44 days was used for each of the four iterations in the bold-line scheme.

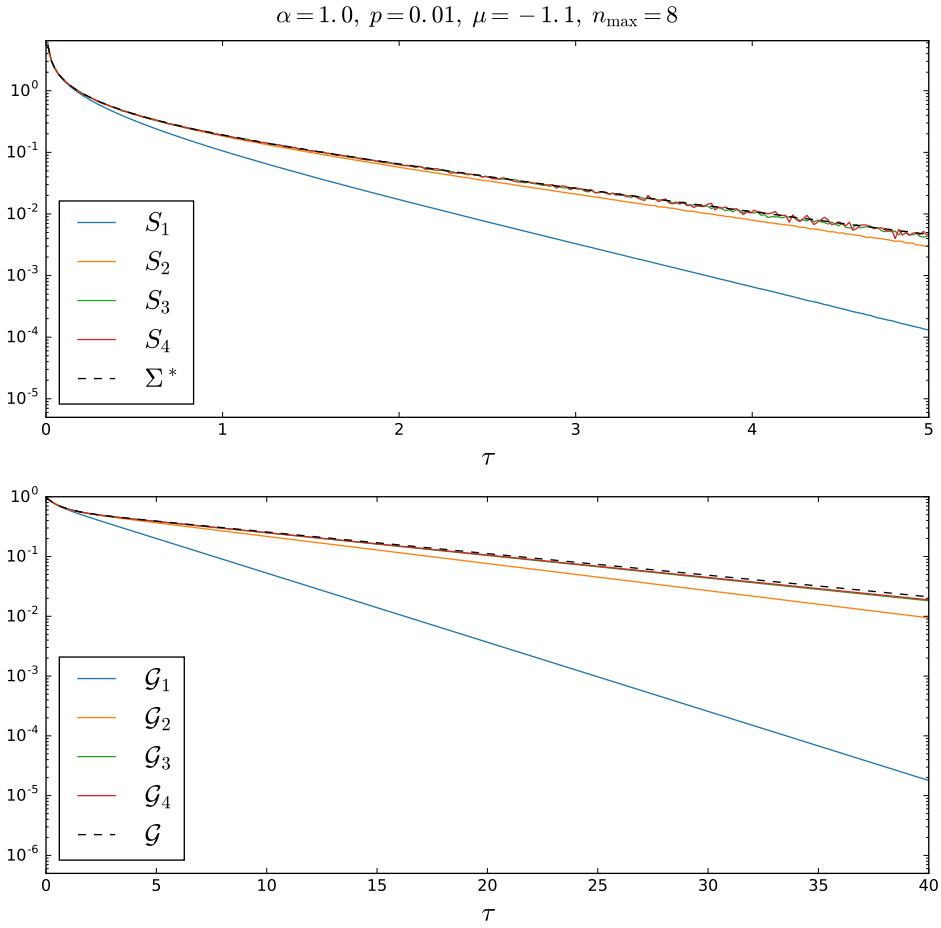


Figure 3.25: A total core time of 65 days was used for each of the four iterations in the bold-line scheme.

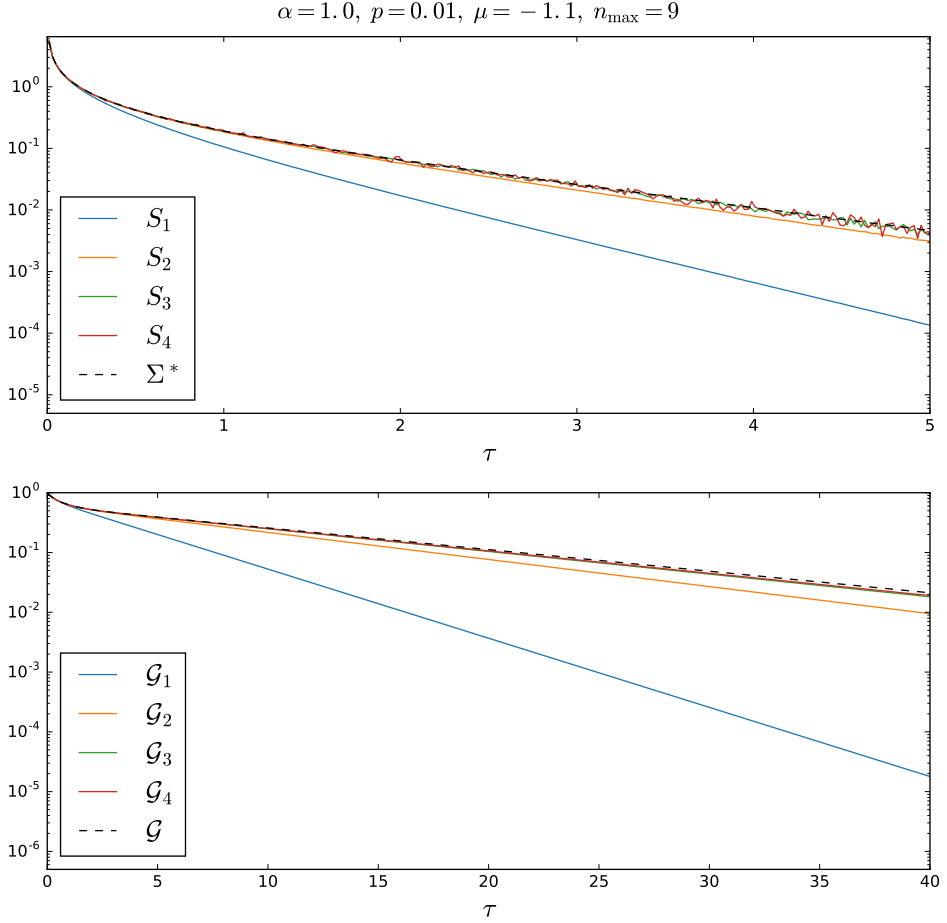


Figure 3.26: A total core time of 203 days was used for each of the four iterations in the bold-line scheme.

Evident from these figures, is that S_k approaches Σ^* as both the bold-line iteration k and the maximum diagram order n_{\max} become larger, just as expected. However, even though an awful amount of computation time was used to calculate the S_k 's for $n_{\max} = 8, 9$, it seems that it was not enough since there is still much noise present.

By fitting the logarithm of these \mathcal{G}_k 's to a straight line $y = k\tau + m$ at large imaginary-times, one can extract the corresponding $E_0(n_{\max}, k)$ and $Z_0(n_{\max}, k)$ using (2.19). This has been done and the result is presented in figures 3.27 and 3.28.

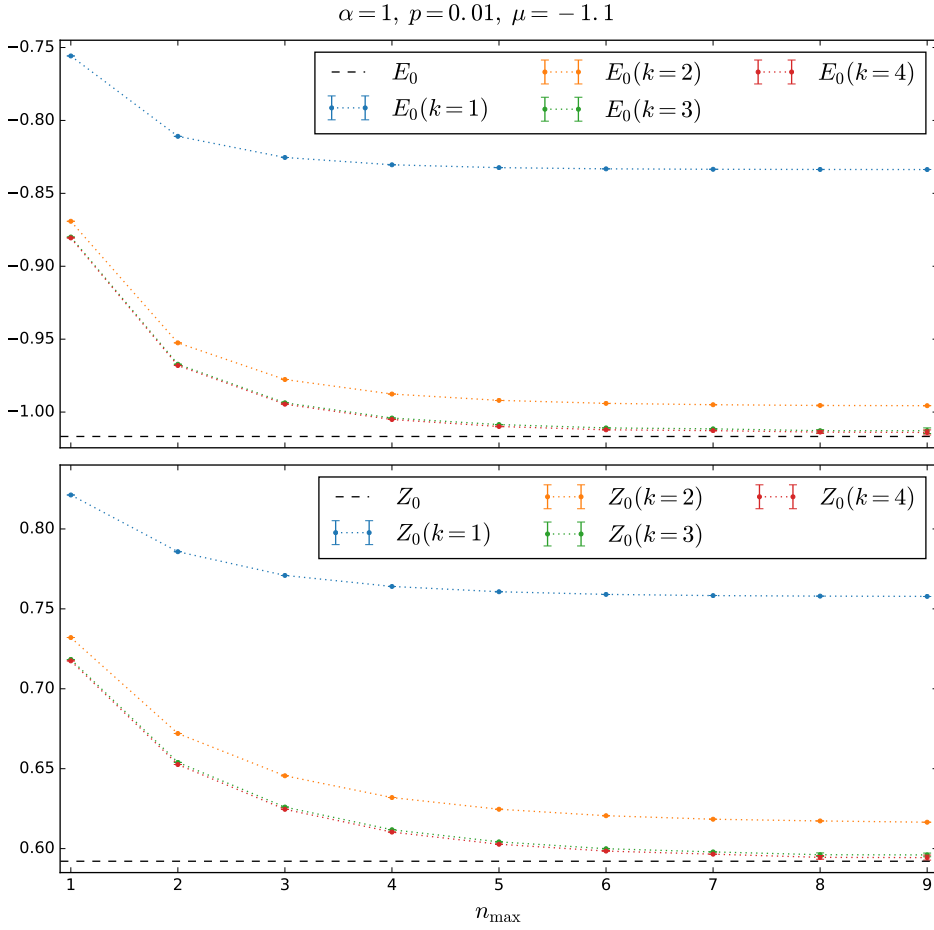


Figure 3.27: Here $E_0(n_{\max}, k)$ and $Z_0(n_{\max}, k)$ obtained from the bold-line simulations are shown next to the true values E_0 and Z_0 .

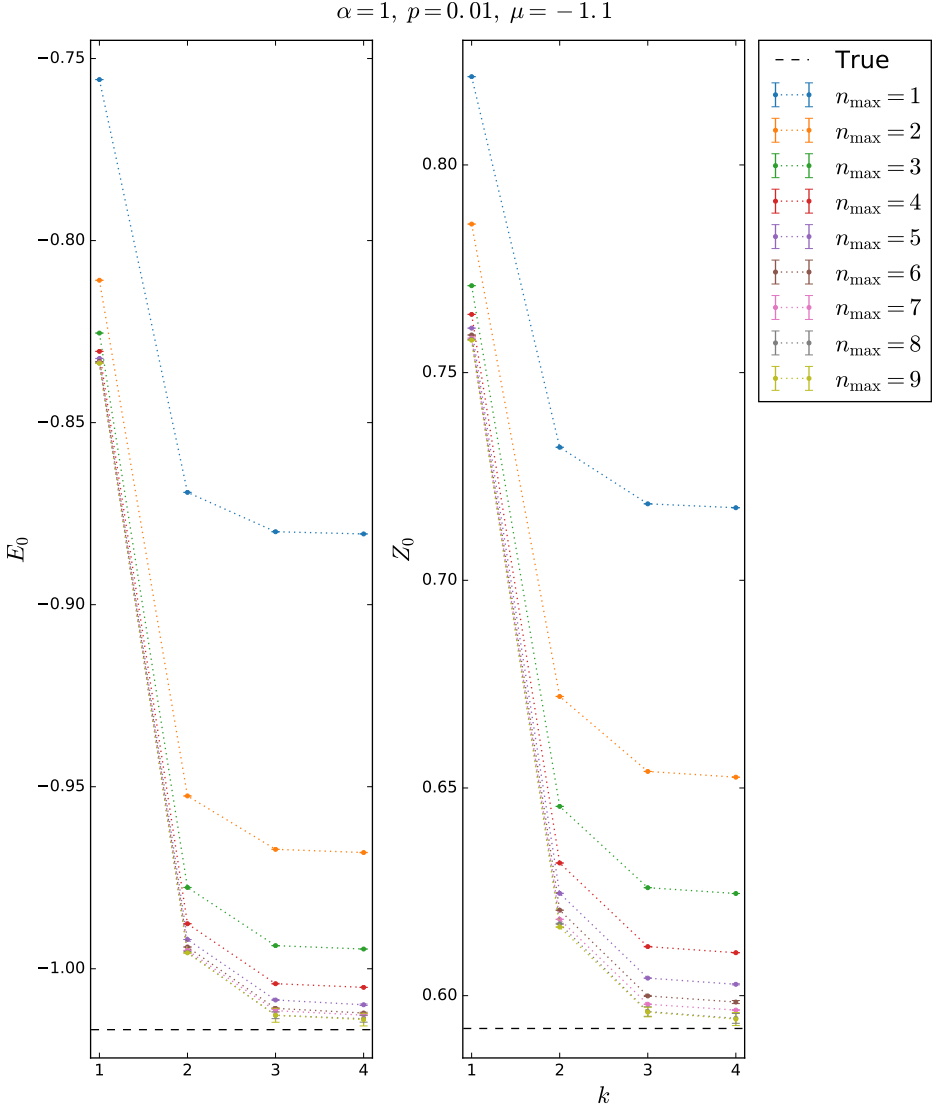


Figure 3.28: Here $E_0(n_{\max}, k)$ and $Z_0(n_{\max}, k)$ obtained from the bold-line simulations are shown next to the true values E_0 and Z_0 .

Unfortunately there was only four iterations used in the bold-line scheme, which according to figure 3.28 was not enough to reach a steady state value for E_0 and Z_0 . This steady state could nevertheless not have been very far away, by the looks of it a fifth or perhaps a sixth iteration would probably have been sufficient for

the trends in that figure to level out. Additionally, it would presumably also have been necessary to use a larger n_{\max} in order to overlap with the curves of the true E_0 and Z_0 . Such a computation would however require an immense amount of computation time in order for the error bars to be of satisfactory size which was also the reason for it not being carried out. The quantities obtained after the fourth iteration with $n_{\max} = 8, 9$ already have a bit too much uncertainty in them due to the noisy statistics.

Even with these shortcomings, it is from the presented result apparent that $E_0(n_{\max}, k)$ and $Z_0(n_{\max}, k)$ approach the true values E_0 and Z_0 respectively as n_{\max} and k increase.

3.6 Numerical *and analytical (!?)* Results

This thesis would not be complete without presenting some general quantities of interest to do with the polaron. Here numerous simulations of \mathcal{G} has been carried out using the bare scheme for Σ^* with different values of the interaction parameter α and the external momentum \mathbf{p} from which E_0 and Z_0 then have been extracted. The result is presented in figures 3.29 and 3.30 but also in table 3.4. The computation time for each data point range from two to twelve core hours, providing a standard deviation smaller than $5 \cdot 10^{-4}$. For comparison these numerically computed quantities are presented next to corresponding ones obtained using traditional analytical perturbative methods.

Present the analytical perturbative quantities here instead of doing it in the caption of the figures.

Data in agreement with the two papers + thesis

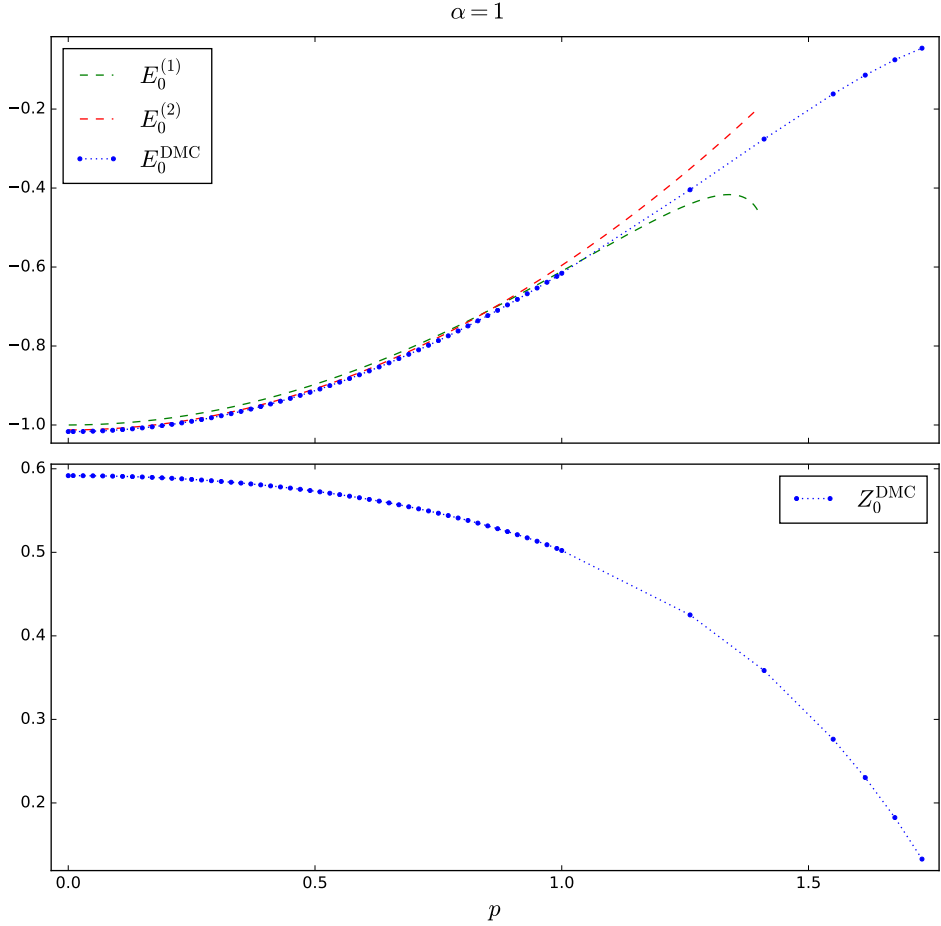


Figure 3.29: Here the numerically obtained E_0^{DMC} and Z_0^{DMC} are plotted against the external momentum magnitude p at $\alpha = 1$. The perturbative analytical result of E_0 up to first [8][2] and second [14] order are also outlined and happen to agree quite well for $p < 1$. The error bars are here omitted since they would not have been visible due to the low uncertainty.

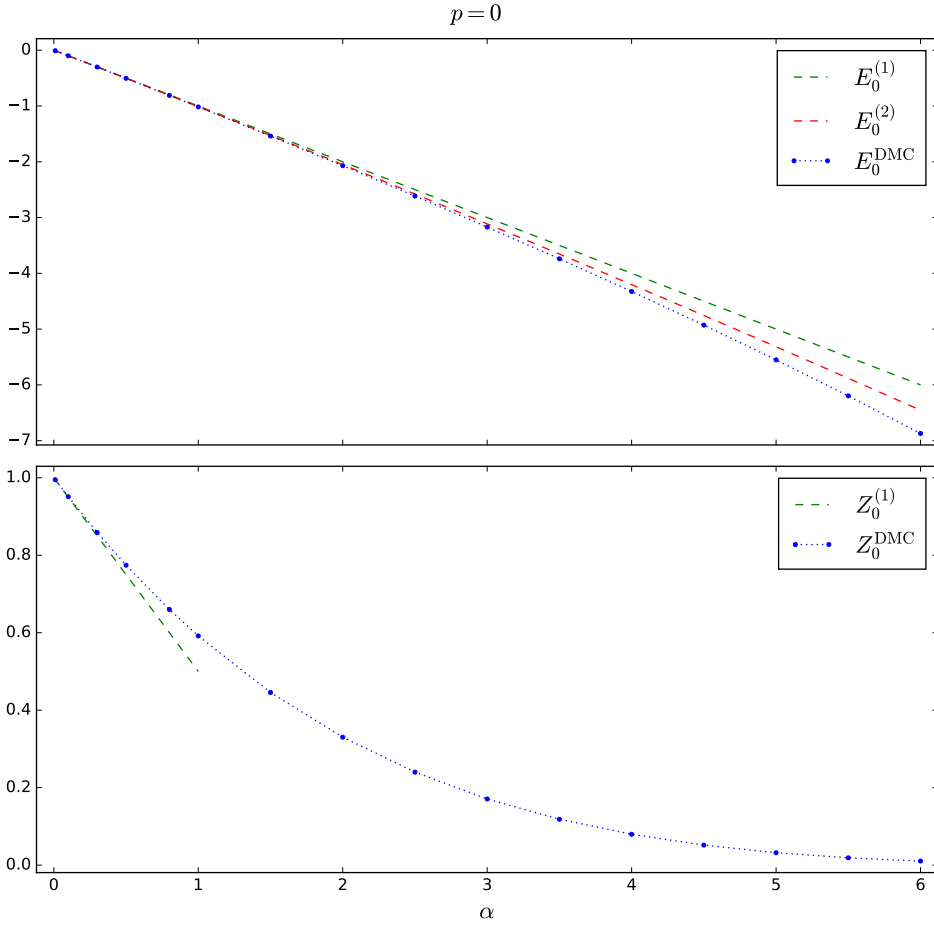


Figure 3.30: Here the numerically obtained E_0^{DMC} and Z_0^{DMC} are plotted against the interaction parameter α at $p = 0$. Again analytical perturbative results up to the first and second order are outlined. Since $\mathcal{G}^{(1)}(\mathbf{p} = \mathbf{0}, \tau) = [1 - \alpha/2] \mathcal{G}^{(0)}(\mathbf{p} = \mathbf{0}, \tau)$ it is apparent that $Z_0^{(0)} = 1 - \alpha/2$ by comparing against 2.19. The error bars are here omitted since they would not have been visible due to the low uncertainty.

$\alpha = 1$			$p = 0$		
p	E_0^{DMC}	Z_0^{DMC}	α	E_0^{DMC}	Z_0^{DMC}
0	-1.0168	0.5918	0.01	-0.0100	0.9950
0.11	-1.0117	0.5909	0.1	-0.1002	0.9511
0.21	-0.9984	0.5886	0.3	-0.3015	0.8590
0.33	-0.9714	0.5839	0.5	-0.5041	0.7743
0.45	-0.9326	0.5769	0.8	-0.8107	0.6600
0.55	-0.8915	0.5691	1	-1.0168	0.5918
0.67	-0.8320	0.5569	1.5	-1.5389	0.4458
0.79	-0.7619	0.5411	2	-2.0711	0.3303
0.89	-0.6959	0.5248	2.5	-2.6147	0.2401
1	-0.6158	0.5022	3	-3.1705	0.1708
1.26	-0.4044	0.4251	3.5	-3.7403	0.1184
1.41	-0.2760	0.3585	4	-4.3256	0.0797
1.55	-0.1618	0.2763	4.5	-4.9284	0.0516
1.615	-0.1141	0.2303	5	-5.5514	0.0320
1.675	-0.0753	0.1825	5.5	-6.1976	0.0188
1.73	-0.0458	0.1328	6	-6.8709	0.0104

Table 3.4: Some of the data from figures 3.29 and 3.30.

Chapter 4

Summary, conclusions and outlook

- Summarize what has been done in the thesis. What was the main objectives?
- What could have been improved (better statistics for bold)? What more could have been done?
- Other studies about the polaron using DMC.

Bibliography

- [1] A. S. Alexandrov and J. T. Devreese, *Advances in Polaron Physics (Springer Series in Solid-State Sciences)* (Springer, 2009).
- [2] R. P. Feynman, *Statistical Mechanics: A Set Of Lectures (Advanced Books Classics)* (Westview Press, 1998).
- [3] H. Wimmel, *Quantum Physics & Observed Reality: A Critical Interpretation of Quantum Mechanics* (World Scientific Pub Co Inc, 1992).
- [4] A. L. Fetter and J. D. Walecka, *Quantum Theory of Many-Particle Systems* (Dover Publications, 2003).
- [5] A. A. Abrikosov, L. P. Gorkov and I. E. Dzyaloshinski, *Methods of Quantum Field Theory in Statistical Physics (Dover Books on Physics)* (Dover Publications, 2012).
- [6] T. Matsubara, *A New Approach to Quantum-Statistical Mechanics*, Progress of Theoretical Physics **14**, 351 (1955).
- [7] A. Mishchenko *et al.*, *Diagrammatic quantum Monte Carlo study of the Fröhlich polaron*, Physical Review B **62**, 6317 (2000).
- [8] H. Fröhlich, *Electrons in lattice fields*, Advances in Physics **3**, 325 (1954), <http://dx.doi.org/10.1080/00018735400101213>.
- [9] H. Goldstein, *Classical Mechanics (Addison-Wesley series in physics)* (Addison-Wesley, 1980).
- [10] K. Binder, *Monte Carlo Methods in Statistical Physics (Topics in Current Physics)*, Second edition. ed. (Springer, 1986).
- [11] M. E. J. Newman and G. T. Barkema, *Monte Carlo Methods in Statistical Physics* (Clarendon Press, 1999).
- [12] N. Prokof'ev and B. Svistunov, *Bold Diagrammatic Monte Carlo Technique: When the Sign Problem Is Welcome*, Phys. Rev. Lett. **99**, 250201 (2007).

- [13] R. Mattuck, *A Guide to Feynman Diagrams in the Many-Body Problem: Second Edition* Dover Books on Physics (Dover Publications, 2012).
- [14] E. Haga, *Note on the Slow Electrons in a Polar Crystal*, Progress of Theoretical Physics **11**, 449 (1954).